12-2014

FLEXURAL STRENGTHENING OF ONE-WAY CONTINUOUS REINFORCED CONCRETE SLABS WITH CUTOFFS IN SAGGING AND HOGGING REGIONS Jafer Husni

Jafer Husni Alshawa

Follow this and additional works at: https://scholarworks.uaeu.ac.ae/all_theses

Part of the Civil and Environmental Engineering Commons

United Arab Emirates University

College of Engineering

Department of Civil and Environmental Engineering

FLEXURAL STRENGTHENING OF ONE-WAY CONTINUOUS REINFORCED CONCRETE SLABS WITH CUTOFFS IN SAGGING AND HOGGING REGIONS

Jafer Husni Alshawa

This thesis is submitted in partial fulfillment of the requirements for the degree of Master of Science in Civil Engineering

Under the supervision of Dr. Tamer El Maaddawy

December 2014

Declaration of Original Work

I, Jafer Husni Alshawa, the undersigned, a graduate student at the United Arab Emirates University (UAEU), and the author of the thesis entitled "Flexural Strengthening of One way Continuous Reinforced Concrete Slabs with Cutoffs in Sagging and Hogging" hereby, solemnly declare that this thesis is an original research work done and prepared by me under the supervision of Dr. Tamer El Maaddawy, in the College of Engineering at UAEU. This work has not been previously formed as the basis for the award of any academic degree, diploma or similar title at this or any other university. The materials borrowed from other sources and included in my thesis have been properly cited and acknowledged.

Student's Signature ……………………..   Date ……………………...

Approval of the Master Thesis

This Master Thesis is approved by the following Examining Committee Members:

1) Advisor (Committee Chair): Dr. Tamer El Maaddawy

   Title: Associate Professor

   Department of Civil and Environmental Engineering

   College of Engineering

   Signature _____   Date _____

2) Member (Internal Examiner): Dr. Said ElKhouly

   Title: Assistant Professor

   Department of Civil and Environmental Engineering

   College of Engineering

   Signature _____   Date _____

3) Member (External Examiner): Dr. Mark Green

   Title: Professor

   Department of Civil Engineering

   Institution: Queen's University, Ontario, Canada

   Signature _M.F. Green_   Date _23 Dec 2014_

This Master Thesis is accepted by:

Dean of the College of Engineering: Prof. Mohsen Sherif

Signature_____   Date_____

Dean of the College of Graduate Studies: Prof. Nagi Wakim

Signature _____   Date_____

Copy ____of ____

Abstract

Installation of cutouts in existing reinforced concrete (RC) floor slabs to accommodate utility services reduces the slab load capacity and ductility. This research examines the effectiveness of using near-surface-mounted (NSM) carbon fiber-reinforced polymer (CFRP) reinforcement to improve the flexural response of continuous RC slabs with cutouts. The study comprised experimental testing and analytical modeling. A total of eleven two-span RC slab strips, 400 x 125 x 3800 mm each, were tested. Test parameters included the location of the cutout, and amount and distribution of the NSM-CFRP reinforcement between the sagging and hogging regions.

Installation of a cutout in the sagging region reduced the load capacity and ductility index by 27% and 12%, respectively. When the cutout was installed in the hogging region, a 23% reduction in both load capacity and ductility index was recorded. The NSM-CFRP strengthening fully restored the original load capacity of all deficient specimens, except one specimen with a cutout in the hogging region where only 90% of the original load capacity was restored. The enhancement in load capacity due to strengthening was in the range of 53% to 81% for the specimens with a cutout in the sagging region and 18% to 54% for the specimens with a cutout in the hogging region. The ductility index of the specimens strengthened in the sagging region only was, on average, 16% lower than that of the control specimen, whereas for the specimens strengthened in the hogging region only, the ductility index was almost the same as that of the control slab. For the specimens heavily strengthened in both sagging and hogging regions, the ductility index was on average 40% lower

than that of the control slab. A maximum moment redistribution ratio of 26% was recorded for the continuous RC slabs strengthened with NSM-CFRP.

An analytical model that can predict the load capacity of two-span RC slab strips containing cutouts and strengthened with NSM-CFRP has been introduced. The ratio of the predicted to measured load capacity was in the range of 0.74 to 1.02 with an average of 0.85, standard deviation of 0.09, and coefficient of variation of 10%.

Keywords: strengthening, slabs, continuous, cutouts, flexural, NSM-CFRP.

Title and Abstract in Arabic

تقوية عزوم الانحناء للبلاطات الخرسانية المتصلة أحادية التحميل التي تحوي فتحات في أماكن الارتخاء و التقوس

الملخص

إن احداث فتحات في البلاطات الخرسانية المسلحة من أجل استيعاب خدمات المرافق، يؤدى الى تخفيض قدرة تحمل البلاطة وليونتها. يتناول هذا البحث فعالية استخدام البوليمر المقوى بالألياف الكربونية والمثبت في ممرات سطحية لتحسين قدرة تحمل البلاطات الخرسانية التي تحتوي على فتحات. وتضمنت الدراسة اجراء اختبارات معملية وطرح نموذج تحليلي. تم اختبار عدد إحدى عشر بلاطة خرسانية مسلحة من مقطعين بأبعاد 400 × 125 × 3800 مم. تضمنت متغيرات البحث موقع الفتحات في جسم البلاطات الخرسانية المسلحة، وعدد شرائح البوليمر المقوى بالألياف الكربونية المثبتة في ممرات سطحية وتوزيعها بين مناطق الارتخاء والتقوس.

احداث فتحات في مناطق الارتخاء أدى الى تخفيض قدرة التحمل ومؤشر الليونة بنسبة 27٪ و12٪ على التوالي. عندما تم احداث فتحات في منطقة التقوس لوحظت نسبة انخفاض قدرها 23٪ في كل من قدرة التحمل ومؤشر الليونة. استخدام البوليمر المقوى بالألياف الكربونية المثبت في ممرات سطحية أدى الى استعادة جميع عينات البلاطات الخرسانية التي تحتوي على فتحات لقدرة التحمل الأصلية بالكامل، باستثناء عينة واحدة تحتوي على فتحة في منطقة التقوس حيث تم استعادة 90٪ فقط من قدرة التحمل الأصلية. نسبة زيادة قدرة التحمل للبلاطات التي تحتوي على فتحات في منطقة الارتخاء كانت في حدود 53٪ إلى 81٪ اما بالنسبة للعينات التي تحتوي على فتحات في منطقة التقوس فكانت نسبة زيادة قدرة التحمل في

حدود 18٪ إلى 54٪. كان مؤشر الليونة في العينات التي تم تقويتها في منطقة الارتخاء فقط، 16٪ اقل من مؤشر الليونة لعينة التحكم، في حين أن العينات التي تم تقويتها في منطقة التقوس فقط، كان مؤشر الليونة مشابها تقريبا لمؤشر عينة التحكم. بالنسبة الى العينات التي تم تقويتها في مناطق الارتخاء والتقوس في وقت واحد كان مؤشر الليونة أقل بنسبة 40٪ مقارنة بمؤشر الليونة لعينة التحكم. وكانت النسبة القصوى لمؤشر إعادة توزيع أحمال الانحناء 26٪ في البلاطات الخرسانية المستمرة التي تحتوي على فتحات والتي تم تقويتها بالبوليمر المقوى بالألياف الكربونية المثبت في ممرات سطحية.

تم طرح نموذج تحليلي يمكنه أن يتنبأ بقدرة التحمل للبلاطات الخرسانية المكونة من مقطعين وتحتوي على فتحات وتم تقويتها البوليمر المقوى بالألياف الكربونية المثبت في ممرات سطحية. كانت نسبة قدرة التحمل التي تم حسابها باستخدام النموذج التحليلي مقارنة بقدرة التحمل من التجربة المعملية في حدود 0.74 إلى 1.02 مع متوسط 0.85 ومعيار انحراف قدره 0.09، ومعامل اختلاف قدره 10٪.

كلمات البحث: التقوية، بلاطات، مستمرة، فتحات، انحناء، البوليمر المقوى بالألياف الكربونية المثبت في ممرات سطحية.

Acknowledgements

Dedication

To my parents Eng. Husni Alshawa, and Fatina Kaduora, brother Eng. Abdul Raouf

Alshawa, and sisters Dr. Haya and Dr. Farah Alshawa.

Table of Contents

List of Tables

List of Figures

List of Notations

A_f　　Cross sectional area of a NSM-CFRP strip

$A_{f,eff}$　Effective cross section area of all CFRP strips used in strengthening

$A_{f,s}$　Cross section area of all CFRP strips used in the sagging regions

$A_{f,h}$　Cross section area of all CFRP strips used in the hogging region

A_i　　Area of concrete layer i

A_{si}　Cross sectional area of steel bar i

b　　Width of the slab section

c　　Depth of the neutral axis measured from the compression face of the slab

CFRP　Carbon fiber reinforced polymers

C_c　　Load capacity of the control specimen without cutouts

C_s　　Load capacity of the strengthened specimen with cutouts

d　　Depth of the tensile steel measured from the compression face of the slab

d'　　Depth of the compression steel measured from the compression face of the slab

d_{ci}　Distance between plastic centroid of concrete section and centroid of concrete layer i

d_f　　Distance between plastic centroid of concrete section and center of the CFRP strip

d_{si}　Distance between plastic centroid of the concrete section and center of steel bar i

E_c　　Young's modulus of the concrete

E_f　　Young's modulus of the CFRP

EF	Efficiency factor
E_s	Modulus of steel reinforcement before yielding (pre-yield stage)
E_{sp}	Modulus of steel reinforcement after yielding (post-yield stage)
f_c	Concrete stress for given concrete strain
f_c'	Concrete compressive strength
f_{ci}	Concrete stress at the center of the layer i
f_{ct}	Concrete splitting strength
f_f	Stress in NSM-CFRP reinforcement
f_{fr}	Tensile strength of the CFRP
f_s	Steel stress corresponding to ε_s
f_{si}	Stress in the steel bar i
f_{su}	Steel ultimate strength
f_y	Steel yield stress
h	Thickness of slab
L	Length of one span of the slab strip
l_c	Length of the cutout
LER	Load enhancement ratio
$L_{f,s}$	Length of all CFRP strips used in the sagging regions
$L_{f,h}$	Length of all CFRP strips used in the hogging region
L_i	Length of span i of the continuous slab
$LVDT$	Linear variable deferential transformer
$No.\ 10$	10 mm diameter steel reinforcing bar
$No.\ 8$	8 mm diameter steel reinforcing bar
MER	Moment enhancement ratio

M_{exp}	Moment from elastic analysis
M_{exp}	Moment from experiment
$M_{h,e}$	Hogging moment from elastic analysis
$M_{h,exp}$	Hogging moment from experiment
M_n	Nominal moment strength
M_{nh}	Nominal moment strength of the hogging section
M_{ns}	Nominal moment strength of the sagging section
$M_{s,e}$	Sagging moment from elastic analysis
$M_{s,exp}$	Sagging moment from experiment
NSM	Near surface mounted
P_{cr}	Cracking load
P_n	Nominal load capacity predicted by the model
P_u	Ultimate load
P_y	Yielding load
S_g	Strength gain
T_{fe}	Effective tensile strength of all CFRP strips
w_c	Width of the cutout
ε_c	Concrete strain for a given loading condition
ε_{co}	Concrete strain corresponding to the concrete compressive strength
ε_f	Strain in longitudinal NSM-CFRP reinforcement
$\varepsilon_{f,max}$	CFRP strain at peak load
ε_{fr}	Rupture CFRP strain
ε_s	Strain in tensile steel reinforcement
$\varepsilon_s{}'$	Strain in the compression steel reinforcement
ε_{su}	Steel strain corresponding to the steel ultimate strength f_{su}

ε_{sy} Steel strain corresponding to the yield stress f_y

μ Ductility index

Δ_p Mid-span deflection at peak load

Δ_{y1} Mid-span deflection at first yielding (second change in load-deflection response)

$\beta\%$ Moment redistribution ratio

ρ_f CFRP reinforcement ratio

CHAPTER 1: INTRODUCTION

1.1 Introduction

Installation of cutouts in existing reinforced concrete (RC) continuous slabs for the passage of service ducts will reduce the flexural capacity. When such cutouts are unavoidable, adequate measures shall be undertaken to strengthen the concerned slab and restore the flexural strength. The ACI 318-08 Building Code permits presence of openings of any size in flat plate floor systems provided that an analysis is performed to ensure that strength and serviceability requirements are satisfied.

Externally-bonded composite plates or sheets are vulnerable to premature delamination which would limit the gain in flexural capacity and reduce the slab ductility. Sudden failure of the externally-bonded composite system would not allow moment redistribution between sagging and hogging regions. Consequently, most of the current design guidelines on the use of composites in strengthening do not allow moment redistribution in continuous RC structures strengthened with externally-bonded composites. The externally-bonded composite system is also susceptible to acts of vandalism, fire, mechanical damage, and other weather conditions.

To protect the composite reinforcement from mechanical and environmental damage, it has been proposed to use a near-surface-mounted (NSM) composite system, where composite strips or reinforcing bars are inserted into grooves precut on the concrete surface and held in place using an epoxy adhesive as shown in Figure 1.1 (ISIS Canada, 2004). The NSM composite plates are less susceptible to premature delamination than composite sheets or plates bonded on the surface of the concrete. The use of post-installed NSM composite reinforcement as an alternative solution to upgrade continuous RC slabs with cutouts would reduce the risk of

premature delamination and could allow for moment redistribution in continuous structures.
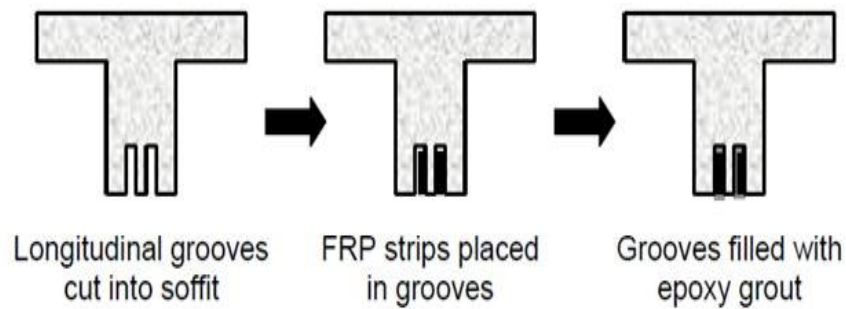
Figure 1.1 : Near Surface Mounted (NSM) Technique for a T- Beam (ISIS Canada, 2004)

1.2 Scope and Objectives

This research aims to examine the viability of using post-installed NSM composite reinforcement to upgrade the flexural response of one-way continuous RC slabs with cutouts in either the sagging and hogging regions. The main objectives of the present study are:

1. to investigate the effect of creating cutouts in either the sagging or hogging regions on the flexural response of one-way continuous reinforced concrete slabs.
2. to examine the effectiveness of using post-installed NSM composite reinforcement to upgrade the flexural response of one-way continuous reinforced concrete slabs with cutouts.
3. to investigate the effect of varying the amount of NSM composite reinforcement in the sagging and hogging regions on the flexural response.

4. to introduce an analytical approach for prediction of the flexural capacity of one-way unstrengthened and strengthened continuous reinforced concrete slabs with and without cutouts.

1.3 Thesis Outline

This research thesis consists of six chapters as follows.

Chapter 1: Introduction

This chapter highlights the importance of the research topic. It discusses the problem briefly and identifies the major objectives. The thesis outline and organization of this research work is also provided in the same chapter.

Chapter 2: Literature Review

This chapter presents a literature review of the available previous studies on flexural strengthening of RC elements containing openings using composites. Available studies on strengthening of continuous RC structures with composites are also reviewed and discussed.

Chapter 3: Experimental Program

This chapter presents details of the experimental program, description of test specimens, fabrication process, material properties, and strengthening methodology. Details of test set-up and instrumentation are also presented in this chapter.

Chapter 4: Experimental Results

Results of the experimental testing are presented in this chapter. The effectiveness of using NSM composite reinforcement to upgrade the flexural

capacity of continuous RC slab strips is discussed. The experimental results include load capacity, failure mode, deflection response, ductility index, strain response of internal steel and NSM composite reinforcement, concrete strain response, support reactions, moment-deflection response, and load versus moment relationships. The moment redistribution ratios of the sagging and hogging regions have been calculated and discussed. The efficiency of strengthening schemes are discussed at the end of the chapter.

Chapter 5: Analytical Modeling

This chapter introduces an analytical approach that can predict the load carrying capacity of one-way continuous reinforced concrete slabs with cutouts and strengthened with NSM composite reinforcement. The accuracy of the proposed analytical approach has been demonstrated by comparing its predictions with the experimental results.

Chapter 6: Conclusions and Recommendations

General conclusions of the work along with recommendation for future studies are presented in this chapter.

CHAPTER 2: LITERATURE REVIEW

2.1 Introduction

Although, significant research work has been carried out during the last three decades to investigate the structural performance of RC structures strengthened with composites, few studies focused on continuous RC structures with cutouts. This chapter presents a brief review of the available experimental research work on strengthening of RC slabs with cutouts using composite reinforcement. Available studies on strengthening of continuous RC flexural elements have also been reviewed and presented in this chapter.

2.2 Studies on Strengthening of RC Slabs with Cutouts Using Composites

Vasquez and Karbhari (2003) examined the viability of using externally-bonded pultruded carbon fiber reinforced polymer (CFRP) strips to upgrade the capacity of RC slabs with cutouts. A total of four slabs with a rectangular cross section were constructed and tested. A typical test specimen had a length of 6000 mm and a cross section dimensions of 3200 x 180 mm. Each slab contained a central cutout with a size of 1 x 1.6 m. The test specimens were divided into two groups based on the applied load position as shown in Figure 2.1. Each group contained a slab without strengthening to act as the base line. Test parameters included the location of the applied load and the externally bonded CFRP configuration. The concrete compressive strength was 27.6 MPa and the steel reinforcement nominal yield strength was 420 MPa. The strengthening regime consisted of bonding of

pultruded CFRP strips with a width of either 50 mm or 100 mm on the concrete surface around the cutout. The pultruded CFRP strips had a tensile modulus of 155 GPa, tensile strength of 2400 MPa, and thickness of 1.2 mm. The strengthened slabs failed by debonding of the CFRP strips and peeling of concrete cover. The externally bonded CFRP strips increased the flexural capacity of the slabs with cutouts. The strength of the strengthened slabs was almost the same as the original strength before the cutout.
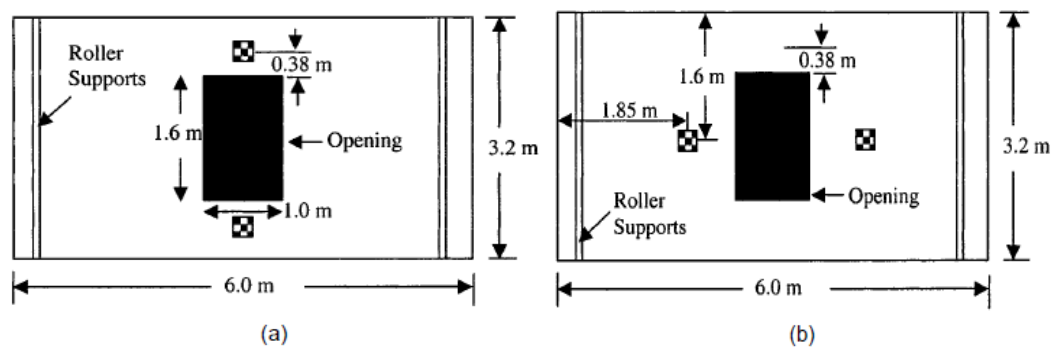
Figure 2.1: Load position for tested slabs (Vasquez and Karbhari 2003)

Tan and Zhao (2004) investigated the structural behavior of one way reinforced concrete slabs with openings strengthened with CFRP composites. A total of eight slabs with a rectangular cross section were constructed and tested. Test specimen had a length of 2700 mm and cross section dimensions of 2400 x 150 mm. Each slab had two edge beams with cross section dimensions of 200 x 300 mm as shown in Figure 2.2. Test parameters included the location of the cutout, the size of the cutout, the load application, and the strengthening system. The concrete compressive strength was 30 MPa. The steel yield strength was 600 MPa for the longitudinal bars and 640 MPa for the transversal bars. The strengthening regime consisted of two systems applied using an externally bonded technique. The first system consisted of fiber sheets. The second system consisted of precured strips. The

strengthened specimens experienced a higher load capacity than the unstrengthened specimens with or without a cutout. The failure mode depended on the opening size. The specimens experienced flexural mode of failure initiated by CFRP debonding. The CFRP sheets were more effective in improving the flexural capacity than the precured CFRP strips because of their better bonding condition.
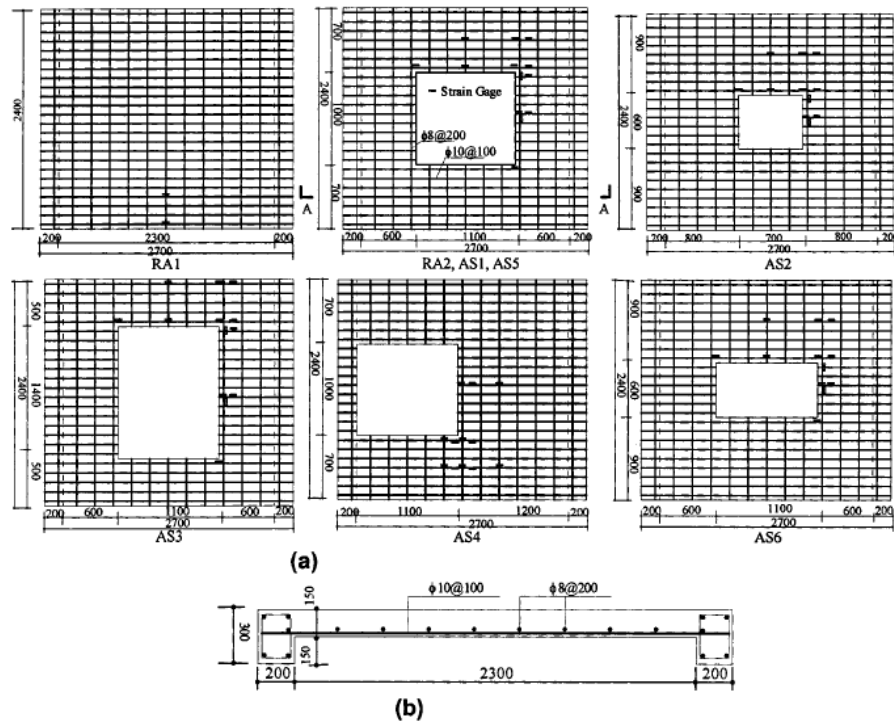
Figure 2.2: (a) Schematic plan layout (b) section A-A (Tan and Zhao 2004)

Boon et al. (2009) studied the flexural behavior of reinforced concrete slabs with an opening. A total of five slabs with a rectangular cross section were constructed and tested. Test specimen had a length of 1100 mm and a cross section dimension of 300 x 75 mm. Test parameters included the direction of the additional reinforcement surrounding the opening. The opening size was 150 x 300 mm. The opening reduced the slab area by 15%. The concrete compressive strength was 25 N/mm^2. The strengthening regime consisted of adding additional steel surrounding

the opening. The test specimens were divided according to the strengthening regime, hence the first specimen did not contain any additional steel or opening. The second specimen did not contain additional steel but it contained an opening. The third specimen contained an opening with longitudinal and transverse steel surrounding it. The fourth specimen contained an opening with diagonal steel placed at the corners of the opening. The last specimen contained an opening with longitudinal, transverse and diagonal steel surrounding it. The rectangular opening reduced the flexural strength of the slab by 37%. Although, the additional steel increased the flexural strength of the specimens with the opening, it could not restore the flexural capacity of the control slab without the opening. The use of longitudinal, transverse and diagonal additional reinforcement was the most effective method to increase the slab capacity.

Kim and Smith (2009) conducted a study on strengthening of reinforced concrete slabs with large penetrations using anchored CFRP composites. A total of three one-way reinforced concrete slabs with a rectangular cross section were constructed and tested. Test specimens had a length of 3400 mm and cross section dimensions of 3200 x 160 mm. Test parameters included the availability of an anchorage system to support the CFRP sheet. The concrete compressive strength was in the range of 35 to 42 MPa. The steel yield strength was 546 MPa. The strengthening regime consisted of using externally-bonded CFRP sheets attached to the slab surface with and without CFRP spike anchors. The control specimen experienced crushing of the compressive concrete in the constant moment region. The strengthened unanchored specimen failed by debonding of the CFRP as shown in Figure 2.3. The strengthened anchored specimen failed by initial debonding of the CFRP followed by concrete compressive failure and rupture of the internal steel

reinforcement. Test results indicated that flexural strengthening with CFRP sheets around the opening increased the load capacity of the slab compared with the control specimen. The use of CFRP spike anchors delayed the debonding of the CFRP sheets, and hence slightly increased the load capacity. The spike anchors offered also a post-peak reserve of strength and improved the slab ductility.

Figure 2.3: Debonding of CFRP (Kim and Smith 2009)

Smith and Kim (2009) carried out a study on strengthening of one-way spanning reinforced concrete slabs with cutouts using CFRP composites. A total of six slabs with a rectangular cross section were constructed and tested. Tested specimen had a length of 3400 mm and cross section dimensions of 2500 x 160 mm for type 1 and 800 x 160 mm for type 2 as shown in Figure 2.4. Test parameters included the position of the applied load and the presence of the cutouts. The average concrete compressive strength was 44 MPa. The steel yield strength was 557 MPa. The strengthening regime consisted of adding two layers of CFRP sheets using externally bonded technique. Two control specimens without a cutout acted as a baseline. Test results indicated that the unstrengthened specimens encountered a peak load of 48.5 kN; however, the strengthened specimen experienced an enhanced average peak load of 75.9 kN. All strengthened slabs failed due to debonding of CFRP sheets. The range of debonding was dependent on the location of the applied

load. The specimens with a line load adjacent to the cutout experienced a transverse bending action, which delayed debonding of the CFRP sheet and thus increased the load capacity.

Figure 2.4: Test slabs (Smith and Kim 2009)

Seliem et al. (2011) reported a case study on restoration of flexural capacity of continuous one-way reinforced concrete slabs with cutouts. A total of five field tests were conducted on RC building slab required demolition as shown in Figure 2.5. The concrete compressive strength was 17.5 MPa and the steel yield strength was 586 MPa. Two strengthening techniques were investigated, namely externally bonded CFRP sheets with and without spike anchors, and NSM-CFRP reinforcement. The test was conducted under four point bending configuration to develop a constant moment zone. The efficiency of each method was evaluated based on the failure mode. Flexure started at the mid span, and then developed from the four corners of the cutouts in longitudinal direction. The slab without a cut-out failed in flexure due to a major crack developed on the top surface. The specimens strengthened with NSM-CFRP reinforcement had higher effective CFRP strain than the specimen with externally bonded CFRP sheets. The NSM-CFRP strengthening system increased the load capacity of the slab with a cut-out by 10%, but it did not enhance the stiffness of the specimen. The use of externally bonded CFRP without anchors insignificantly

increased the slab strength. The strength of the slabs strengthened with NSN-CFRP or externally bonded CFRP without anchors was lower than that of the control. On the contrary, externally bonded CFRP system with spike anchors restored the full flexural capacity.
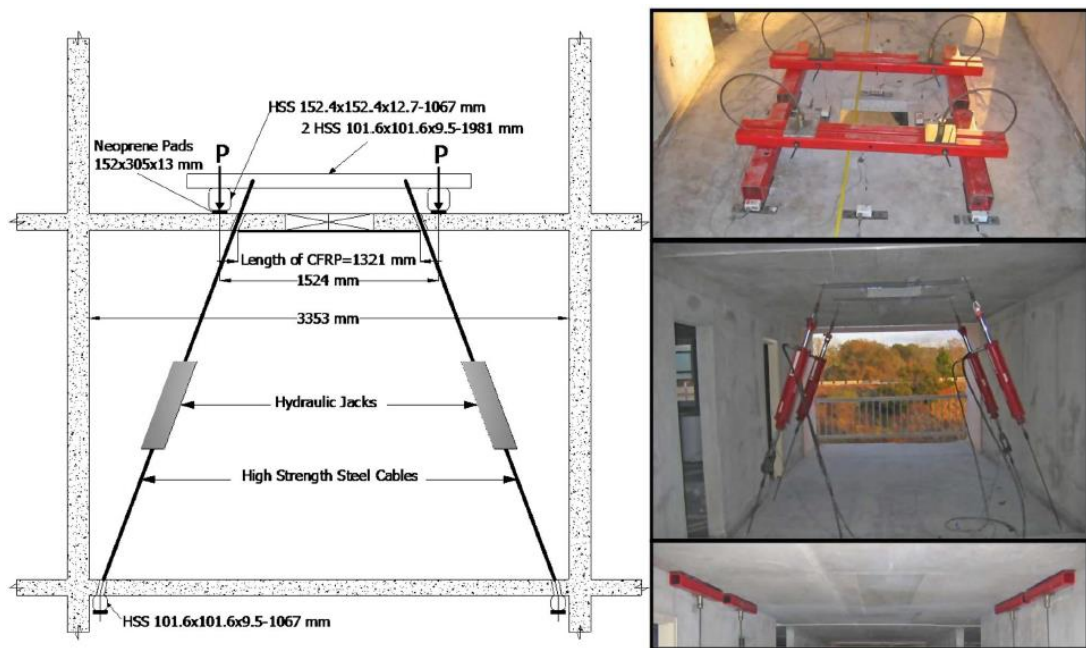
Figure 2.5: Test setup (Seliem et al 2011)

2.3 Studies on Strengthening of Continuous Structures with Composites

El-Refaie et al. (2003) carried out a study in sagging and hogging strengthening of continuous reinforced concrete beams using CFRP sheets. A total of eleven reinforced concrete two-span beams with a rectangular cross section were constructed and tested. Test specimen had a length of 4250 mm and cross section dimensions of 150 x 250 mm. Test parameters included the position, length, and number of CFRP layers. The concrete compressive strength was 30 N/mm^2. The

nominal steel yield strength was 520 N/mm^2. The specimens were divided into two groups. Each group contained one unstrengthened control specimen. An externally bonded technique was used to strengthen the specimens with CFRP sheets. Test results indicated that the external CFRP sheets increased the beam load capacity by more than 18% for the first group and more than 34% for the second group relative to the load capacity of the corresponding control beam. The moment redistribution was reduced for both groups compared with the corresponding control specimen in both sagging and hogging regions. The ductility index was reduced as the number of CFRP sheets increased, since as the strengthening increased the structure element tended to be more brittle. It was also concluded that the adding additional number of CFRP layer more than an optimal limit did not have any effect on the flexural response. Also, increasing the length of the CFRP sheet did not prevent a peeling mode of failure in the strengthened beams. It was noted that the moment capacity enhancement due to strengthening was higher than the load capacity enhancement.

Ashour et al. (2004) performed a study on flexural strengthening of reinforced continuous beams using CFRP laminates. A total of sixteen reinforced concrete continuous beams with a rectangular cross section were constructed and tested. Test specimen had a length of 8500 mm and cross section dimensions of 150 mm x 250 mm. Test parameters included length, thickness, position and form of the CFRP laminates. The average concrete compressive strength was 37 N/mm^2. The longitudinal steel had nominal yield strength of 520 N/mm^2. The specimens were divided into three groups and each group had a different arrangement of internal steel bars and external CFRP reinforcement. All strengthened specimens had higher load capacity and lower ductility than those of the control specimen. The strengthened specimens failed by either peeling failure of the concrete cover adjacent

to the CFRP sheets or tensile rupture of CFRP as shown in Figure 2.6. Increasing the length of the CFRP sheet to cover the entire negative or positive moment zones did not alter the mode of failure and was not effective in further improving the capacity of continuous beams with a tensile rupture mode of failure. It was also concluded that the enhancement of the bending moment capacity of a continuous beam due to external strengthening was higher than the enhancement of the load capacity. This happened because increasing the moment capacity locally may not always lead to a corresponding increase in the load capacity applied to the continuous beam. The load capacity in continuous RC structures depends on the global behavior rather than local behavior.

Tensile rupture of CFRP   Peeling failure of concrete cover
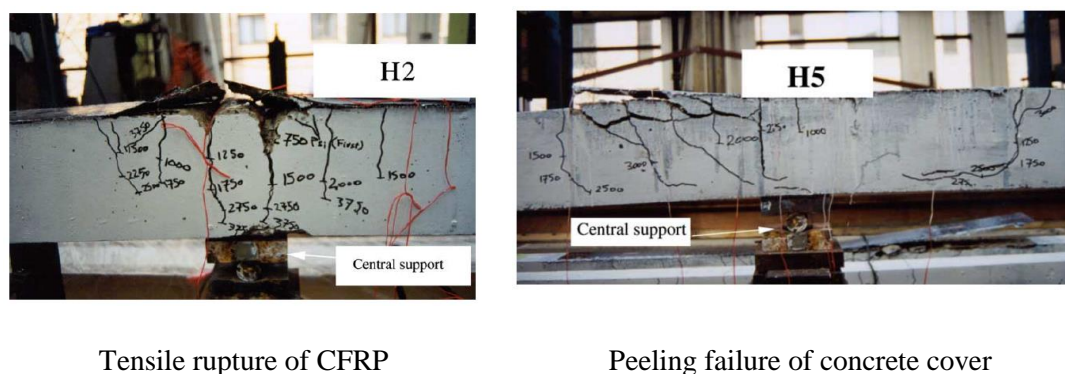
Figure 2.6: Failure Mode (Ashour et al. 2003)

Arduini et al (2004) studied the performance of one-way reinforced concrete slabs strengthened with an externally bonded fiber reinforced polymer system. A total of twenty six slabs with and without an overhang were constructed and tested. The geometry and loading configuration allowed for the study of positive and negative moment regions. Test specimen had a length of either 5000 mm or 6500 mm and cross section dimensions of 1500 x 240 mm. The strengthening regime consisted of manually lay-up CFRP laminates. Test parameters included the amount of internal steel reinforcement, number and width of the CFRP plies. The concrete

compressive strength was 38.8 MPa. The steel yield strength was 557 MPa. The test results indicated that the unstrengthened specimens failed due to steel yielding, while the dominate failure mode for the strengthened specimens was fiber rupture followed by peeling in the concrete cover. The CFRP strengthening enhanced the peak load by up to 122% relative to that of the benchmark specimen. It was also concluded that flexural cracks developed at the tangential stress distribution at the surface between the CFRP laminate and concrete.

Grace et al. (2004) conducted a study on strengthening of cantilever and continuous beams using a triaxially braided ductile fabric shown in Figure 2.7. A total of six beams with a rectangular cross section were constructed and tested. Test specimen had a length of 4267 mm and cross section dimensions of 152 x 254 mm. Test parameters included the location of the support and the number of triaxial ductile fabric or CFRP layers. The concrete compressive strength was 41.5 MPa. The steel yield strength was 490 MPa. The specimens were divided into two groups. Specimens of the first group were tested with one overhanging cantilever, while specimens of the second group were tested with two continuous spans. Each group included an unstrengthened specimen to act as a control specimen. The remaining two beams in the first group were strengthened with two layers of triaxial ductile fabric for the first beam, and four CFRP layers for the second beam. The remaining two beams in the second group were strengthened with one layer of triaxial ductile fabric for the first beam, and two CFRP layers for the second beam. Test results indicated that flexural strengthening with triaxial ductile fabric and CFRP sheets increased the failure load by 36% and 42%, respectively. It was also noted that the strength of the specimens strengthened with CFRP sheets was higher than that of the specimens strengthened with the triaxial ductile fabric system. Although the

strengthened specimens exhibited lower ductility than the control specimens, the triaxial ductile fabric was capable of providing reasonable ductility.
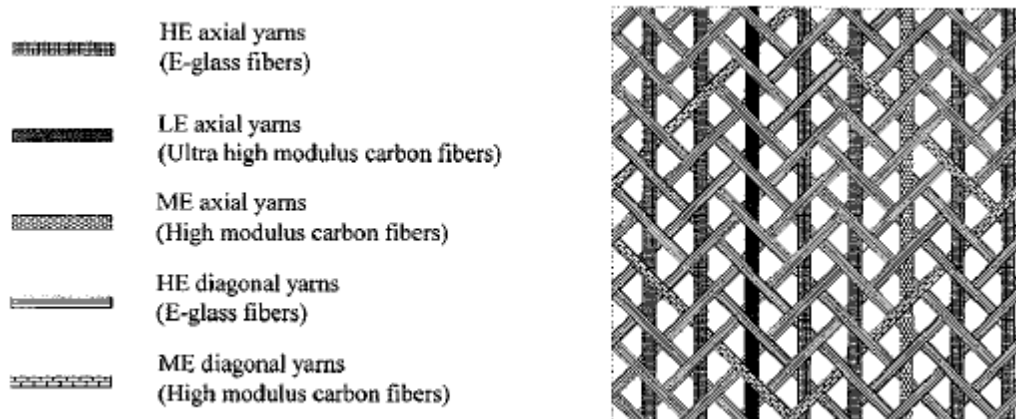
Figure 2.7: Details of triaxial ductile fabric geometry (Grace et al. 2004)

Liu et al. (2006) investigated the moment redistribution of FRP and steel surface plated RC beams and slabs. There were several types of debonding mechanisms such as plate end debonding, critical diagonal crack debonding, and intermediate crack debonding. The rate of moment redistribution for the plated strengthened specimens was lower than the unplated specimens. It was noted that strengthening the hogging and sagging regions of the specimen with a steel plate tended to have an intermediate debonding in the hogging region before yielding of the steel plate. It was found that the moment redistribution occurred only if debonding took place after yielding of internal steel reinforcement. It was concluded that in poorly designed continuous beams, premature debonding of external reinforcement can happen in a certain region before the other region has achieved its moment capacity. Hence, it was suggested to consider moment redistribution in the

analysis of strengthened RC structures because simply allowing for no moment redistribution might not always be a safe assumption.

Coccia et al. (2008) carried out a study to investigate the redistribution of bending moment in continuous reinforced concrete beams strengthened with FRP. An analytical model was developed to define the relationship of bending moment versus curvature. The moment-curvature relationship was divided into three phases. The post cracking phase (first phase) was important to reveal the transition between the uncracked and cracked stages. In the second phase, all the elements in the specimen were subjected to stress and strain. Therefore; after cracking the concrete and FRP interference occurred with a redistribution of stress and strain. In the failure stage, the steel stress tended to have a linear behavior along the reinforcing bar, while the strain patterns were bilinear. The addition of FRP at the hogging and sagging regions of the beams enhanced the ultimate load by 20 %; however, it produced the worst case senior in terms of global ductility. It was also concluded that increasing the amount of FRP at the sagging or hogging region reduced the moment redistribution ratio by 20% and 50% for specimens with one and four FRP sheets, respectively.

Silva and Ibell (2008) conducted an analytical study to evaluate the moment redistribution in continuous FRP-strengthened reinforced concrete beams. The investigation of moment redistribution in FRP-strengthened concrete structures was conducted by connecting such behavior to the level of ductility at the critical section. Generated results from a theoretical model were based on ductility demand. Results of an analytical model were compared to limited experimental data published by others. Evaluation of the moment redistribution in FRP-strengthened RC sections

was found to be more complex than that of conventionally reinforced concrete sections. Moment redistribution developed in FRP-strengthened RC beams immediately after yielding of the longitudinal steel reinforcing. Analytical results showed that if a section can develop a curvature ductility capacity greater than 2.0, moment redistribution in the order of at least 7.5% can be achieved.

Jumaat et al (2010) reviewed published articles on flexural strengthening of reinforced concrete beams and slabs. The researchers concluded that few studies focused on continuous beams. Particularly, experiments on strengthening the negative moment regions of continuous T beams were rare to find continuous T-beam using CFRP laminate. The researchers pointed out that studying the strengthening of the negative moment region was important because this region included maximum moment and shear simultaneously. Externally bonded technique enhanced the load capacity of the beams but reduced the ductility. A simple method of applying CFRP sheets in the negative moment regions was proposed.

Farahbod and Mostofinejad (2011) examined the moment redistribution in reinforced concrete frames strengthened with CFRP sheets. A total of six two-span reinforced frames with a rectangular cross section were constructed and tested. The lengths of the beam and column of the frames were 4300 mm and 2200 mm, respectively with cross section dimensions of 200 x 200 mm as shown in Figure 2.8. The study investigated the response of unstrengthened frames, and strengthened frames with different layers of CFRP with and without mechanical anchors. The concrete compressive strength was 33 MPa. The CFRP had ultimate strength of 3900 MPa, tensile modulus of 230 GPa, and ultimate strain of 1.69%. Test results indicated that the load carrying capacities of the frames increased by 20% to 38% after strengthening, while the flexural capacities had an increase of 9% to 20% and

35% to 55% at the negative and positive moment regions, respectively. It was also concluded that the load capacity of the strengthened frames with mechanical anchors was enhanced by 3% to 5% over that of the strengthened frames without anchors. On the other hand, the flexural moment capacity of the strengthened frames with mechanical anchors exhibited an enhancement of 6% to 8% compared to the frames without anchors. It was concluded that moment redistribution can occur in continuous frames strengthened with CFRP sheets as a result of concrete cracking, yielding of tensile steel, and gradual slip of the strengthening sheet at the contact point with concrete. The moment redistribution value depended on quantity and configuration of CFRP retrofitting, and presence of mechanical anchorage. A maximum moment redistribution value of around 56% was recorded. Moment redistribution in frames strengthened with CFRP and mechanical anchorage was reduced by 10% to 15% compared to their corresponding strengthened frames without mechanical anchorage.

Figure 2.8: Test setup (Farahbod and Mostofinejad 2011)

Aiello and Ombres (2011) studied the moment redistribution in continuous concrete beams strengthened with FRP. A total of six beams with a rectangular cross

section were constructed and tested. Test specimen had a length of 3500 mm and cross section dimensions of 150 x 200 mm. The concrete compressive strength was 21.1 MPa. The steel yield strength was 557 MPa. The strengthening regime consisted of adding CFRP strips at the sagging and hogging regions. A test in progress is shown in Figure 2.9. Test results indicated that strengthening the specimen in sagging region only resulted in approximately 35% increase in load capacity. The load capacity of the specimen strengthened in both sagging and hogging regions was approximately 6% higher than that of the specimen strengthened only in the sagging region. A 12% enhancement in load capacity was recorded when the specimen was strengthened in the hogging region only. It was also concluded that proper strengthening configuration allowed for up to 20% moment redistribution in FRP-strengthened continuous RC beams.

Figure 2.9: Test in progress (Aiello and Ombres 2011)

Dalfré and Barros (2011) studied the effectiveness of using NSM-CFRP flexural strengthening technique to improve the flexural response of continuous RC slabs. A total of two slabs with a rectangular cross section were constructed and

tested. Test specimen had a length of 5850 mm and cross section dimensions of 375 mm x 120 mm. The test parameters included the location of the applied CFRP laminates. The concrete compressive strength was 30 MPa. The steel yield strength was 446 MPa. The strengthening regime consisted of using NSM-CFRP technique as shown in Figure 2.10. The test results indicated that NSM-CFRP strengthening enhanced the load capacity by 29%. Appreciable moment redistribution values of 21% and 27% were recorded for the strengthened slab strips.
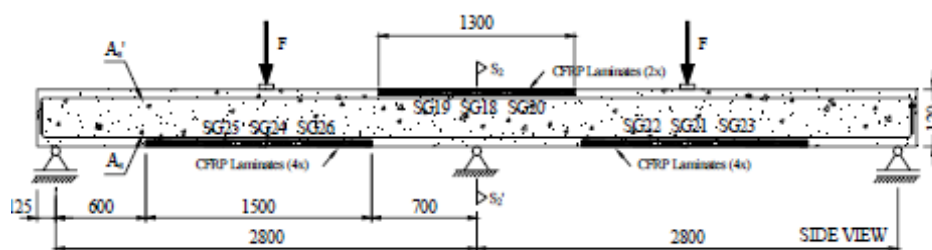
Figure 2.10: NSM-CFRP laminates layout (Dalfré and Barros 2011)

Kai et al (2011) conducted experiments on four two-span continuous RC T-beams. The test specimen had a length of 5400 mm, web width of 200, flange width of 900 mm, flange thickness of 80 mm, and total depth of 300 mm. Three specimens were pre-heated for 75 minutes and one specimen was not. Two of the pre-heated specimens were strengthened with externally bonded CFRP sheets. The concrete compressive strength was 30 N/mm^2. The steel nominal yield strength was 350 N/mm^2. The strengthening regime consisted of applying CFRP sheet using externally bonded technique at either the hogging or sagging regions. The test results indicated that pre-heating slightly reduced the load capacity by 3.5%. Flexural strengthening in the hogging region only had insignificant effect on the load capacity. A 16% increase in the load capacity was recorded after strengthening in the sagging region

only. The load capacity of the pre-heated strengthened specimens were the same as or higher than that of the control specimen. The strengthened specimens exhibited a tensile rupture of the CFRP sheets as a failure mode. The specimens strengthened in the hogging region and that strengthened in the sagging region experienced CFRP effective strain values of 63% and 68% of the ultimate CFRP strength, respectively. The strengthened specimens experienced significant reduction in ductility index compared with that of the control specimen.

2.4   Research Significance

Installation of cutouts in existing RC continuous slabs for the passage of service ducts would result in a significant reduction in the flexural capacity. When such openings are unavoidable, adequate measures shall be undertaken to strengthen the concerned slab and restore the flexural strength. Few studies on flexural strengthening of simply-supported slabs with cutouts were found in the literature. The response of continuous RC beams or slab strips strengthened with composites has also been investigated by few researchers. To the best knowledge of the author, no studies were carried out on flexural strengthening of continuous RC slab strips with cutouts. This research examines the viability of using NSM composite reinforcement as a potential solution to safeguard an acceptable margin of safety and serviceability of continuous RC slabs with cutouts. The results are expected to assist practitioners and researchers in obtaining a satisfactory design solution for retrofitting one-way RC continuous slabs with cutouts. Findings of this research are anticipated to develop existing design guidelines and standards for flexure-deficient RC continuous structures strengthened with composite reinforcement.

CHAPTER 3: EXPERIMENTAL PROGRAM

3.1 Introduction

The experimental program of the current study consisted of testing eleven one-way two span continuous reinforced concrete (RC) slabs. Five slabs had a cutout in the sagging regions, five slabs had a cutout in the hogging region, and one slab had no cutouts to act as a benchmark. The cutout went completely through the full thickness of the slab. The slabs with cutouts were either unstrengthened or strengthened in flexure with near-surface-mounted (NSM) carbon fiber-reinforced polymer (CFRP) composite strips.

This chapter presents details of the experimental program, description of test specimens, fabrication process, material properties, and strengthening methodology. Details of the test set-up and instrumentation are also presented in this chapter.

3.2 Test Program

The main objectives of this experimental work are to:

- investigate the effect of creating a cutout in the sagging or hogging region on the flexural response of one-way continuous RC slabs.

- examine the effectiveness of using post-installed NSM-CFRP composite reinforcement to upgrade the flexural response of one-way continuous RC slabs with cutouts.

- study the effect of varying amount and distribution of the NSM-CFRP reinforcement between the sagging and hogging regions on the flexural response of continuous RC slabs with cutouts.

The test matrix is given in Table 3.1. The test program consisted of eleven one-way two span continuous RC slabs with a cutout in either the hogging or sagging region, except the control slab that had no cutouts. The control slab was not strengthened. The remaining ten specimens were divided into two groups, [A] and [B], based on the location of the cutout.

Table 3.1: Test Matrix

Group	[*]Tension Steel Reinforcement		Strengthening Regime		Designation
	Sagging	Hogging	Sagging	Hogging	
Control No Cutouts	4 No. 10	4 No. 10	-	-	Control
Group [A] Cutout in Sagging Region	2 No. 10	4 No. 10	-	-	A-NS
			NSM-CFRP (2 strips)	-	A-S2-H0
			NSM-CFRP (4 strips)	-	A–S4-H0
			NSM-CFRP (2 strips)	NSM-CFRP (2 strips)	A–S2-H2
			NSM-CFRP (4 strips)	NSM-CFRP (2 strips)	A–S4-H2
Group [B] Cutout in Hogging Region	4 No. 10	2 No. 10	-	-	B-NS
			-	NSM-CFRP (2 strips)	B-S0-H2
			-	NSM-CFRP (4 strips)	B–S0-H4
			NSM-CFRP (2 strips)	NSM-CFRP (2 strips)	B–S2-H2
			NSM-CFRP (2 strips)	NSM-CFRP (4 strips)	B–S2-H4

[*]Diameter of No. 10 steel bar = 10 mm

In Table 3.1, No. 10 refers to a reinforcing steel bar with a nominal diameter of 10 mm. The symbols A and B refer to specimens of groups [A] and [B], respectively. The symbol NS refers to no strengthening. The symbols S0, S2, S4 refer to strengthening with zero, two, and four NSM-CFRP strips in the sagging region, respectively. The symbols H0, H2, H4 refer to strengthening with zero, two, and four NSM-CFRP strips in the hogging region, respectively.

3.2.1 Control Specimen

The control specimen did not have a cutout in neither the sagging nor hogging region to act as benchmark for the other test specimens. The slab is reinforced with 4 No. 10 steel bars in the hogging region and 4 No. 10 steel bars in the sagging regions. Geometry and details of reinforcement of the control specimen is shown in Figure 3.1 and described in section 3.3.

3.2.2 Group [A]

This group comprised five specimens. All specimens of this group had a cutout in each sagging region. The cutout had a width of 150 mm in transverse direction and a length of 450 mm in longitudinal direction. The centre of the cutout coincided with the mid-point of the sagging region. Installation of the cutout reduced the tension steel reinforcement in the sagging region to be 2 No. 10 instead of 4 No. 10 reinforcing bars. Since the cutout was only in the sagging region, the steel reinforcement in the hogging region remained unchanged as 4 No. 10 bars. Four slabs were strengthened in flexure using NSM-CFRP reinforcement, and one slab was not strengthened. Specimens A-S2-H0 and A-S4-H0 were strengthened in each sagging region with two and four NSM-CFRP strips, respectively. Specimen A-S2-H2 was strengthened with two NSM-CFRP strips in both sagging and hogging

regions. Specimen A-S4-H2 was strengthened with four NSM-CFRP strips in each sagging region and two NSM-CFRP strips in the hogging region. Results of specimen A-NS have been used to study the effect of creation of a cutout in the sagging regions on the flexural response of one-way continuous RC slabs. Results of the strengthened specimens have been used to examine the effectiveness of the NSM-CFRP strengthening system to restore the flexural capacity of one-way continuous RC slabs with a cutout in the sagging regions.

3.2.3 Group [B]

This group involved five specimens. All specimens had a cutout of 150x450 mm in the hogging region over the central support. Installation of the cutout reduced the tension steel reinforcement in the hogging region to be 2 No. 10 bars instead of 4 No. 10 bars. The tension steel in the sagging region, 4 No. 10 bars, was not changed. Four slabs were strengthened with NSM-CFRP reinforcement while one slab was not strengthened. Specimens B-S0-H2 and B-S0-H4 were strengthened with two and four NSM-CFRP strips in the hogging region, respectively. Specimens B-S2-H2 and B-S2-H4 were strengthened with two and four NSM-CFRP strips in the hogging region, respectively and two NSM-CFRP strips in each sagging region. Results of specimen B-NS have been used to study the effect of creation of a cutout in the hogging region on the slab's flexural response. Results of other specimens of this group have been used to evaluate the viability of the NSM-CFRP strengthening system to restore the flexural capacity of continuous RC slabs with a cutout in the hogging region.

3.3 Specimens Details

Figure 3.1 shows geometry, reinforcement, and load configuration of the control test specimen. The geometry and details of reinforcement of specimens of groups [A] and [B] are shown in Figure 3.2 and 3.3, respectively. The control test specimen was 3800 mm long, 400 mm wide, and 125 mm deep. The specimen comprised two equal spans of 1800 mm each. The specimen was tested to failure under two point loads, one in the mid of each span. The control specimen was reinforced by 4 No. 10 longitudinal steel reinforcement in tension zone of both sagging and hogging regions as shown in Figure 3.1. The clear concrete cover was 25 mm while the cover to centre of steel was 38 mm. The compression steel reinforcement in both the sagging and hogging regions consisted of 2 No. 10 steel bars. Shear reinforcement in the form of 4-leg No. 8 (8 mm diameter) closed stirrups spaced at $s = 50$ mm was provided along the length of the specimen to avoid shear mode of failure. Shear reinforcement is often used at the supports (columns) in flat plate floor systems to improve the punching shear resistance. For RC members subjected to bending moments without axial compression forces, the confinement provided by the shear reinforcement would have a negligible effect on the flexural capacity.

Specimens of group [A] had the same dimensions as that of the control specimen but a cutout was installed in the sagging region of each span. The cutout had a width of $w_c = 150$ mm and length of $l_c = 450$ mm. The centre of the cutout coincided with the mid-span point. The cutout width-to-slab width ratio, w_c/b, was 0.375 and the cutout length-to-span length ratio, l_c/L, was 0.25. Similarly, specimens of group [B] had the same dimension as that of the control specimen but a cutout

having a width of $w_c = 150$ mm and length of $l_c = 450$ mm was installed in the hogging region over the middle support. The steel reinforcement intersected by the cutout was removed to resemble the case of inclusion of a cutout in an existing floor slab which would typically result in cutting of existing steel reinforcement. As a result, specimens of group [A] had 2 No. 10 tension steel reinforcement in the mid-span section (sagging region) and specimens of group [B] had 2 No. 10 tension steel reinforcement over the middle support (hogging region).
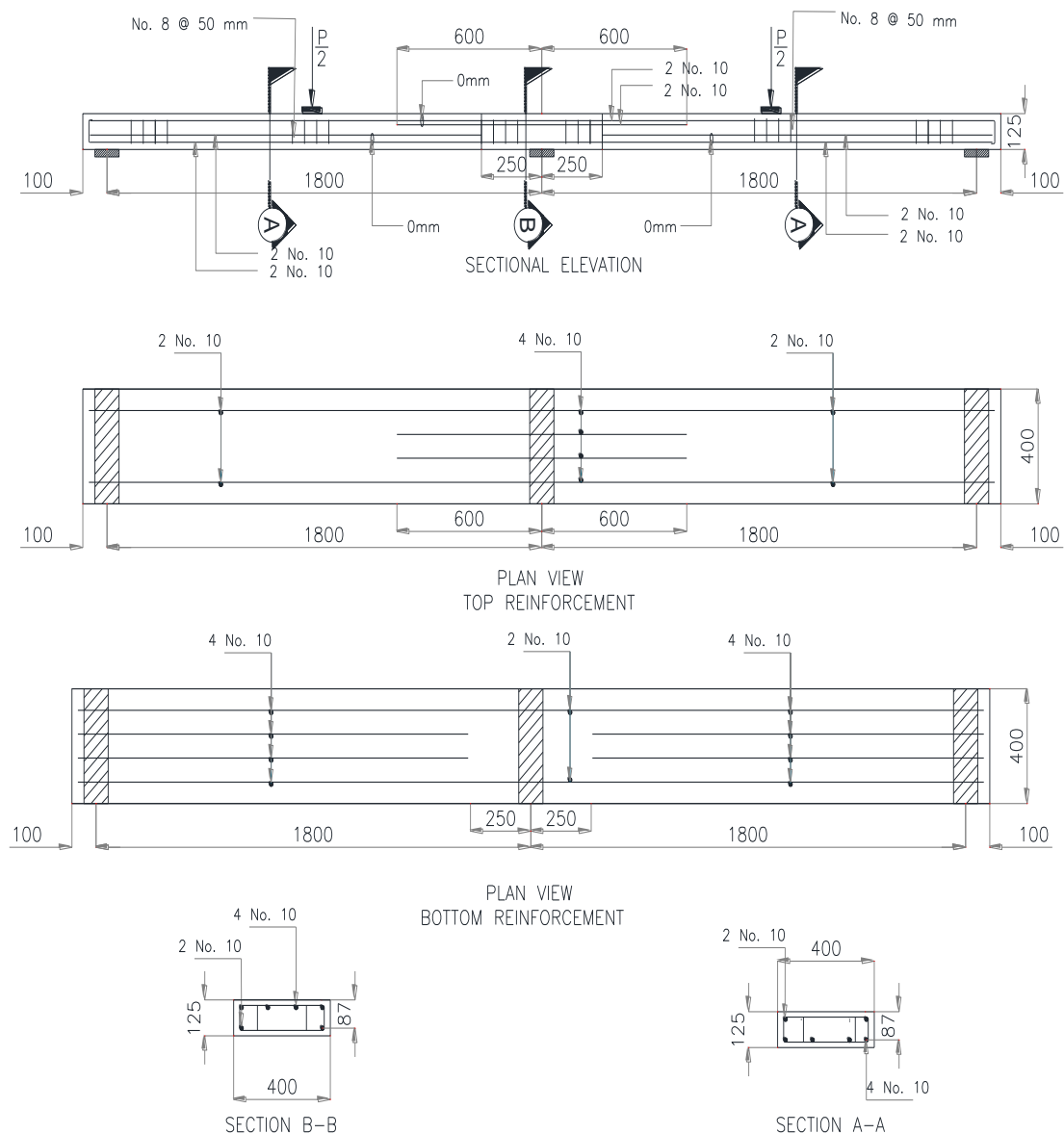
Figure 3.1: Geometry and details of reinforcement of the control specimen
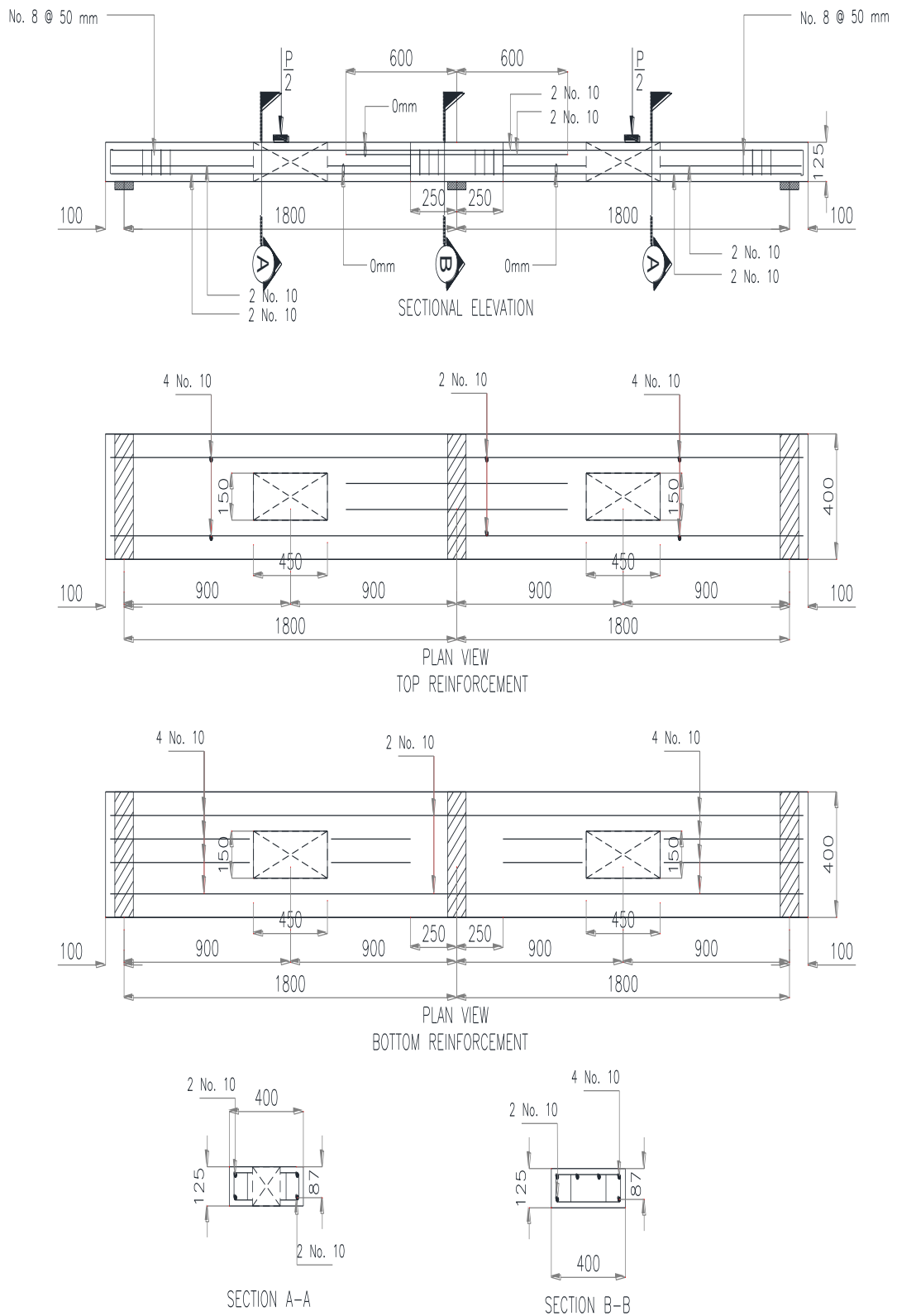
Figure 3.2: Geometry and details of reinforcement of specimens of group [A]
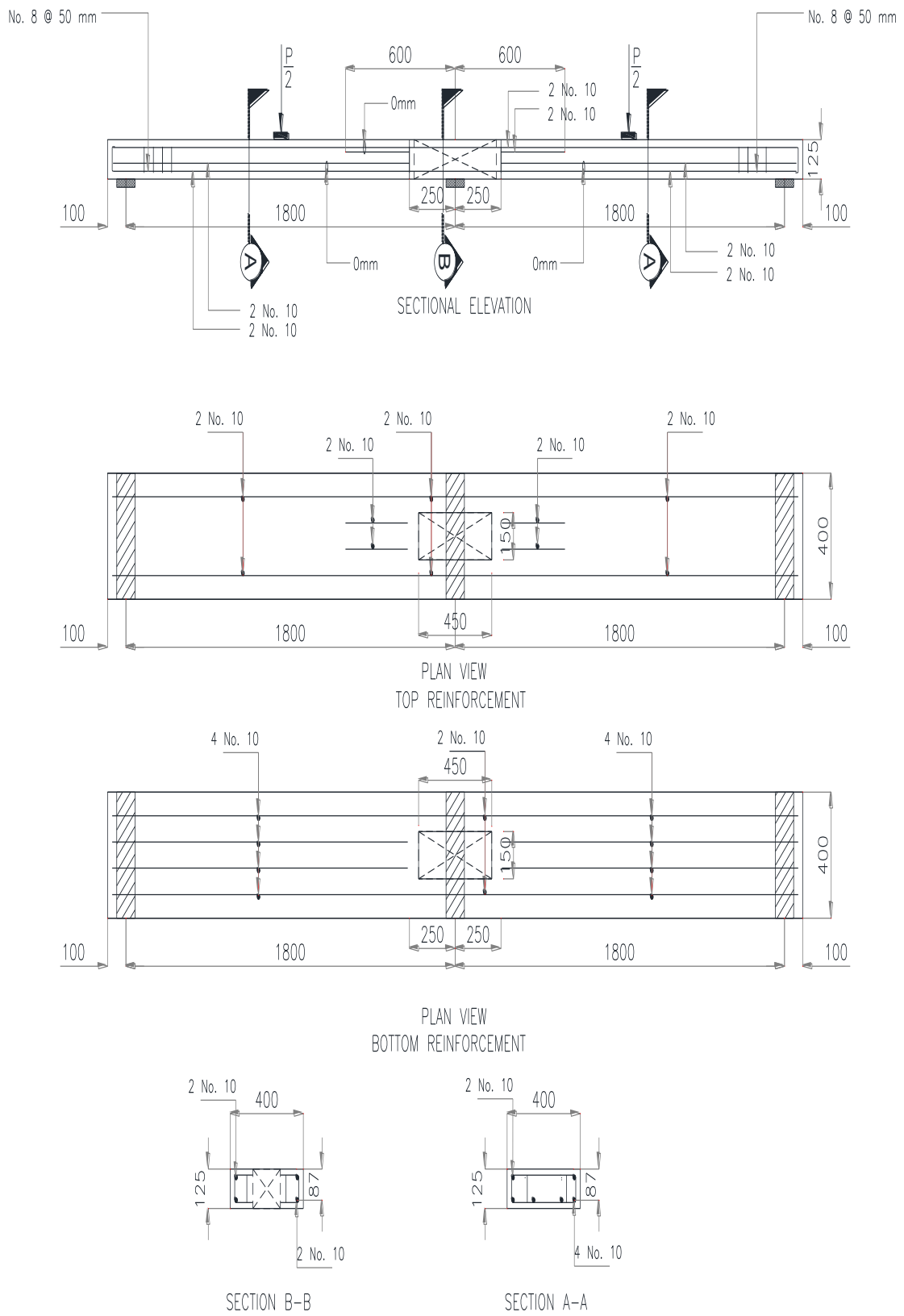
Figure 3.3: Geometry and details of reinforcement of specimens of group [B]

3.4 Specimens Fabrication

Wooden forms were fabricated using 18 mm plywood sheets and 240x240 mm white timbers as shown in Figure 3.4(a). A wooden box with dimensions of 150x450 mm was fabricated and then installed in the form at the location of the cutout to provide the required opening in test specimens. The steel bars were cut and bent to desired dimensions. The steel bars were tied together using bending steel wires to form the steel cages. A photo of steel cages is shown in Figure 3.4(b).

Strain gauges (S.G.) were bonded to the tensile steel reinforcement at the mid spans and over the central support. The surface of steel was first prepared using a grinder at the location of the S.G. to acquire a smooth surface. The steel surface was then cleaned by alcohol. The S.G. was then bonded to the steel surface using an adhesive. The wires of the S.G. were isolated from being in contact with the steel bars. A coating material was then applied to protect the S.G. and wires during concrete casting. Photos taken during installation of a typical S.G. are shown in Figure 3.5.

Small concrete cubes having the same dimensions as those of the clear concrete cover were prepared. The concrete cubes were attached to the main steel bars prior to casting at discrete locations to maintain the concrete clear cover. The steel cages were then installed inside the forms prior to casting as shown in Figure 3.6.

(a) Fabricated wooden forms   (b) Steel cages

Figure 3.4: Formwork and steel cages

(a) Surface preparation using grinder   (b) Cleaning of steel surface by alcohol
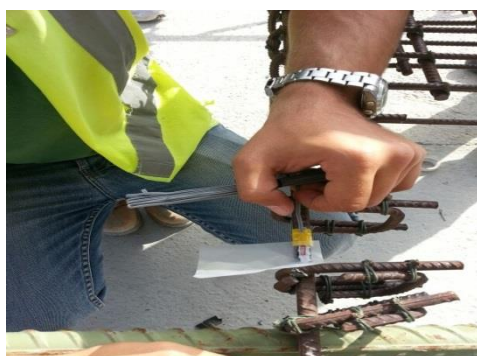
(c) Bonding of S.G. to steel surface   (d) Application of coating tape

Figure 3.5: Installation of strain gauges to steel bars

Figure 3.6: Steel cages installed inside the forms

The concrete was prepared and delivered by a local ready-mix concrete producer. All specimens were cast in a horizontal position as shown in Figure 3.7. The concrete was compacted using hand-held vibratos to prohibit any segregation as shown in Figure 3.8. Concrete cubes and cylinders were sampled during casting as shown in Figure 3.9. The concrete surface was finished and leveled using a trowel as shown in Figure 3.10. After casting, polythene sheets, 500 gauges each, were wrapped around test specimens for one day. The sides of the forms were then removed. Following removal of forms, concrete specimens were covered with burlap sheets as shown in Figure 3.11. The burlap sheets were sprayed with water five times per day for seven days. The specimens were then left air-cured until the time of strengthening and/or testing.

Figure 3.7: Concrete casting

Figure 3.8: Concrete vibration

Figure 3.9: Preparation of concrete cylinder samples

Figure 3.10: Concrete finishing

Figure 3.11: Concrete curing

3.5 Material Properties

3.5.1 Concrete

The concrete mix proportion is given in Table 3.2. The concrete mixtures included ordinary Type I Portland Cement. The course aggregate included crushed limestone with nominal sizes in of 5 mm, 10 mm, and 20 mm. The fine aggregate was dune sand. The aggregate distribution is demonstrated in Table 3.3. The water cement ratio was 0.42. Before casting of concrete, a slump test was conducted to ensure workability of concrete as shown in Figures 3.12 and 3.13. The concrete slump was 120 mm which was within the acceptable limits (160±40 mm). Six concrete cylinders 150x300 mm each, and six concrete cubes, 150x150 mm each, were sampled during casting. The concrete cubes and cylinders were subjected to the same curing regime as that of test specimens.

Table 3.2: Concrete mix proportion

Mix Proportion	
Materials	Batch Weight kg/m^3
Cement	360
20 mm cr. L/S Agg.	600
10 mm cr. L/S Agg.	400
5 mm cr. L/S Agg.	600
Dune Sand	325
Free Water	150
Total Weight	2441

Table 3.3: Aggregate distribution

Aggregates Percentage		
Size	Type	%
20 mm	Crushed Limestone	31.2
10 mm	Crushed Limestone	20.8
0-5 mm	Crushed Limestone	31.2
Dune Sand	Alain	16.9

The cubes and cylinders were tested at the time of structural testing as shown in Figure 3.14. The cubes were tested under compression to determine the concrete cube compression strength. Three cylinders were tested under compression to determine the concrete cylinder compression strength and three cylinders were used to determine the concrete splitting strength. The compression and splitting strength results are given in Tables 3.4 and 3.5, respectively. The concrete cylinder and cube strengths were on average 24.8±3 MPa and 41.2±2 MPa with coefficient of variations of 12% and 5%, respectively. For general construction testing, the

coefficient of variation for strength results of the concrete cylinders is considered fair whereas for the strength results of the concrete cubes, it is considered excellent (ACI 214R-02). The concrete splitting strength was on average 2.6 MPa with a standard deviation of 0.4 MPa.

Table 3.4: Concrete compression strength results

Property	Sample No. 1	Sample No. 2	Sample No. 3	Sample No. 4	Sample No. 5	Sample No. 6	AVG. (MPa)	SD (MPa)
Cylinders f'_c (MPa)	23.65	28.29	22.47	-	-	-	24.8	3
Cubes f_{cu} (MPa)	41.56	40	42.22	38.89	40	44.44	41.2	2

Table 3.5: Concrete splitting strength results

Property		Sample No. 1	Sample No. 2	Sample No. 3	Average (MPa)	Standard deviation (MPa)
f_{ct} (MPa)		2.89	2.18	2.57	2.6	0.4

Figure 3.12: Concrete delivery

Figure 3.13: Slump test

(a) Cube compression test   (b) Cylinder compression test   (c) Cylinder splitting test

Figure 3.14: Cube and cylinder compression and splitting tests

3.5.2 Steel Reinforcement

The longitudinal steel reinforcement was No. 10 (10 mm diameter), while the shear reinforcement was No. 8 (8 mm diameter). Three steel coupons from both diameters were tested under uniaxial tension force to determine the yield and ultimate strengths. The tensile test results of the steel coupons are provided in Table 3.6. The No. 10 steel reinforcing bars had average yield and ultimate strengths of 515 MPa and 599 MPa, respectively with corresponding standard deviations of 30 MPa and 22 MPa, respectively. The No. 8 steel reinforcing bars had average yield and ultimate strength of 530 MPa and 609 MPa, respectively with corresponding standard deviations of 37 MPa and 22 MPa, respectively.

Table 3.6: Tensile test results of steel coupons

Nominal bar size	Property (MPa)	Sample No. 1	Sample No. 2	Sample No. 3	Average (MPa)
No. 10[*]	Yield Strength	520	542	483	515 ± 30
	Ultimate Strength	598	622	578	599 ± 22
No. 8[**]	Yield Strength	514	503	572	530 ± 37
	Ultimate Strength	605	589	633	609 ± 22

[*]No. 10 = 10 mm diameter steel reinforcing bar
[**]No. 8   = 8 mm diameter steel reinforcing bar

3.5.3 Composite Reinforcement

The CFRP composite strips used in the NSM strengthening had cross section dimensions of 2.5 x 15 mm, average tensile modulus and strength of 165 GPa and 3100 MPa, respectively, and a strain at break of approximately 1.9 % (Sika® CarboDur® Plates). The NSM composite strips were bonded to sides of the concrete

grooves using an epoxy adhesive having a tensile modulus of 4.5 GPa, tensile strength of 24.8 MPa, and elongation at break of 1% (Sikadur® 30). Properties of the CFRP strips and epoxy adhesive were obtained from the manufacturer. Figure 3.15 shows the materials used in strengthening.

| (a) CFRP strips (Sika® Carbo Dur) | (b) Epoxy adhesive (Sikadur®30) |

Figure 3.15: Material used in the NSM strengthening system

3.6 Strengthening Methodology

The strengthening regimes adopted for specimens of group [A] are shown in Figure 3.16 through Figure 3.19 while those of specimens of group [B] are shown in Figure 3.20 through Figure 3.23. The CFRP strips used in the sagging region were cut to length of 1530 mm which corresponded to 85% of the span length. The CFRP strips in the hogging region were cut to a length of 1200 mm and extended inside each span for a 600 mm. The extended length of the hogging CFRP reinforcement corresponded to one-third of the span length (i.e. *L/3*) which would resemble practical applications. A slitting machine was used to cut grooves on concrete surface at desired locations. Each groove had a width of 10 mm and depth of 23 mm. The grooves were cleaned of dust and loose particles using an air blower. The grooves were partially filled with the epoxy adhesive. The CFRP strips were then inserted

into the grooves and lightly pressed until the adhesive overflowed around them. The concrete surface was then cleaned and leveled using a trowel. The strengthening procedures are summarized in Figure 3.24. The slabs were left air-cured until time of structural testing.
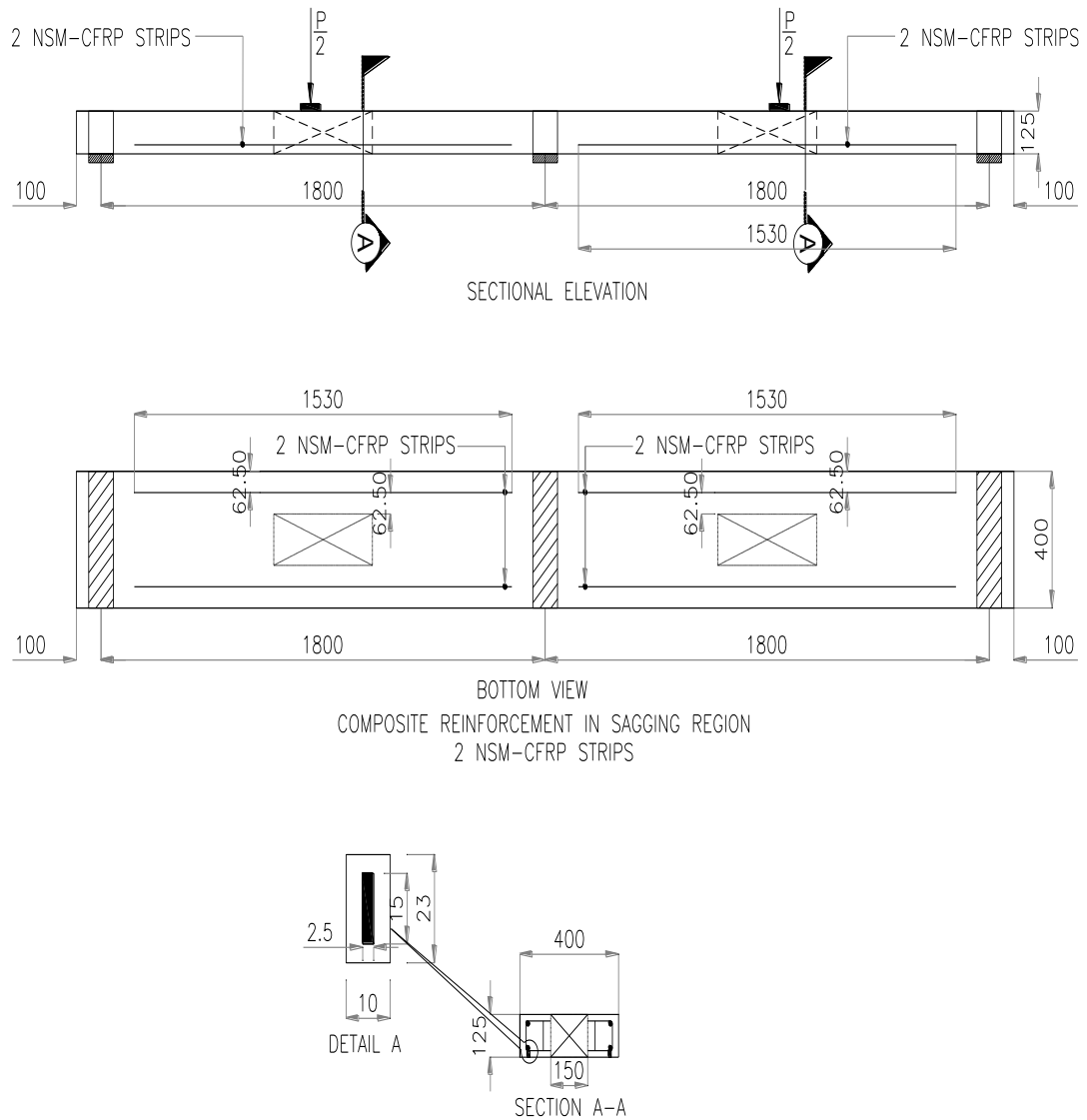
Figure 3.16: Strengthening regime for specimen A-S2-H0

4 NSM-CFRP STRIPS

P/2

4 NSM-CFRP STRIPS

P/2

125

100 1800 100

1800

1530

A A

SECTIONAL ELEVATION

1530 1530

4 NSM-CFRP STRIPS 4 NSM-CFRP STRIPS

400

30 30 30 30

65 65

100 1800 1800 100

BOTTOM VIEW
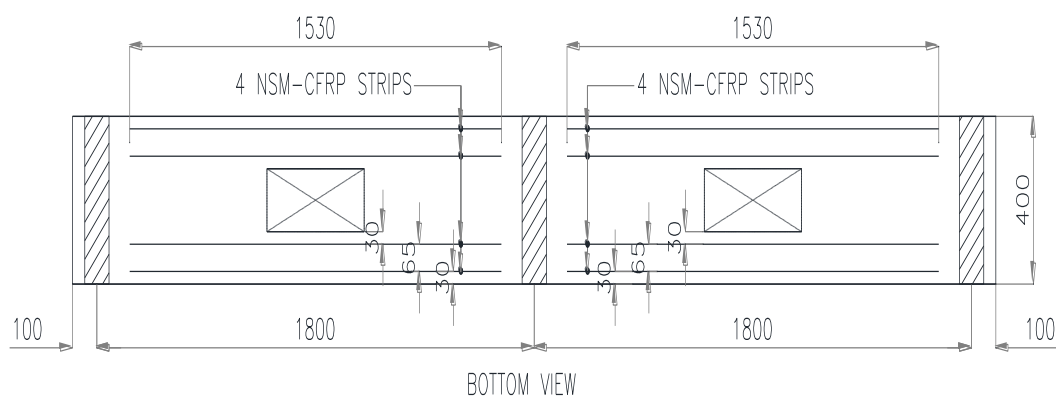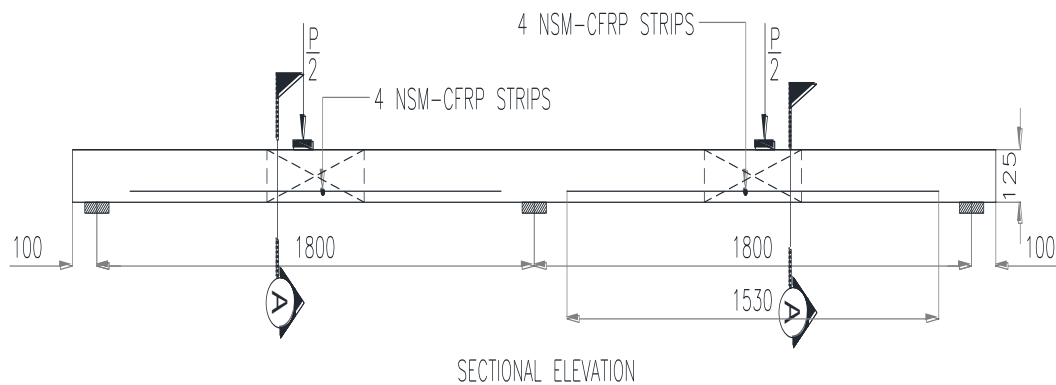
COMPOSITE REINFORCEMENT IN SAGGING REGION

4 NSM-CFRP STRIPS

23

15

2.5

10

DETAIL A

400

125

150

SECTION A-A
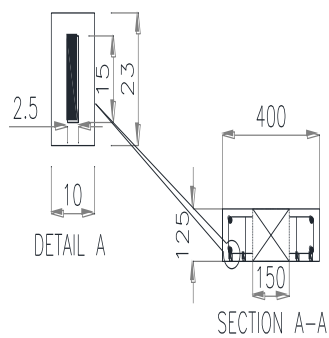
A-S4-H0

Figure 3.17: Strengthening regime for specimen A-S4-H0
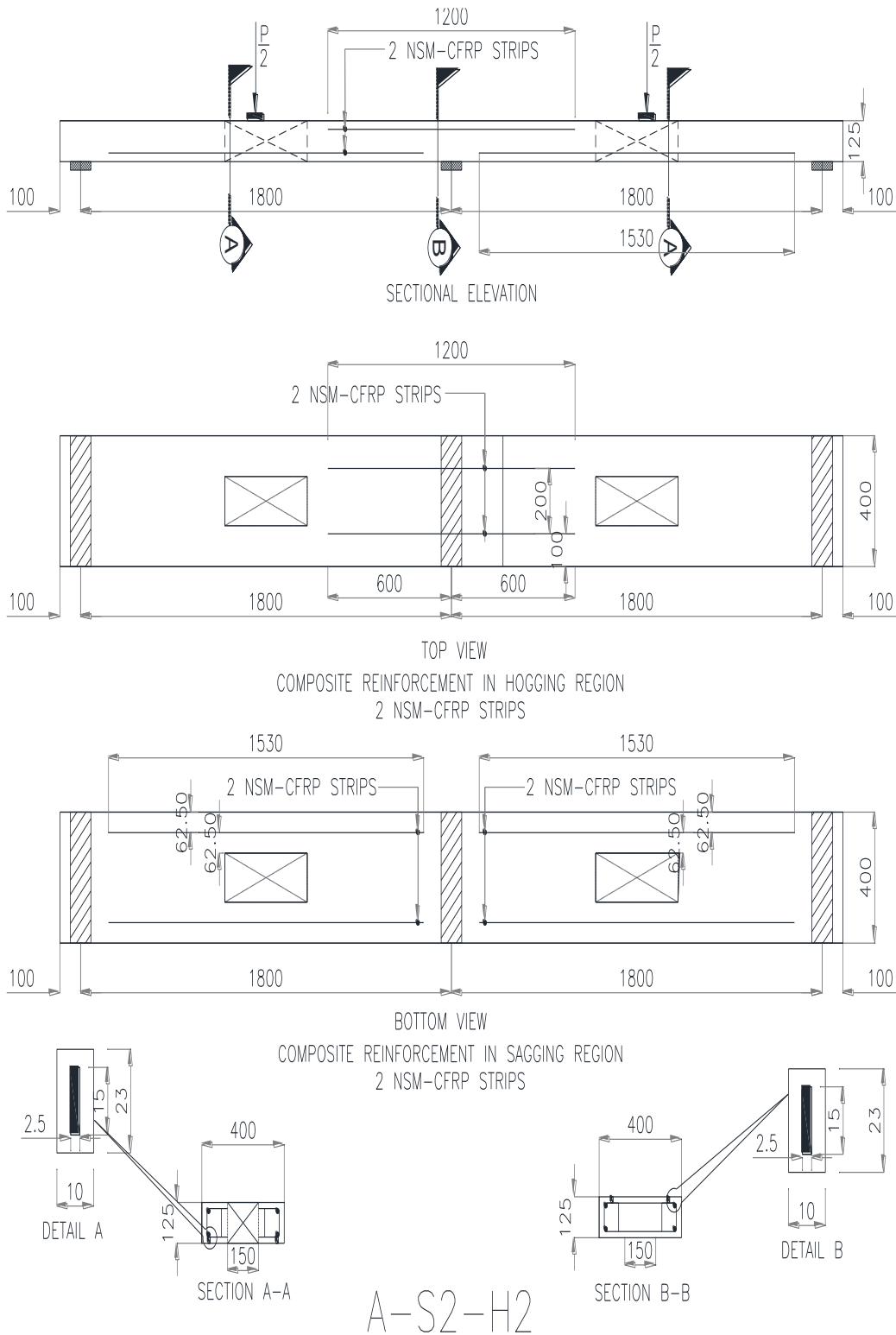
Figure 3.18: Strengthening regime for specimen A-S2-H2
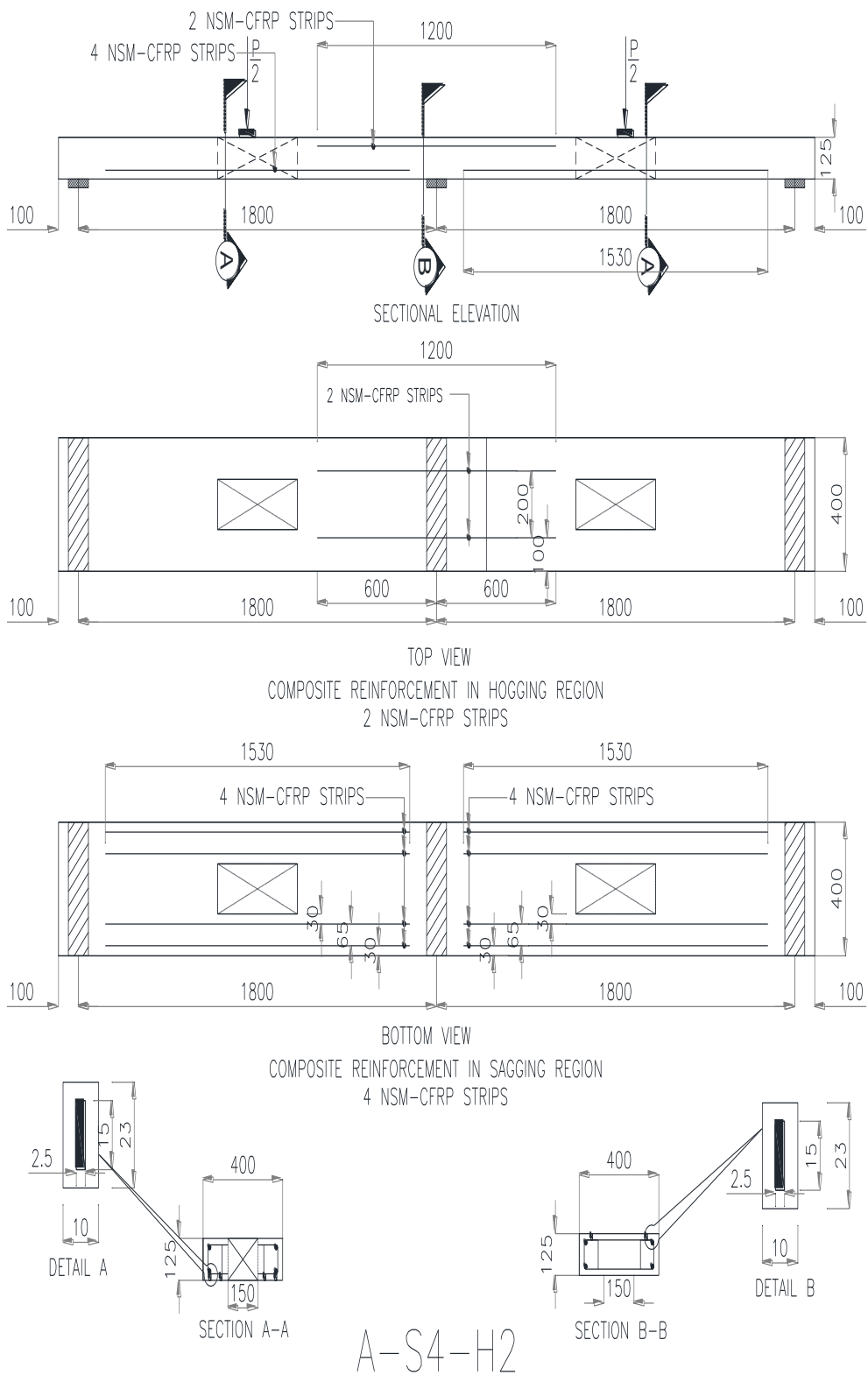
Figure 3.19: Strengthening regime for specimen A-S4-H2

1200

2 NSM-CFRP STRIPS

P/2   P/2

125

100   1800   1800   100

SECTIONAL ELEVATION

1200

2 NSM-CFRP STRIPS

62.50

275

400

62.50

100   1800   600   600   1800   100
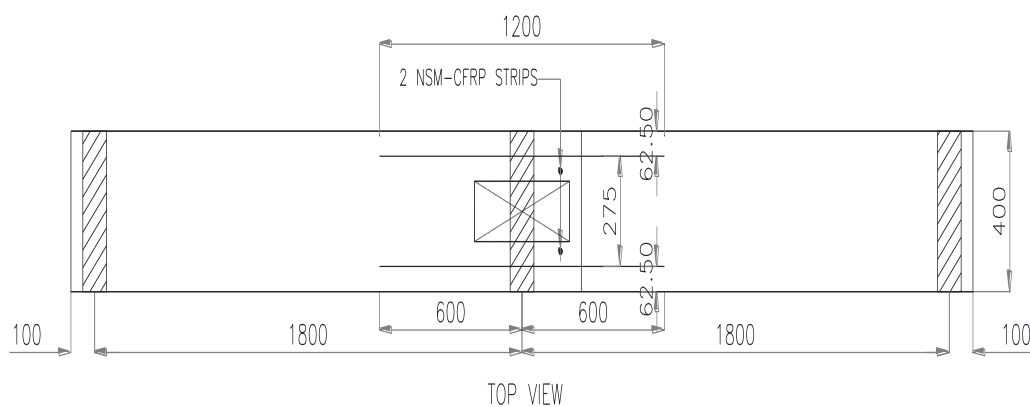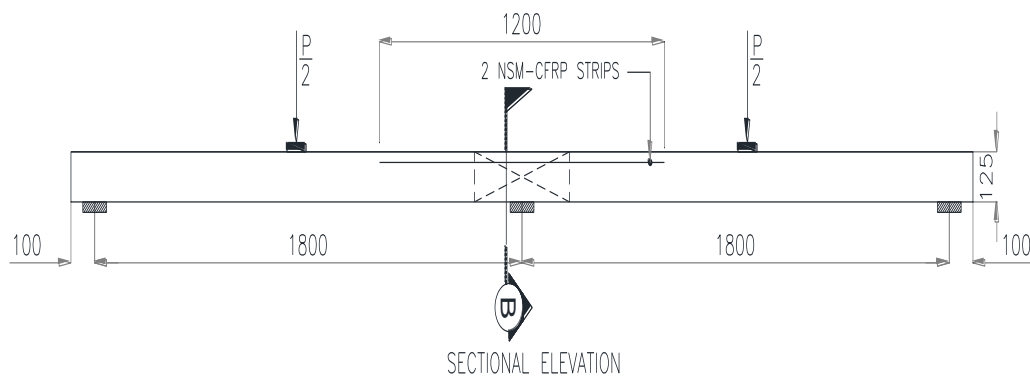
TOP VIEW
COMPOSITE REINFORCEMENT IN HOGGING REGION
2 NSM-CFRP STRIPS

400

23

15

2.5

125

10

150

DETAIL B

SECTION B-B
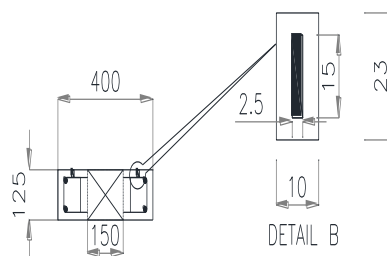
B-S0-H2

Figure 3.20: Strengthening regime for specimen B-S0-H2

1200

4 NSM-CFRP STRIPS

P/2   P/2

125

100   1800   1800   100

SECTIONAL ELEVATION

1200

4 NSM-CFRP STRIPS

30
65
30

400

100   1800   600   600   1800   100

TOP VIEW
COMPOSITE REINFORCEMENT IN HOGGING REGION
4 NSM-CFRP STRIPS

15
23

2.5

10

DETAIL B

400

125

150

SECTION B-B
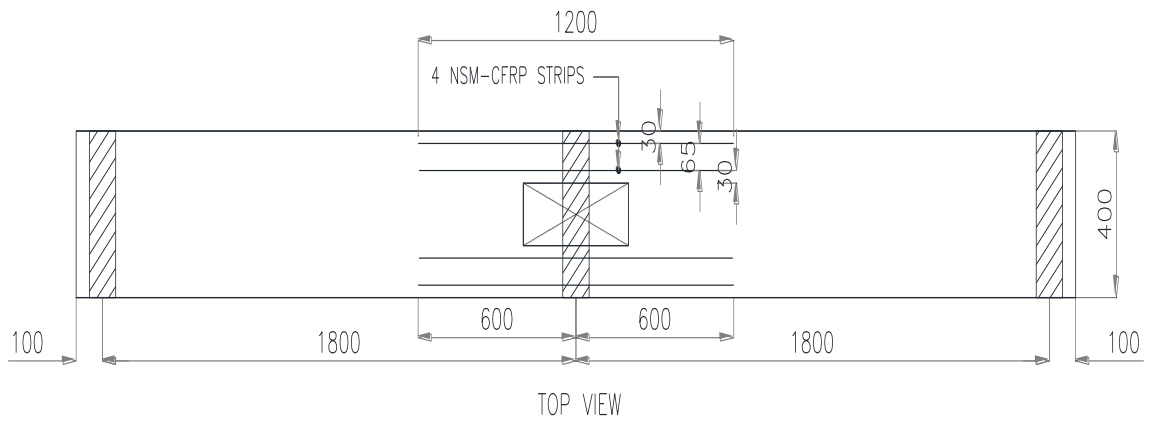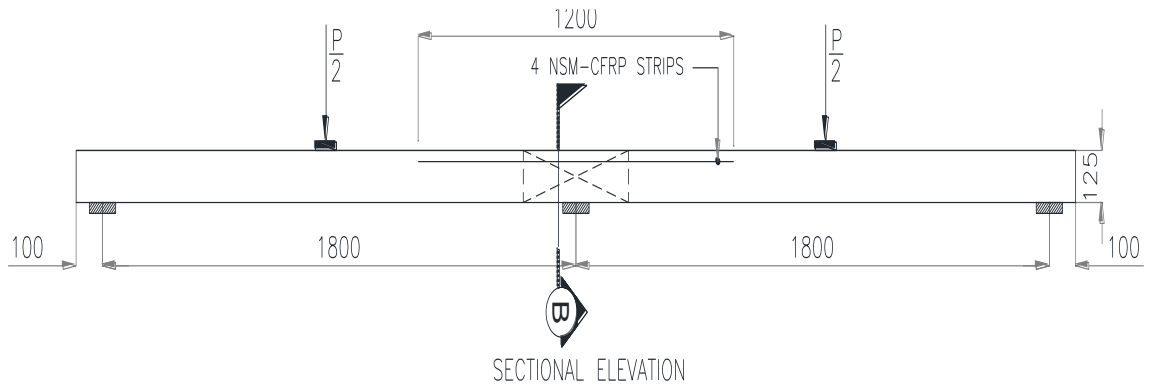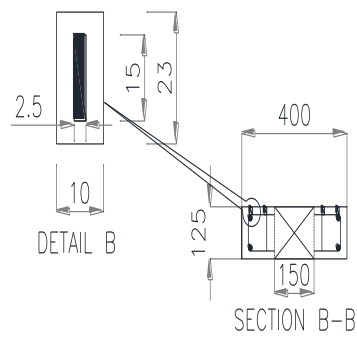
B-S0-H4

Figure 3.21: Strengthening regime for specimen B-S0-H4
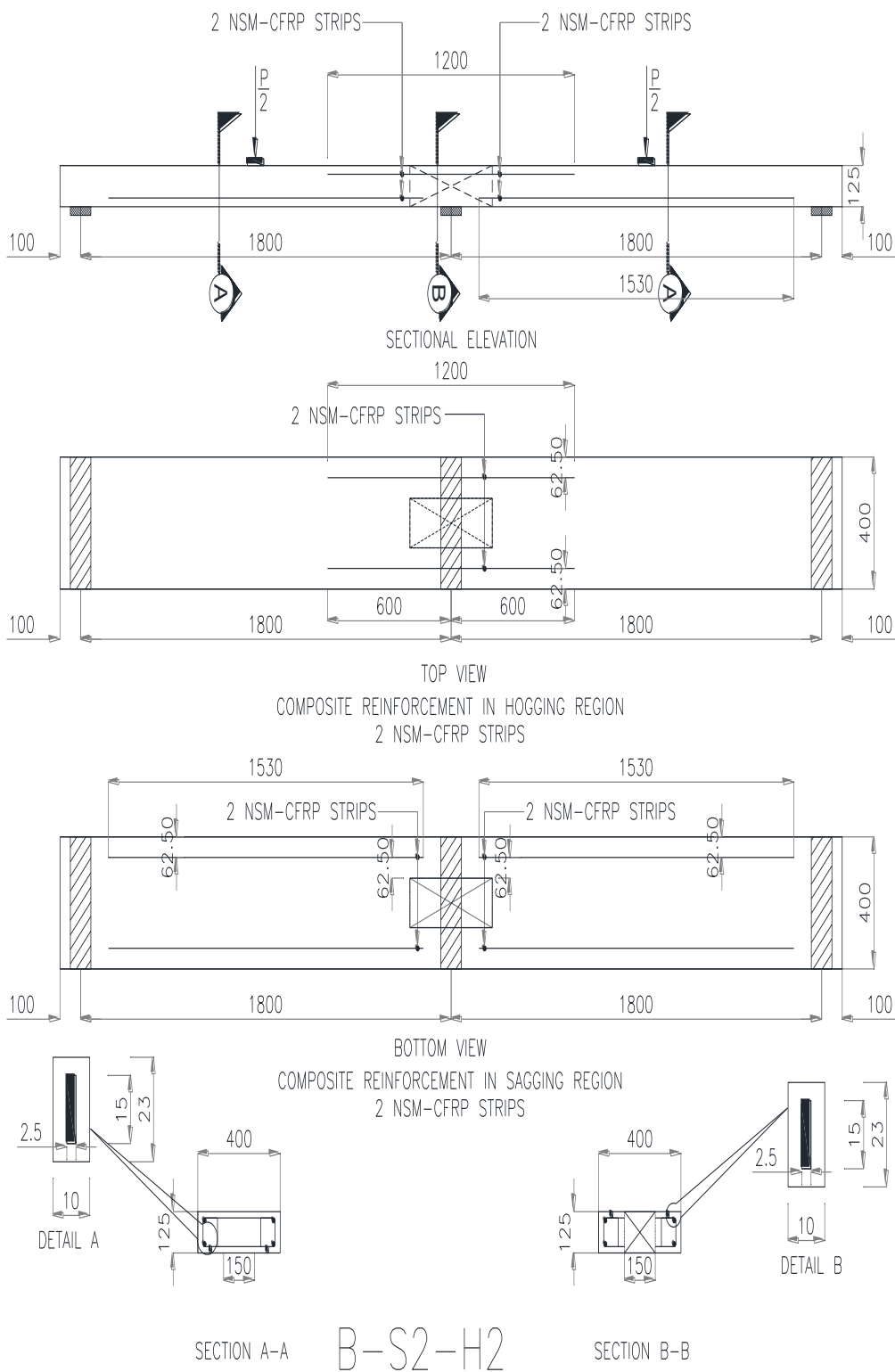
Figure 3.22: Strengthening regime for specimen B-S2-H2
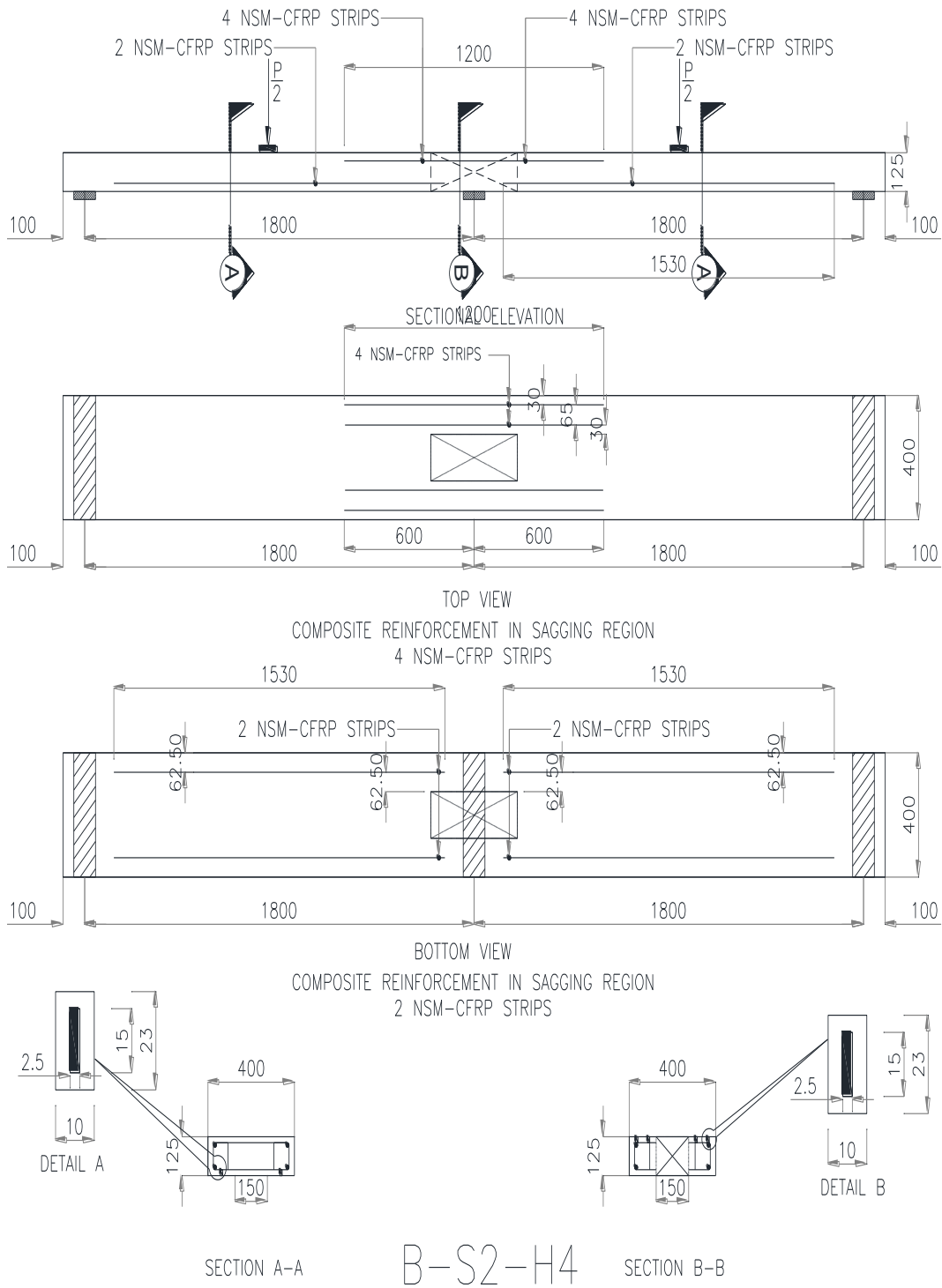
Figure 3.23: Strengthening regime for specimen B-S2-H4

(a) Cutting of CFRP strips

(b) Cutting of grooves

(c) Cleaning of grooves

(d) Installation of epoxy adhesive

(e) Installation of CFRP strips

(f) Finishing of concrete surface

Figure 3.24: Strengtheing procedure

3.7 Test Set-up and Instrumentation

The test specimens consisted of two equal spans, 1800 mm each. The specimens were tested in flexure under two point loads, one at the mid of each span. The specimens rested on three supports 1.8 m apart during testing.

3.7.1 Strain Measurements

Electrical resistance strain gauges (S.G.) with a gauge length of 5 mm and coefficient of thermal expansion of $11X10^{-6}$ /C^O and a gauge resistant of 120 Ω were bonded to the internal tensile steel reinforcement and external NSM-CFRP reinforcement at the mid-spans and over the middle support.

Strain gauges with a gauge length of 60 mm and coefficient of thermal expansion of $11X10^{-6}$ /C^O and a gauge resistant of 120 Ω were bonded to the concrete surface at the extreme compression fiber in the mid span sections and over the central support.

3.7.2 Displacement and Load Measurement

A schematic diagram showing the test set-up is given in Figure 3.25. The load was applied incrementally by means of a hydraulic jack located at the mid-point of the specimen. A spreader steel beam was used to spread the load equally into two point loads. Each point load is located at the middle of each span. In order to measure the mid-span deflections of the slab, one Linear Variable Differential Transformer (LVDT) was placed below the slab at the mid-point of each span. The total applied load was measured using a 500 kN load cell placed between the hydraulic jack and the steel spreader beam. The reaction of the middle support was measured using a 200 kN load cell placed between the slab soffit and the top surface of the middle support. A data acquisition system was used to record the data during testing. A photo of a test in progress is shown in Figure 3.26.
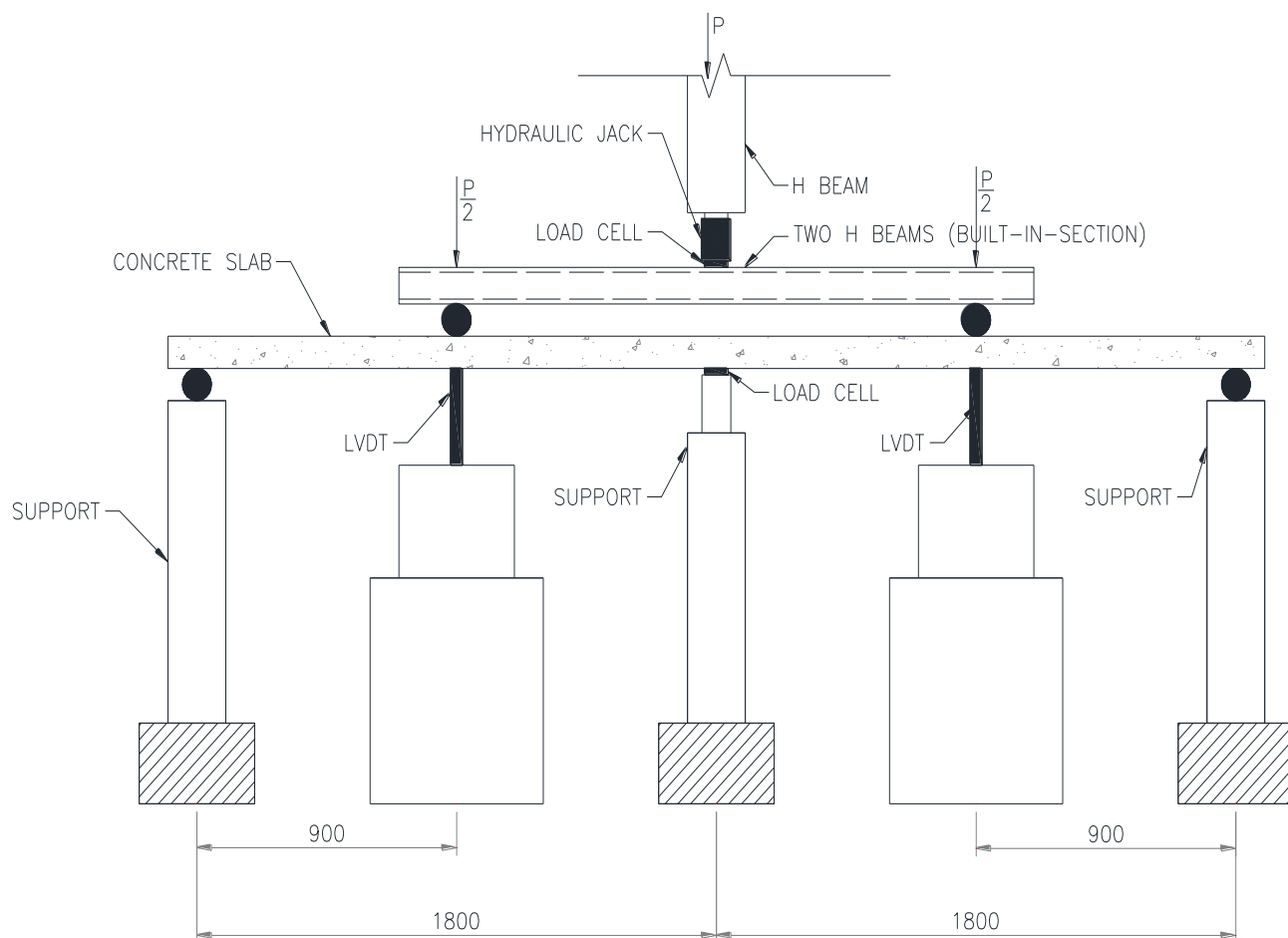
Figure 3.25: Schematic view of the test setup

Figure 3.26: A test in progress

CHAPTER 4: EXPERIMENTAL RESULTS

4.1 Introduction

The feasibility of flexural strengthening of continuous reinforced concrete (RC) slab strips using NSM-CFRP reinforcement has been investigated in this research work. Results of the experimental work are presented in this chapter. The results are presented in terms of load measurement, deflection response, tensile strain response, concrete strain response, CFRP strain response, support reactions, and load versus moment relationship.

4.2 Test Results

The results were collected during testing using a data acquisition system. The results were maintained in Excel sheet format where all the necessary graphs and figures were produced. Results of test specimens with cutouts, before and after strengthening were compared with those of the control specimen to evaluate the effectiveness of the NSM-CFRP strengthening system.

4.2.1 Group [A]

In this section, results of the five specimens of group [A] with a cutout in each sagging region are presented. Four specimens were strengthened with NSM-CFRP reinforcement in the sagging region, while one specimen was not strengthened. Results of specimens of this group are also compared to those of the control specimen that did not include a cutout and was not strengthened.

4.2.1.1 Load Capacity

Results of the load measurements for specimens of group [A] along with those of the control are summarized in Table 4.1. The symbols P_{cr}, P_y, and P_u refer to the cracking, yield, and ultimate loads, respectively. The ultimate load enhancement ratios (*LER*) for the strengthened specimens with respect to that of the unstrengthened specimen A-NS are given in the same table. The cracking and yielding load of the sagging and hogging regions were taken from the steel strain graphs. The cracking load was taken as the load where the first change in the slope of the tensile steel strain response took place. The yield load was taken as the load where the second change in the slope of the tensile steel strain response was acquired. The cracking and yield loads of some specimens were not reported due to malfunction of the corresponding steel strain gauges.

The control specimen exhibited flexural cracking in the west and east sagging regions at load values of approximately 14.6 kN and 27.1 kN, respectively. For the hogging region, flexural cracks initiated at a load value of approximately 29.8 kN. The tensile steel in the west and east sagging regions yielded almost at the same time at load values of approximately 83.4 kN and 94.3 kN, respectively. The tensile steel in the hogging region yielded at a load value of approximately 87.8 kN. The ultimate load of the control specimen was 116.9 kN.

Specimen A-NS with a cutout in the sagging regions without strengthening experienced flexural cracking in the west and east sagging regions at load values of approximately 5.9 kN and 11.4 kN, respectively. For the hogging region, flexural cracks initiated at a load value of approximately 7.5 kN. The tensile steel in the west and east sagging regions yielded almost at load values of approximately 54.5 kN and

64.4 kN, respectively. The tensile steel in the hogging region yielded at a load value of approximately 70.2 kN. The tensile steel in the sagging region yielded prior to the tensile steel in the hogging region, because of the presence of the cutout in the sagging regions, which reduced the amount of steel and reduced the concrete section size. The west and east sagging yield loads of specimen A-NS were 35% and 32% lower than those of the control specimen, respectively. The hogging yield load of specimen A-NS was 20% lower than that of the control specimen. Specimen A-NS achieved an ultimate load of 85.80 kN. The ultimate load of specimen A-NS was 27% lower than that of the control specimen.

Table 4.1: Results of load measurement for specimens of group [A]

Specimen	P_{cr} (kN)			P_y (kN)			P_u (kN)	LER^*
	Sagging		Hogging	Sagging		Hogging		
	West	East		West	East			
control	14.6	27.1	29.8	83.4	94.3	87.8	116.90	-
A-NS	5.9	11.4	7.5	54.5	64.4	70.2	85.80	1.00
A-S2-H0	10.9	-	36.7	97.5	-	98.3	131.02	1.53
A-S4-H0	8.4	8.5	32.2	133	120.3	105.3	151.12	1.76
A-S2-H2	18.2	18.2	30.5	94	104.2	121.6	140.00	1.63
A-S4-H2	17.6	32.5	30.8	143	115.4	136.6	155.00	1.81

[*]Load enhancement ratio with respect to that of specimen A-NS

Flexural cracks initiated in the west sagging region of specimen A-S2-H0 at a load value of approximately 10.9 kN whereas they were initiated in the hogging region at a load value of 36.7 kN. The cracking and yield loads of the east sagging region were not reported due to malfunction of the corresponding steel strain gauges.

The steel in the sagging and hogging regions yielded almost at the same time at a load value of approximately 98 kN. The yield load of specimen A-S2-H0 of the sagging regions was approximately 64% higher than that of specimen A-NS whereas a 40% increase in the yield load was recorded in the hogging region. Specimen A-S2-H0 experienced a load enhancement ratio of 53% relative to the ultimate load of specimen A-NS. The load capacity of specimen A-S2-H0 was even higher than that of the control specimen by approximately 12%.

Specimen A-S4-H0 with four NSM-CFRP strips in each sagging region experienced flexural crack in the sagging and hogging regions at load values of approximately 8.45 kN and 32.2 kN, respectively. Yielding of steel in the hogging region occurred first at a load value of approximately 105.3 kN followed by yielding of steel in the west and east sagging regions at load values of approximately 133 kN and 120.3 kN, respectively. This occurred because of the high amount of NSM-CFRP reinforcement (four NSM-CFRP strips) installed in the sagging region. The yield loads of specimen A-S4-H0 recorded in the west and east sagging regions were 144 % and 87 %, higher than those of specimen A-NS, respectively. For the hogging region, a 50% enhancement in yield load was recorded compared to that of specimen A-NS. The load capacity of specimen A-S4-H0 was 76% higher than that of specimen A-NS and 30% higher than that of the control specimen.

Flexural cracks initiated in the sagging regions of specimen A-S2-H2 at a load value of approximately 18.2 kN. For the hogging region, the flexural cracks initiated at a load value of approximately 30.5 kN. Specimen A-S2-H2 exhibited west and east sagging yield loads of 94 kN and 104.2 kN, respectively. The average sagging yield load of specimen A-S2-H2 was almost the same as that of specimen A-S2-H0. The hogging yield load of specimens A-S2-H2 was, however, higher than

that of specimen A-S2-H0 by approximately 24%. This indicates that the addition of NSM-CFRP reinforcement in the hogging region had no effect on the sagging yield load, but slightly increased the hogging yield load. The ultimate load of specimen A-S2-H2 was 63% higher than that of specimen A-NS and only 7% higher than that of specimen A-S2-H0.

Specimen A-S4-H2 experienced flexural cracks in the west and east sagging regions at load values of approximately 17.6 kN and 32.5 kN, respectively. For the hogging region, flexural cracks initiated at a load value of approximately 30.8 kN. The tensile steel in the west and east sagging regions yielded at load values of approximately 143 kN and 115.4 kN, respectively. The average sagging yield load of specimen A-S4-H2 was almost the same as that of specimen A-S4-H0. This confirms that installation of NSM-CFRP reinforcement in the hogging region had no effect on the sagging yield load. For the hogging region, the tensile steel yielded at a load value of 136.6 kN. The hogging yield load of specimen A-S4-H2 was approximately 30% higher than that of specimen A-S4-H0. The ultimate load of specimen A-S4-H2 was insignificantly higher than that of specimen A-S4-H0, 81% higher than that of specimen A-NS, and 33% higher than that of the control specimen.

4.2.1.2 Failure Mode

The control specimen failed in a flexural mode of failure. The tensile steel in the sagging and hogging regions yielded almost at the same time. Following the yielding of tensile steel, crushing of concrete occurred at the top face of the specimen in the mid-span section and at the bottom face over the middle support. Photos of the control specimen at failure are shown in Figure 4.1.

Specimen A-NS failed in a flexural mode of failure. The tensile steel yielded first in the sagging region then in the hogging region. Following yielding of tensile steel, crushing of concrete occurred at the top face of the specimen in the mid-span section then at the bottom face over the middle support. Photos of specimen A-NS at failure are shown in Figure 4.2.

Failure of mid-span section
(sagging region)
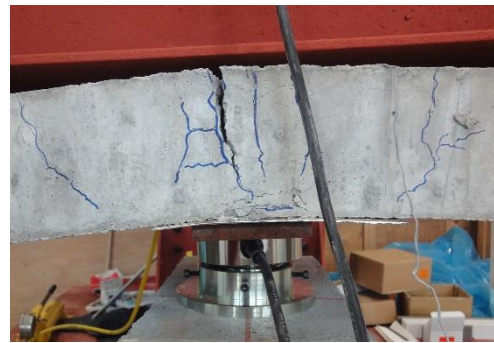
Failure of section over central support
(hogging region)

Figure 4.1: Photos of the control specimen at failure

Failure of mid-span section
(sagging region)

Failure of section over central support
(hogging region)

Figure 4.2: Photos of specimen A-NS at failure

Failure of specimen A-S2-H0 initiated by formation of flexural cracks in both sagging and hogging regions. As the load progressed, yielding of tensile steel occurred in both sagging and hogging regions almost at the same time. Following yielding of tensile steel, crushing of concrete occurred at the top face of the specimen in the mid-span section. A shear crack developed in the mid-span section at the onset of concrete crushing. This shear crack occurred due to the weakness of the concrete section in the sagging region caused by the cutout. A photo of specimen A-S2-H0 at failure is shown in Figure 4.3.

Specimen A-S4-H0 failed in a flexural mode of failure. The tensile steel yielded first in the hogging region then in the sagging region. Following yielding of tensile steel, crushing of concrete occurred at the top face of the specimen in the mid-span section and at the bottom face over the middle support. No shear cracks were developed at the onset of concrete crushing. This can be attributed to the high amount of longitudinal NSM-CFRP reinforcement used around the cutout in each sagging region, which may have improved the shear resistance by the dowel action, and hence, kept the concrete section intact at failure. More research is needed to investigate the effect of longitudinal NSM-CFRP reinforcement on the shear resistance of concrete. Photos of specimen A-S4-H0 at failure are shown in Figure 4.4.

Specimen A-S2-H2 failed in a flexural mode of failure. The tensile steel yielded first in the sagging region then in the hogging region. Following yielding of tensile steel, crushing of concrete occurred at the top face of the specimen in the mid-span section then at the bottom face over the middle support. Photos of specimen A-S2-H2 at failure are shown in Figure 4.5.

Figure 4.3: Photo of specimen A-S2-H0 at failure

Failure of mid-span section
(sagging region)

Failure of section over central support
(hogging region)

Figure 4.4: Photos of specimen A-S4-H0 at failure

Failure of mid-span section
(sagging region)

Failure of section over central support
(hogging region)

Figure 4.5: Photos of specimen A-S2-H2 at failure

Failure of specimen A-S4-H2 initiated by formation of flexural cracks in both sagging and hogging regions then yielding of tensile steel. The tensile steel yielded in the hogging region at a load value of 136.6 kN. The last yielding occurred in the west sagging region at a load value of 143 kN. Following yielding of tensile steel, crushing of concrete occurred at the top face of the specimen in the mid-span sections. A shear crack developed in the west mid-span section at the onset of concrete crushing due to the weakness caused by the cutout. A photo of specimen A-S4-H2 at failure is shown in Figure 4.6.

Figure 4.6: Photo of specimen A-S4-H2 at failure

4.2.1.3 Load Deflection Response

The load-deflection response of the control specimen is shown in Figure 4.7. The load-deflection response of specimens of group [A] are depicted in Figures 4.8 to 4.12. From Figure 4.7, it can be seen that the east and west spans of the control specimen featured a very similar deflection response. Both spans exhibited a linear deflection response until initiation of flexural cracks. In the post-cracking stage, the deflection increased at a higher rate after initiation of cracks until yielding of tensile steel took place in the sagging and hogging region concurrently. Following yielding of steel, the deflection continued to increase at a higher rate until the specimen reached its peak load at an average mid-span deflection value of approximately 26.4

mm. Then, the specimen featured a plastic deflection response until failure as shown in Figure 4.7.

For specimen A-NS, both spans experienced a very similar deflection response. A linear response was maintained up to an average mid-span deflection of approximately 1.2 mm. Then, the specimen exhibited a quasi-linear deflection response until first yielding took place in the sagging region at an average deflection of 7.5 mm. The second (last) yielding occurred in the hogging region at an average mid-span deflection of approximately 10 mm. Following last yielding, the deflection continued to increase but at a higher rate until the specimen reached its peak load of 85.80 kN at corresponding east and west span deflections of 19.9 mm and 24.4 mm, respectively as shown in Figure 4.8
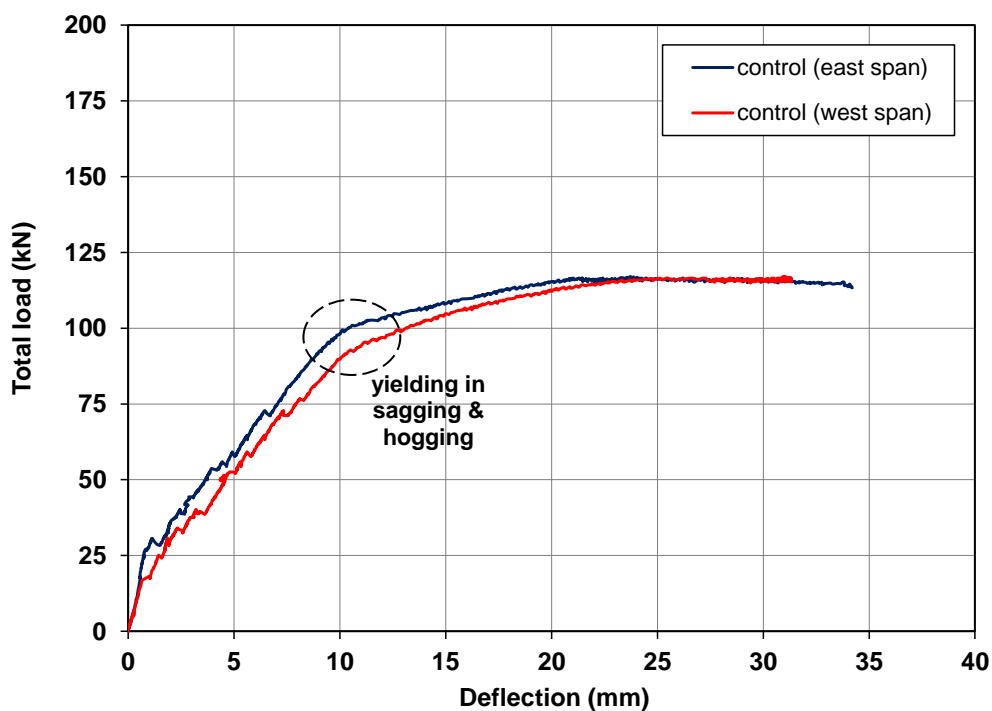
Figure 4.7: Load-deflection response of the control specimen
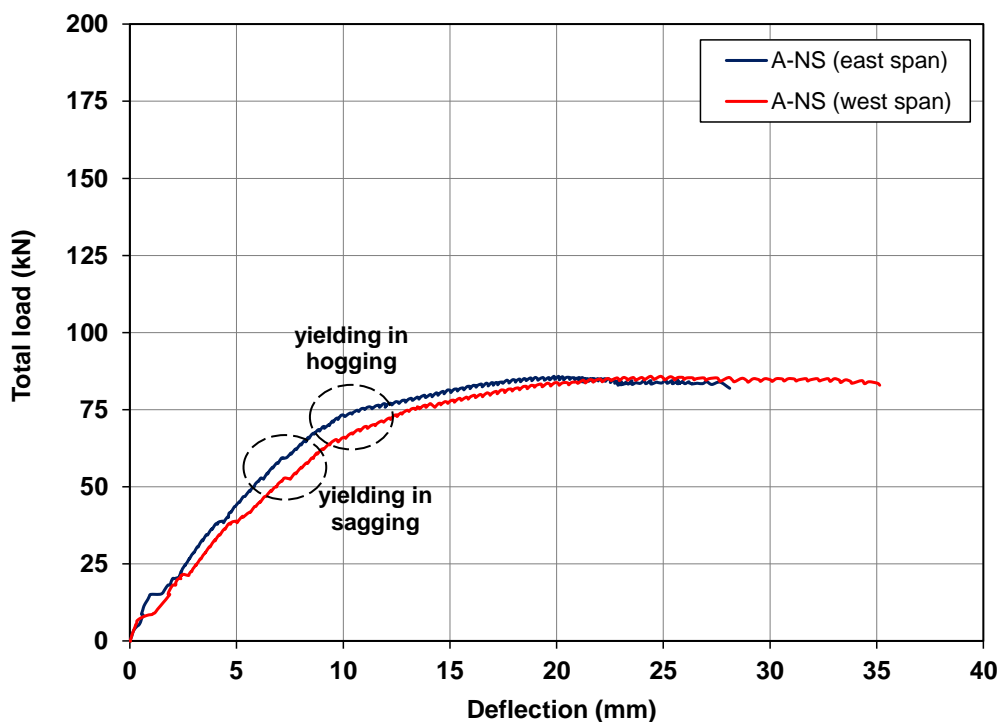
Figure 4.8: Load-deflection response of specimen A-NS

Specimen A-S2-H0 featured a linear deflection response in both spans until initiation of cracks at a deflection value of approximately 2 mm where the first deviation from linearity took place. Following cracking, the specimen experienced a quasi-linear deflection response until yielding of tensile steel took place in the sagging and hogging regions concurrently at an average deflection of approximately 11 mm. Following yielding, the deflection continued to increase but at a higher rate until the specimen reached its peak load of 131.02 kN at corresponding east and west span deflections of 22.21 mm and 24.40 mm, respectively as shown in Figure 4.9.
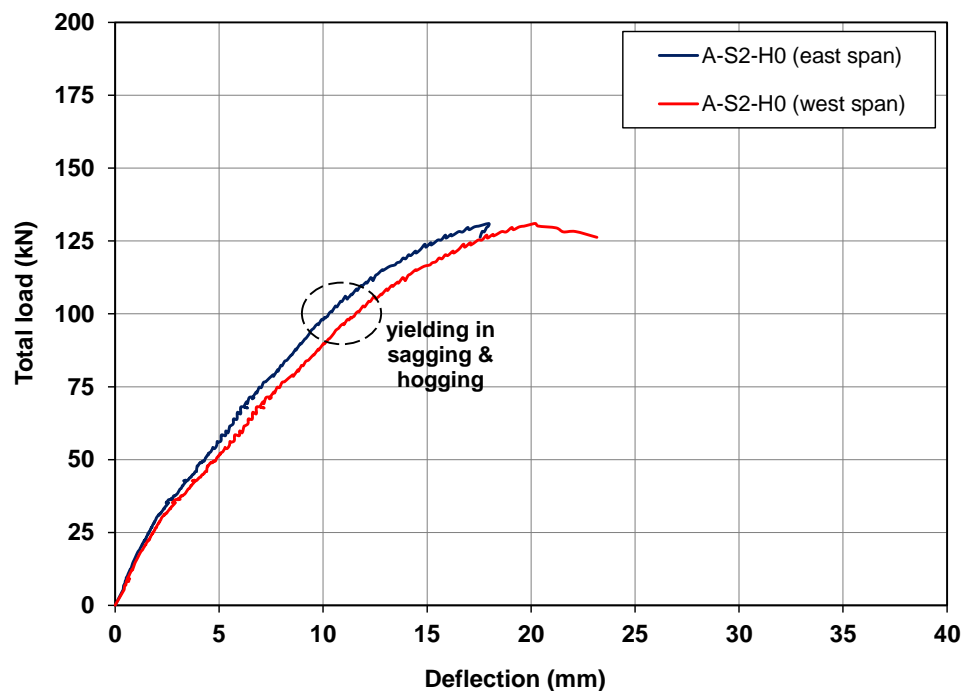
Figure 4.9: Load-deflection response of specimen A-S2-H0

Specimen A-S4-H0 exhibited a linear deflection response up to an average deflection of approximately 1.5 mm where first change in slope took place due to cracking. In the second stage, the deflection continued to increase but at a higher rate until first yielding took place in the hogging region at an average deflection of approximately 9.3 mm. Following first yielding, the deflection increased rapidly until the specimen reached its last yielding in the sagging region at east and west deflections of 14.8 mm and 18.5 mm, respectively. In the last stage, the mid-span deflection of the west span experienced a plastic response until a peak load of 151.13 kN was achieved, shortly after the last yielding, at a deflection of 21.41 mm as shown in Figure 4.10.

For specimen A-S2-H2, the linear deflection response was maintained up to an average mid-span deflection of approximately 1.5 mm. Then, the deflection increased at a higher rate until first yielding of steel took place in the sagging region

at east and west mid-span deflections of 7.4 mm and 10 mm, respectively. Following first yielding, the deflection further increased at a higher rate until second yielding occurred in the hogging region at east and west deflections of 12.4 mm and 18.1 mm, respectively. In the last stage, the deflection in the west span exhibited an almost plastic response until the specimen reached its peak load of 153.37 kN at a mid-span deflection of 23.53 mm in the west span as shown in Figure 4.11.

For specimen A-S4-H2, the deviation from linearity started at east and west deflections of 1.3 mm and 1 mm, respectively due to flexural cracking. In the post-cracking stage, the deflection increased almost linearly up to east and west deflections of 11.5 mm and 13.8 mm, respectively, where first yielding of steel took place in hogging region. Then, the deflection continued to increase until last yielding of steel took place in the sagging region at west span deflection of 17.5 mm. Following yielding of steel in the sagging region, the specimen failed shortly at a peak load of 155 kN and a corresponding west span deflection of 18.8 mm as shown in Figure 4.12.
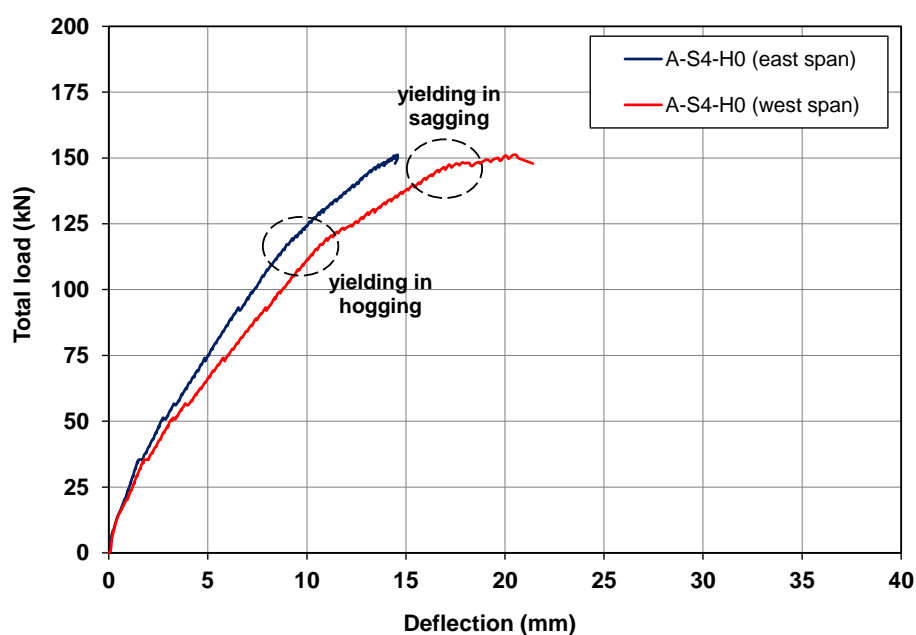
Figure 4.10: Load-deflection response of specimen A-S4-H0
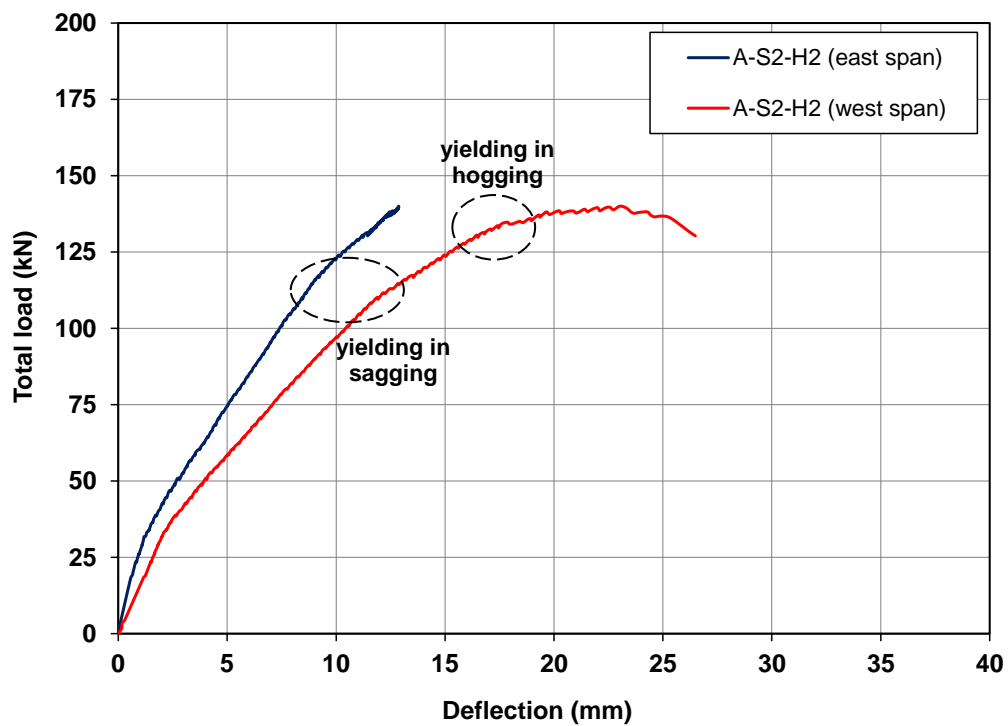
Figure 4.11: Load-deflection response of specimen A-S2-H2
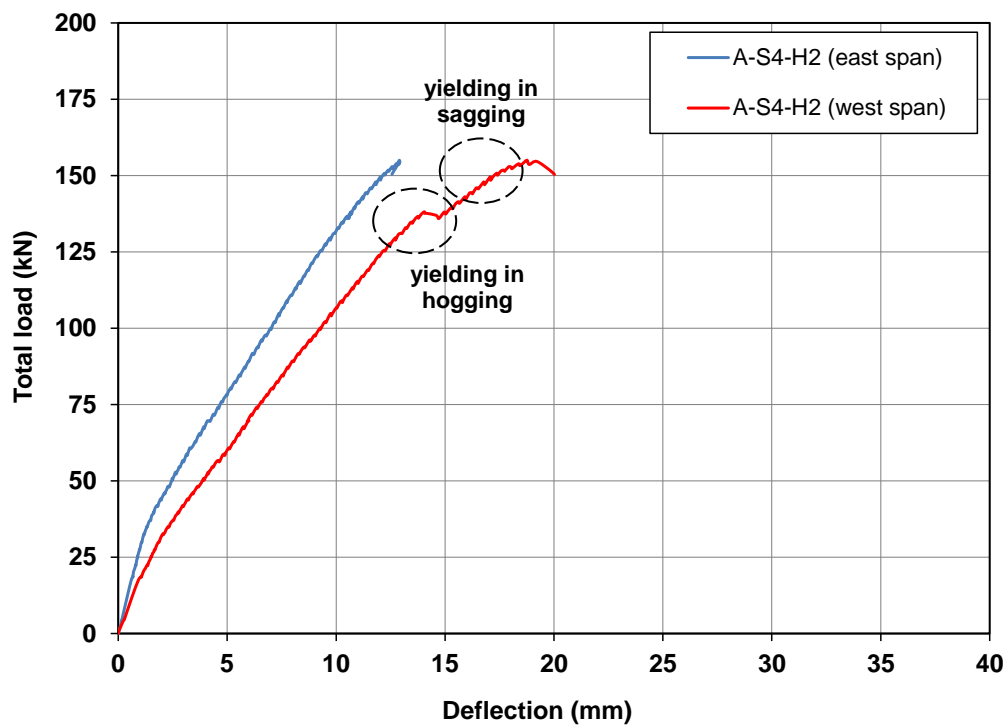
Figure 4.12: Load-deflection response of specimen A-S4-H2

Figure 4.13 compares the deflection response of all specimens of group [A] with a cutout in the sagging region. The deflection of the control specimen is included in the same figure for the purpose of comparison. The response of only one of the two spans that had the greatest deflections was plotted in Figure 4.13 for clarity. From this figure, it is evident that installation of a cutout in the sagging region compromised the stiffness and load capacity of specimen A-NS relative to that of the control. For instance at 50 kN, the deflection of the control specimen was 3.6 mm whereas for specimen A-NS it was 5.8 mm. The deflection at peak load for specimen A-NS was insignificantly lower than that of the control specimen. Flexural strengthening with NSM-CFRP system significantly improved the stiffness and load capacity of the specimens with cutout. The stiffness of specimens A-S2-H0 and A-S2-H2 was almost the same as that of the control whereas specimens A-S4-H0 and A-S4-H2 had higher stiffness than that of the control. The deflection capacity of the strengthened specimens was lower than that of the control.
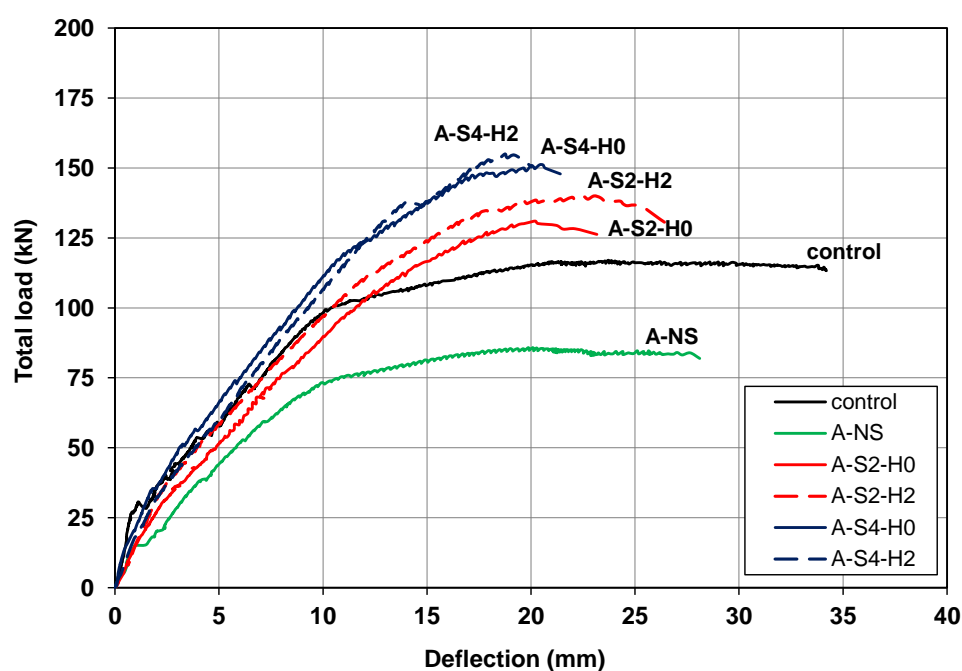
Figure 4.13: Load-deflection response for specimens of group [A]

4.2.1.4 Ductility Index

Ductility is an important aspect in RC structures. When RC structures are strengthened with composites, the ductility could be compromised. Also, the moment redistribution in continuous RC structures is majorly controlled by the ductility ratio of the structure (Liu et al. 2006). The ductility index given in Equation 4.1 is defined as the ratio of the mid-span deflection at peak load to the mid-span deflection at first yielding (second change in slope of the load-deflection response). The deflection values used to calculate the ductility index were taken from Figure 4.13. Table 4.2 gives the ductility indices for specimens of group [A] along with that of the control specimen.

$$\mu = \frac{\Delta_p}{\Delta_{y1}} \tag{4.1}$$

Where:

μ = ductility index

Δ_p = mid-span deflection at peak load

Δ_{y1} = mid-span deflection at second change of load-deflection response (first yielding)

Table 4.2: Ductility indices for specimens of group [A]

Specimen	Δ_{y1} (mm)	Δ_p (mm)	μ
control	10.5	23.8	2.27
A-NS	10.0	20.0	2.00
A-S2-H0	10.5	20.3	1.93
A-S4-H0	11.0	20.6	1.87
A-S2-H2	12.0	23.0	1.91
A-S4-H2	14.0	18.8	1.28

The ductility index of the control specimen was 2.27. The unstrengthened specimen A-NS with a cutout in the sagging region had a ductility index of 2. This indicates that installation of a cutout in the sagging region resulted in slight reduction of 12% in ductility index. The ductility index of all strengthened specimens, except A-S4-H2, was approximately 1.9. This value was 5% lower than that of specimen A-NS and 16% lower than that of the control. Specimen A-S4-H2 that was heavily strengthened with four NSM-CFRP strips in the sagging region and two NSM-CFRP strips in the hogging region was approximately 36% lower than that of specimen A-NS and 44% lower than that of the control specimen. The ductility index of strengthened specimens tended to decrease as the amount of NSM-CFRP reinforcement increased.

4.2.1.5 Tensile Steel Strain Response

The tensile steel strain responses of specimens of group [A] along with those of the control specimen are depicted in Figure 4.14. The steel strain response in the west and east sagging regions was similar, and hence only one of them is shown in Figure 4.14 for clarity. The tensile steel strain response featured three phases. Initially, the steel was not strained until initiation of flexural cracks. Then, the steel strain increased gradually until yielding of tensile steel. In the last stage, the tensile steel increased rapidly or exhibited a strain plateau till failure. Generally, the NSM-CFRP reinforcement decreased the rate of increase of the tensile steel strain relative to that of specimen A-NS. The steel strain in a specific region typically decreased by increasing the amount of the NSM-CFRP reinforcement in the corresponding region.

The control specimen featured a sudden increase in steel strain in the sagging region at the onset of cracking. Flexural cracking occurred first in the sagging region

then in the hogging region. Initiation of cracks in the hogging region was accompanied by a change in slope of the steel strain response. Following cracking, the steel strain in the sagging and hogging regions continued to increase as the load progressed. The steel in the hogging region yielded shortly after yielding of steel in the sagging region. Following yielding of steel, the specimen featured a plastic steel strain response in both sagging and hogging regions.

The unstrengthened specimen A-NS exhibited flexural cracks in the sagging region first then in the hogging region. Initiation of flexural cracks was accompanied by a sudden increase in steel strain in the sagging region and a change in slope of the curve in the hogging region. Following cracking, the steel strain in the sagging and hogging regions continued to increase as the load progressed at a rate higher than that of the control specimen. The steel in the sagging region yielded earlier than the steel in the hogging region. This occurred because specimen A-NS had a cutout in the sagging region without strengthening which significantly reduced the concrete section size and amount of internal steel reinforcement in the sagging region. Following yielding of steel, the specimen featured a strain plateau in both sagging and hogging regions.

Specimen A-S2-H0 experienced flexural cracks in the sagging and hogging regions at load values higher than those of specimen A-NS. In the post cracking stage, the tensile steel in both sagging and hogging regions exhibited similar strains, and hence they yielded simultaneously at a load value of approximately 98 kN. Following yielding, the tensile steel in both regions exhibited a plastic response.

Specimen A-S2-H2 exhibited a sagging steel strain response similar to that of specimens A-S2-H0 because both specimens were strengthened with two NSM-CFRP strips in the sagging region. On the contrary, specimen A-S2-H2 exhibited

lower strains in the hogging region relative to those of specimen A-S2-H0. This occurred because specimen A-S2-H2 had two NSM-CFRP strips in the hogging region but specimen A-S2-H0 had no NSM-CFRP reinforcement in the hogging region. Consequently, the hogging yield load for specimen A-S2-H2 was slightly higher than that of specimen A-S2-H0. It should be noted that the tensile steel in the sagging region of specimen A-S2-H2 yield earlier than the tensile steel in the hogging region.

Specimen A-S4-H0 experienced flexural cracks in the sagging and hogging regions at load values higher than those of specimen A-NR. Following cracking, the tensile steel in the hogging region experienced higher strains than the tensile steel in the sagging region. As a result, the steel in the hogging region yielded earlier than the steel in the sagging region. Following yielding, the tensile steel exhibited a plastic response in the hogging region whereas in the sagging region the tensile steel strain continued to increase but at a higher rate till failure. The sagging yield load of specimen A-S4-H0 with four NSM-CFRP strips in the sagging region was higher than that of its counterpart A-S2-H0 with two NSM-CFRP strips in the sagging region. On the contrary, the hogging yield load of both specimens was insignificantly different because both specimens, A-S2-H0 and A-S4-H0, were not strengthened in the hogging region.

Specimen A-S4-H2 experienced a tensile steel response in the sagging region similar to that of specimen A-S4-H0 because both specimens had the same concrete geometry, same amount of internal steel and NSM-CFRP reinforcement in the sagging region. The tensile steel of specimen A-S4-H2 in the sagging region yielded, however, at a load value slightly higher than that of specimen A-S4-H0 possibly due to moment redistribution. In the hogging region, specimen A-S4-H2 experienced a

lower rate of increase of tensile steel strain than that of specimen A-S4-H0. As a result, the yield load of specimen A-S4-H2 in the hogging region was significantly higher than that of specimen A-S4-H0. This occurred because specimen A-S4-H2 was strengthened by two NSM-CFRP strips in the hogging region whereas specimen A-S4-H0 had no NSM-CFRP reinforcement in the hogging region. The tensile steel of specimen A-S4-H2 in the sagging region yielded shortly after yielding of steel in the hogging region. Following yielding, the steel strain continued to increase but at a higher rate in both sagging and hogging regions until failure.
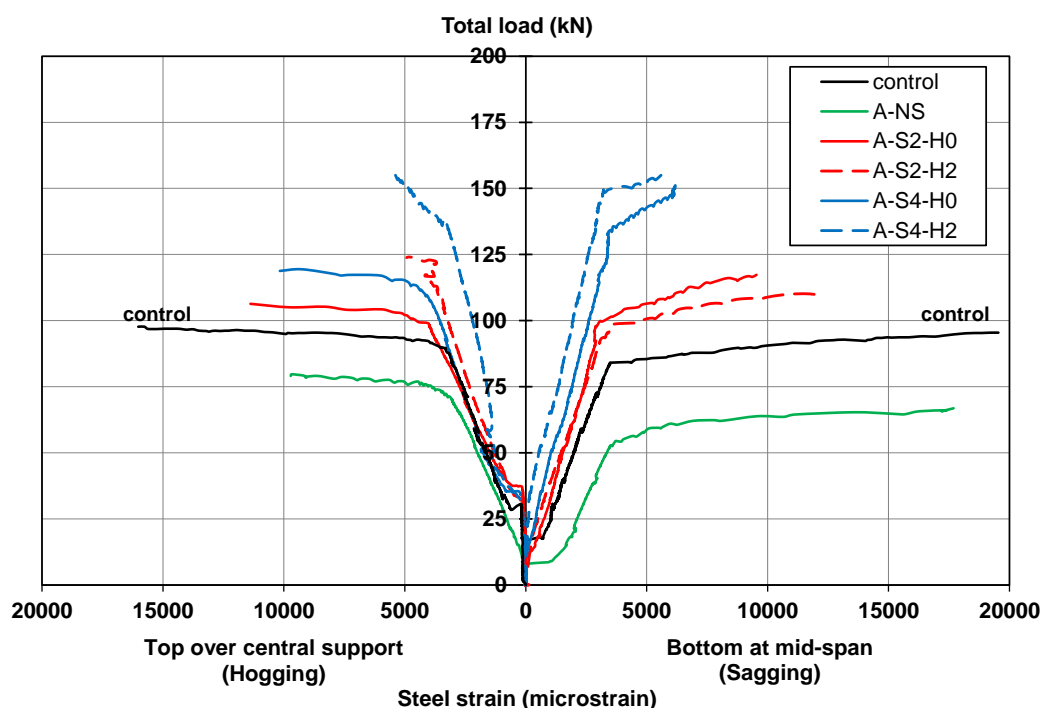
Figure 4.14: Tensile steel strain response for specimens of group [A]

4.2.1.6 CFRP Strain Response

The CFRP strain responses of specimens of group [A] along with that of the control are shown in Figure 4.15. The CFRP strains were not recorded in some specimens due to malfunction of the strain gauge. The specimens exhibited no or minimal CFRP strains prior to flexural cracking. The CFRP strain increased

gradually in the post-cracking stage as the load progressed. The CFRP strain increased at a higher rate after yielding of the tensile steel reinforcement. Specimens A-S2-H0 and A-S2-H2 featured similar FRP strain response in the sagging region because both of them had the amount of NSM-CFRP reinforcement in the sagging region. Similarly, specimens A-S4-H0 and A-S4-H2 featured similar FRP strain response in the sagging region. Increasing the amount of NSM-CFRP reinforcement in the sagging region decreased the rate of increase of the CFRP strains in the corresponding region, and hence specimens A-S4-H0 and A-S4-H2 exhibited lower CFRP strains than specimens A-S2-H0 and A-S2-H2. The reduced rate of CFRP strain in specimens A-S4-H0 and A-S4-H2 with four NSM-CFRP strips in the sagging region delayed yielding of tensile steel and hence increased their load capacity to a level higher than that of specimens A-S2-H0 and A-S2-H2 with two NSM-CFRP strips in the sagging region. It should be noted that the CFRP strain at peak load decreased as the amount of the NSM-CFRP reinforcement increased.
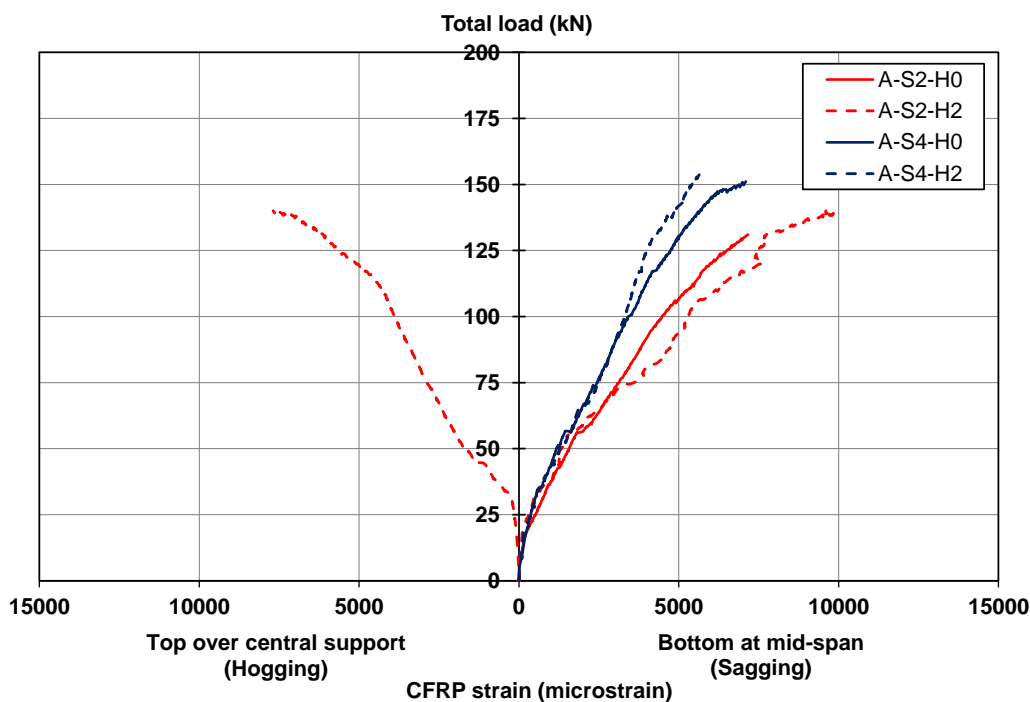
Figure 4.15: CFRP strain response for specimens of group [A]

Specimens A-S2-H0, A-S4-H0, A-S2-H2, and A-S4-H2 reached their peak loads at sagging CFRP strain values of approximately 7167, 7098, 9596, and 5716 microstrain, respectively. The ratios of the CFRP strain at peak load to the rupture CFRP strain for specimens of group [A] are given in Table 4.3. In this table $\varepsilon_{f,max}$ refers to the CFRP strain at peak load whereas ε_{fr} refers to the rupture CFRP strain. The ratios of CFRP strain at peak load to the rupture CFRP strain were 38%, 37%, 51%, and 30% for specimens A-S2-H0, A-S4-H0, A-S2-H2, and A-S4-H2, respectively. The CFRP strain at peak load in the hogging region for specimen A-S2-H2 was 7689 microstrain, which corresponded to approximately 41% of the CFRP rupture strain provided by the manufacturer.

Table 4.3: Ratio of CFRP strain at peak load to rupture CFRP strain (group [A])

Specimen	$(\varepsilon_{f,max})$ CFRP strain at peak load (microstrain)		$(\varepsilon_{f,max} / \varepsilon_{fr})$ (%)	
	Sagging	Hogging	Sagging	Hogging
A-S2-H0	7167	-	38	-
A-S4-H0	7098	-	37	-
A-S2-H2	9596	7689	51	41
A-S4-H2	5716	-	30	-

4.2.1.7 Concrete Strain Response

The concrete strain responses of specimens of group [A] along with that of the control are shown in Figure 4.16. The concrete strains were not recorded in some specimens due to malfunction of the strain gauge. The concrete strain in both sagging and hogging regions featured a tri-linear response as shown in Figure 4.16. Prior to cracking, the concrete experienced minimal concrete strain. Following cracking, the concrete strain increased gradually until yielding of tensile steel. In the final stage,

the concrete strain continued to increase at a higher rate. Generally, the strengthened specimens exhibited lower rate of concrete strain than that of the unstrengthened specimen A-NS.

The concrete strain in the sagging region of specimen A-NS increased at a higher rate than that of the hogging region. The concrete strain in the sagging and hogging regions at yielding was approximately 1400 and 1100 microstrains, respectively. Specimen A-NS reached its peak load at concrete strain values of approximately 3000 and 2300 microstrains in the sagging and hogging regions, respectively.

Flexural strengthening significantly reduced the rate of increase of concrete strain relative to that of specimen A-NS. Specimen A-S2-H2 with two NSM-CFRP strips in the sagging region exhibited higher concrete strains in the sagging region than those of their counterpart specimen A-S4-H2 with four NSM-CFRP strips in the sagging region. The concrete strain response in the hogging region of specimens A-S2-H2 and A-S4-H2 were insignificantly different because both specimens had two NSM-CFRP strips in the hogging region.

It should be noted that due to the presence of the load and support plates, the concrete strain gauges were not placed on the top surface of the specimen at the mid-spans or at the bottom surface over the middle support. The concrete strain gauges were placed on the concrete lateral faces slightly away from the extreme compression fibers. This explains why some concrete strain values at peak load were lower than the concrete crushing strain value of 3000 microstrain specified by the ACI 318-08.
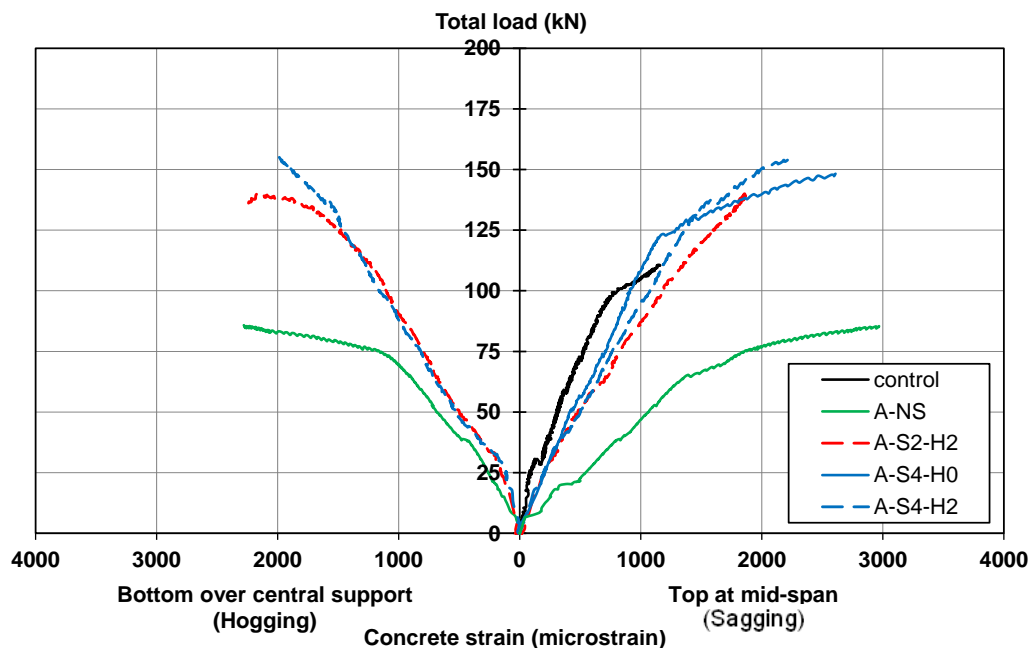
Figure 4.16: Concrete strain response for specimens of group [A]

For specimen A-S2-H2, yielding of tensile steel in the sagging and hogging regions occurred at an average concrete strain value of approximately 1500 microstrain. The specimen reached its peak load at concrete strain values of 2000 and 2150 microstrains in the sagging and hogging regions, respectively.

Specimens A-S4-H0 and A-S4-H2 featured similar concrete strain response in the sagging region because both of them were strengthened with four NSM-CFRP strips in the sagging region. Specimens A-S4-H0 experienced yielding of steel in the sagging region at a concrete strain of approximately 1275 microstrain. A maximum concrete strain of 2600 microstrain was recorded in the sagging region of specimen A-S4-H0 just prior to failure.

Specimen A-S4-H2 experienced similar rate of increase in the concrete strain in both sagging and hogging regions, and hence yielding of tensile steel in both sagging and hogging regions occurred almost at the same time at a concrete strain

value of approximately 1500 microstrain. Concrete strain values of approximately 2250 and 2000 were recorded in the sagging and hogging regions, respectively at the onset of failure of specimen A-S4-H2.

4.2.1.8 Support Reactions

The middle support reaction was measured during testing by means of a load cell. The end support reaction from the experiment was calculated from equilibrium of forces. The support reactions from the experiment are compared to the elastic reactions in Figure 4.17. The elastic reactions were calculated using structural analysis assuming that the slab specimens had uniform stiffness along the two spans. From this figure, it can be seen that the middle and end support reactions of the control specimen was similar to the elastic reactions. This occurred because the sagging and hogging regions had same concrete geometry and amount of steel reinforcement, which resulted in an almost uniform flexural rigidity in both sagging and hogging regions. The reactions of specimen A-NS with a cutout in the sagging region deviated from the elastic reactions. The middle support reactions were higher than the elastic reactions whereas the end support reactions were lower. This occurred because of the presence of a cutout in the sagging region that reduced flexural rigidity of the specimen in the sagging region, reduced the end support reaction, and hence increased the load transferred to the middle support.

Flexural strengthening of a deficient specimen using two NSM-CFRP strips in the sagging region only controlled propagation and growth of cracks in the sagging region, and hence the middle and end support reactions of specimen A-S2-H0 almost coincided with the elastic reactions. The end support reactions of specimen A-S4-H0 with four NSM-CFRP strips in the sagging region were slightly

higher than the elastic reactions and the middle support reactions were slightly lower. This occurred because specimen A-S4-H0 was heavily reinforced with NSM-CFRP strips in the sagging region, which significantly reduced crack propagation in the sagging region and hence reduced the load transferred to the middle support.

Flexural strengthening of specimens A-S2-H2 and A-S4-H2 in the hogging region with two NSM-CFRP strips increased the middle support reactions and reduced the end support reactions relative to elastic reactions. Specimen A-S4-H2 featured higher end support reactions than those of specimen A-S2-H2 because it had doubled the amount of the NSM-CFRP strips in the sagging region. The increased end support reactions of specimen A-S4-H2 reduced the load transferred to the middle support, and hence the specimen exhibited lower middle support reactions than those of specimen A-S2-H2.
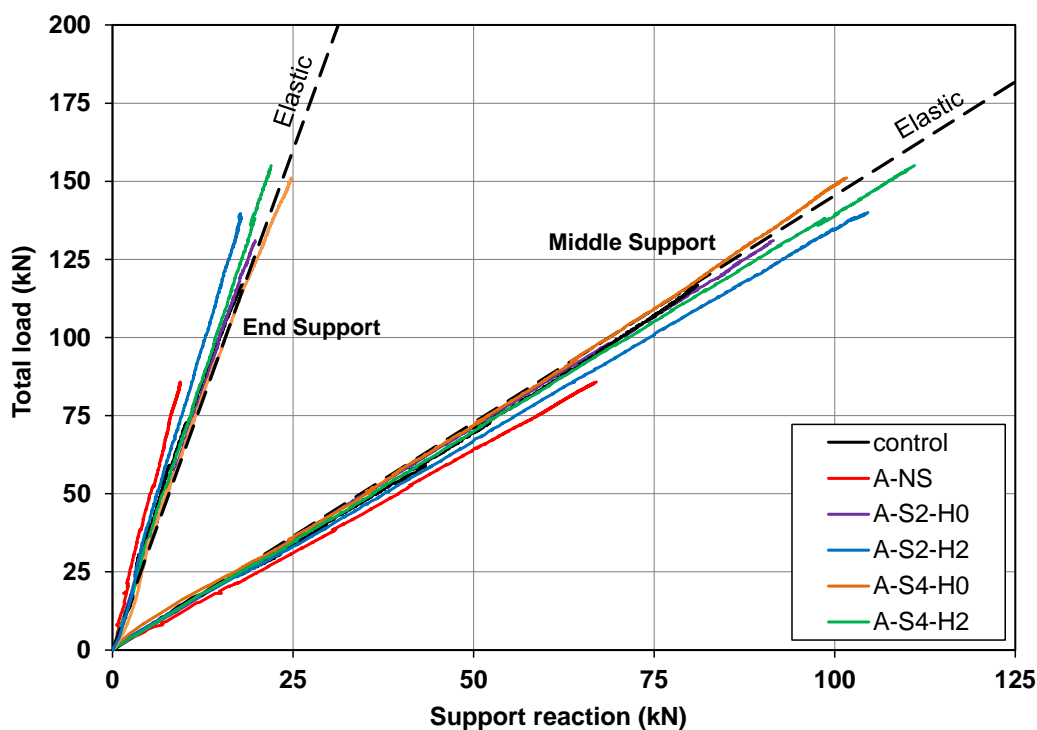
Figure 4.17: Load versus support reactions for specimens of group [A]

4.2.1.9 Moment – Deflection Response

The moment-deflection response of specimens of group [A] along with that of the control specimens are depicted in Figure 4.18. In this figure, the deflection was taken as the average of the west and east mid-span deflections, and the moments were calculated based on the measured supports reactions. The maximum moments from experiments in the sagging and hogging regions are given in Table 4.4 along with the moment enhancement ratio cause by strengthening. In Figure 4.18, the first change in slope of the moment-deflection response corresponds to the cracking moment whereas the second change corresponds to the yield moment. Generally, specimens having same amount of reinforcement in the sagging region experienced similar sagging moment-deflection response whereas specimens with same amount of reinforcement in the hogging region exhibited similar hogging moment-deflection response.
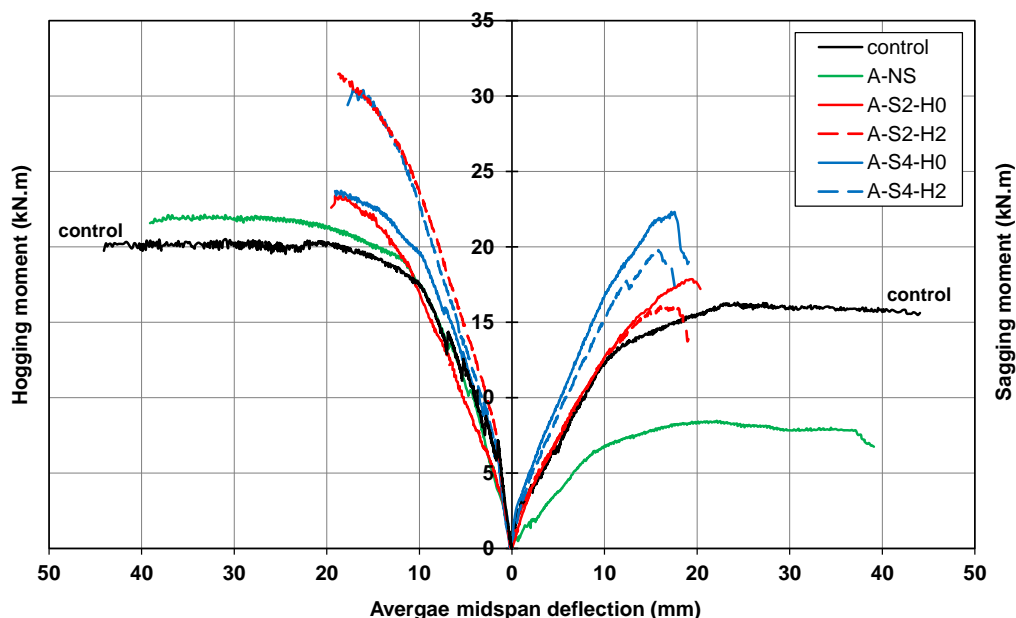
Figure 4.18: Moment-deflection response for specimens of group [A]

Table 4.4: Moment capacity and enhancement ratio for specimens of group [A]

Specimen	Moment capacity from experiment		MER^*
	$M_{s,exp}$ (kN.m)	$M_{h,exp}$ (kN.m)	
control	16.3	20.1	-
A-NS	8.5	21.7	1.0
A-S2-H0	17.8	23.4	2.1
A-S4-H0	22.3	23.5	2.6
A-S2-H2	15.9	31.1	1.9
A-S4-H2	19.8	30.2	2.3

[*]Moment enhancement ratio with respect to sagging moment of specimen A-NS

The unstrengthened specimen A-NS featured a significant reduction in the yield and ultimate sagging moments relative to those of the control because of the cutout that reduced the concrete section and amount of steel reinforcement. The yield and ultimate moments of specimen A-NS were approximately 50% lower than those of the control specimen. The hogging moment of specimen A-NS was insignificantly different from that of the control.

Flexural strengthening in the sagging region only significantly increased the sagging yield and ultimate moments but had almost no effect on the hogging moments. The addition of NSM-CFRP reinforcement in the hogging region increased the hogging yield and ultimate moments but had almost no effect on the sagging moment.

The yield and ultimate sagging moments of specimens A-S2-H0 and A-S2-H2 with two NSM-CFRP strips in each sagging region were approximately 100% higher than those of specimen A-NS and almost the same as those of the control specimen. This indicates that flexural strengthening with two NSM-CFRP strips fully

restored the sagging moment capacity of the specimens with a cutout in the sagging regions.

Increasing the amount of NSM-CFRP reinforcement in the sagging region further increased the ultimate sagging moment to a level even higher than that of the control specimen. For specimens A-S4-H0 and A-S4-H2 with four NSM-CFRP strips in the sagging region, the ultimate sagging moment was on average 148% higher than that of specimen A-NS and 30% higher than that of the control.

The yield and ultimate hogging moments of specimens A-S2-H0 and A-S4-H0 were almost the same as those of specimen A-NS. This occurred because specimens A-S2-H0 and A-S4-H0 were not strengthened in the hogging region. On the contrary, the hogging yield and ultimate moments of specimens A-S2-H2 and A-S4-H2 with two NSM-CFRP strips in the hogging region were on average 40% higher than those of specimen A-NS.

4.2.1.10 Load – Moment Relationship

Figure 4.19 depicts the load-moment relationship of specimens of group [A] and that of the control specimen in the sagging and hogging regions. The moment-deflection response in the sagging and hogging regions followed the same trend as that of the load versus end and middle support reactions, respectively. The sagging and hogging moments in the control specimen in addition to specimens A-S2-H0 and A-S4-H0 were nearly elastic with insignificant moment redistribution because of the similar distribution, propagation, and growth of flexural cracks in both sagging and hogging regions. Conversely, the experimental sagging and hogging moments in specimens A-NS, A-S2-H2 and A-S4-H2 deviated from the elastic moments because of the non-uniform flexural rigidity of the sagging and hogging regions. The

unstrengthened specimen A-NS with a cutout in the sagging region featured the greatest deviation from the elastic behavior because of the significant variation in flexural rigidity between the sagging and hogging regions. The sagging moments in specimen A-NS were lower than the elastic moments whereas the hogging moments were higher than the elastic ones. Specimen A-S4-H2 exhibited higher sagging moments and lower hogging moments than those of specimen A-S2-H2. This occurred because specimen A-S4-H2 had four NSM-CFRP strips in the sagging region whereas specimen A-S2-H2 had only two NSM-CFRP strips in the sagging region. Both specimens had same amount of NSM-CFRP reinforcement in the hogging region. The increased amount of NSM-CFRP reinforcement in the sagging region limited propagation of flexural cracks in the sagging region, increased the end support reactions, and hence increased the sagging moment in specimen A-S4-H2 relative to that of specimen A-S2-H2.
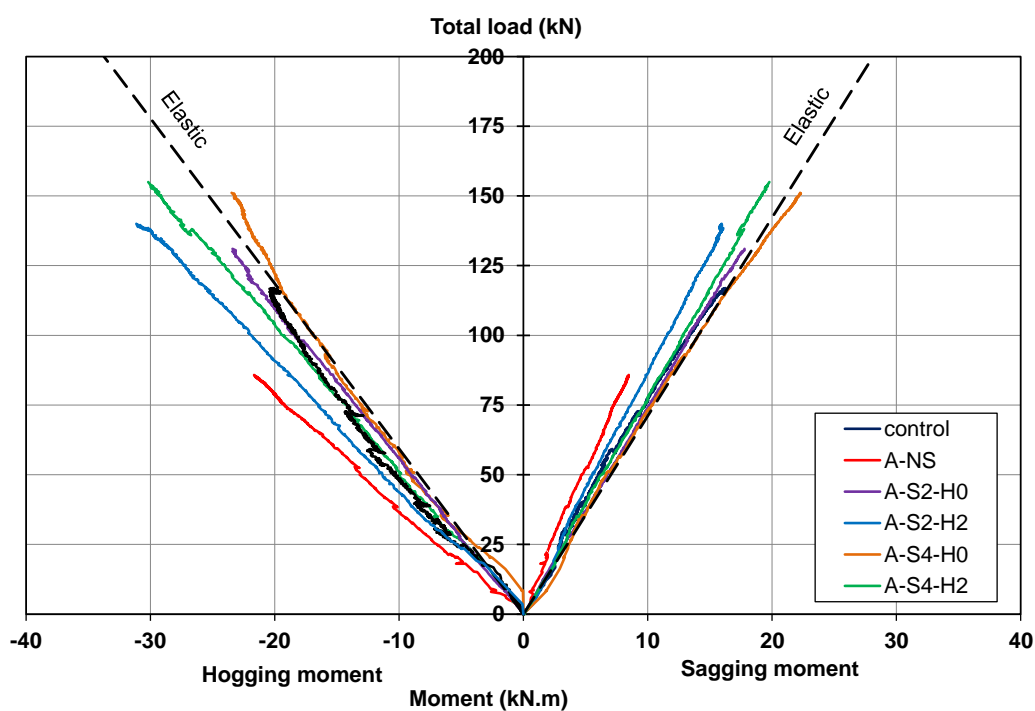
Figure 4.19: Load-moment relationship curves for specimens of group [A]

4.2.1.11 Moment Redistribution

The moment redistribution depends on the difference in flexural rigidity between the sagging and hogging regions. The moment redistribution ratio, β, can be calculated using Equation 4.2. A positive value of moment redistribution ratio indicates that the concerned region has gained moments greater than the elastic moment whereas a negative value indicates that the concerned region has gained moments less than the elastic moments. The elastic moments were calculated using structural analysis assuming that the slab specimens had uniform stiffness along the two spans. The elastic moments are shown in Figure 4.20. Table 4.5 gives the moment redistribution ratio for specimens of group [A] along with that of the control.

$$\beta\% = \frac{M_{exp} - M_e}{M_e} \times 100\% \hspace{3cm} (4.2)$$

Where:

β = moment redistribution ratio

M_{exp} = moment from experiment

M_e = moment from elastic analysis
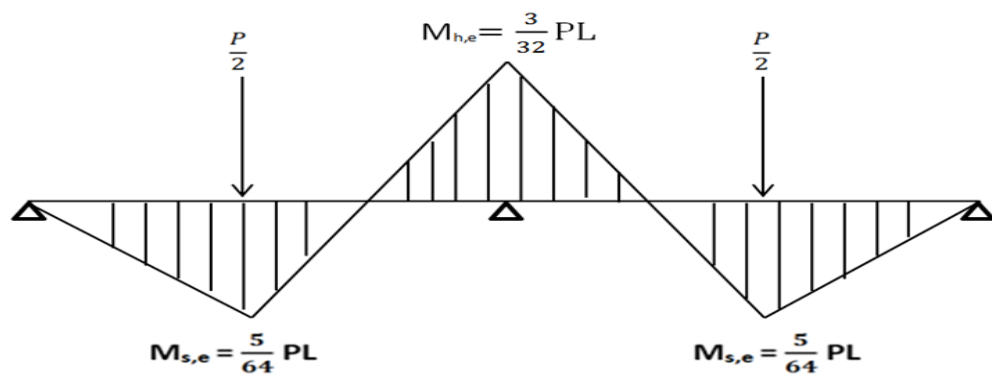
Figure 4.20: Elastic moments

Table 4.5: Moment redistribution ratios for specimens of group [A]

Slab Name	Moment form experiment		Elastic Moment		β (%)	
	$M_{s,exp}$ (kN.m)	$M_{h,exp}$ (kN.m)	$M_{s,e}$ (kN.m)	$M_{h,e}$ (kN.m)	Sagging	Hogging
control	16.3	20.1	16.5	19.7	-1.2	+2.0
A-NS	8.5	21.7	12.1	14.5	-29.8	+49.7
A-S2-H0	17.8	23.4	18.4	22.1	-3.3	+5.9
A-S2-H2	15.9	31.1	21.5	25.9	-26	+20.1
A-S4-H0	22.3	23.5	21.3	25.5	+4.7	-7.8
A-S4-H2	19.8	30.2	21.8	26.2	-9.2	+15.3

From Table 4.5, it is evident that the unstrengthened specimen A-NS with a cutout in the sagging region exhibited the highest moment redistribution ratios of approximately -30% and +50% in the sagging and hogging regions, respectively. This occurred because of the presence of a cutout in the sagging region, which significantly reduced the concrete section and amount of internal steel reinforcement. This in turn resulted in a significant difference in flexural rigidity between the sagging and hogging region. The control specimen exhibited almost no moment redistribution because both sagging and hogging regions had the same concrete geometry and amount of steel reinforcement. Specimen A-S2-H0 and A-S4-H0 exhibited insignificant moment redistribution in the range of 3.3% to 7.8%. Specimen A-S2-H2 featured appreciable moment redistribution values of –26% and +20% in the sagging and hogging regions, respectively whereas for specimen A-S4-H2, moment redistribution values of –9.2% and +15.3% were recorded in the sagging and hogging regions, respectively.

4.2.2 Group [B]

Results of five specimens of group [B] having a cutout in the hogging region are presented in this section. Four specimens were strengthened with NSM-CFRP reinforcement in the hogging region, while one specimen was not strengthened. Results of the control specimen that did not include a cutout and was not strengthened are included for the purpose of comparison.

4.2.2.1 Load Capacity

Results of the load measurements for specimens of group [B] along with those of the control are summarized in Table 4.6. The ultimate load enhancement ratios (*LER*) for the strengthened specimens with respect to that of the unstrengthened specimen B-NS are given in the same table. The cracking and yield loads were taken from the tensile steel strain response. The sagging cracking and yield load of the west span in some specimens were not recorded because of malfunction of the strain gauge.

Table 4.6: Results of load measurement for specimens of group [B]

Specimen	P_{cr} (kN)			P_y (kN)			P_u (kN)	LER^*
	Sagging		Hogging	Sagging		Hogging		
	West	East		West	East			
control	14.6	27.1	29.8	83.4	94.3	87.8	116.90	-
B-NS	-	11.4	25	-	71.2	62.9	89.80	1.00
B-S0-H2	-	15.2	24.7	-	75.1	81.1	105.50	1.18
B-S0-H4	-	15.4	22.6	-	96.7	112.5	122.50	1.36
B-S2-H2	23.2	21.7	23.9	108.5	124.7	112.0	136.9	1.52
B-S2-H4	30.9	27.8	29.6	126.8	121.5	125.9	138.00	1.54

*Load enhancement ratio with respect to that of specimen B-NS

The unstrengthened specimen B-NS cracked at load values of approximately 11.4 kN in the east sagging region and 25 kN in the hogging region. The tensile steel in the hogging region yielded prior to the tensile steel in the east sagging region, because of the presence of the cutout in the hogging region, which reduced the amount of steel and also reduced the concrete section size. The tensile steel in the hogging region yielded at a load value of approximately 63 kN whereas in the east sagging region, it yielded at a load value of approximately 71.2 kN. Specimen B-NS achieved its peak load at a load value of 89.80 kN. This value was approximately 23% lower than that of the control specimen.

Flexural cracks initiated in specimen B-S0-H2 at a load value of approximately 15.2 kN in the east sagging region and 24.7 kN in the hogging region. The steel in the sagging and hogging regions yielded almost concurrently at load values of approximately 75.1 kN and 81.1 kN, respectively. The sagging yield load of specimen B-S0-H2 was almost the same as that of specimen B-NS, whereas the hogging yield load was approximately 29% higher than that of specimen B-NS. Specimen B-S0-H2 strengthened with two CFRP strips in the hogging region experienced a load enhancement ration of 18% relative to the ultimate load of specimen B-NS. The load capacity of specimen B-S0-H2 was, however, 10% lower than that of the control specimen. This indicates that two NSM-CFRP strips were not sufficient to restore the load capacity of the control specimen.

Specimen B-S0-H4 with four NSM-CFRP strips in the hogging region experienced flexural cracks in the sagging and hogging region at load values of approximately 15.4 kN and 22.6 kN, respectively. Yielding of tensile occurred first in the sagging region at a load value of approximately 96.7 kN followed by yielding of steel in the hogging region at a load value of approximately 112.5 kN. This

occurred because of the increased amount of NSM-CFRP strips in the hogging region, which delayed yielding of steel over the middle support. The sagging and hogging yield loads of specimen B-S0-H4 were approximately 36% and 80% higher than those of specimen B-NS, respectively. The load capacity of specimen B-S0-H4 was 36% higher than that of specimen B-NS and also 5% higher than that of the control specimen.

For specimen B-S2-H2, flexural cracks occurred in the west and east sagging regions almost at the same time at load values of approximately 23.2 kN and 21.7 kN, respectively. For the hogging region, flexural cracks initiated at a load value of approximately 23.9 kN. The tensile steel of the west and east sagging regions yielded at load values of approximately 108.5 kN and 124.7 kN, respectively. For the hogging region, the tensile steel yielded at a load value of approximately 112 kN. The ultimate load of specimen B-S2-H2 was 52% higher than that of specimen B-NS and 17% higher than that of the control specimen. It should be noted that the ultimate load of specimen B-S2-H2 was approximately 30% higher than that of specimen B-S0-H2. This indicates that the addition of NSM-CFRP reinforcement in the sagging regions significantly improved the load carrying capacity.

Specimen B-S2-H4 experienced flexural cracks in the west and east sagging regions at load values of approximately 30.9 kN and 27.8 kN, respectively. Flexural cracks initiated in the hogging region at a load value of 29.6 kN. The tensile steel yielded in the west and east sagging regions almost concurrently at load values of 126.8 kN and 121.5 kN, respectively. For the hogging region, the tensile steel yielded at a load value of 125.9 kN. The ultimate load of specimen B-S2-H4 was 54% higher than that of specimen B-NS and 18% higher than that of the control specimen. The ultimate load of specimen B-S2-H4 was approximately 13% higher

than that of specimen B-S0-H4 because of the addition of NSM-CFRP reinforcement in the sagging regions, which improved the load carrying capacity. The increase in load capacity due to increasing the NSM-CFRP reinforcement in the sagging region was less pronounced in specimen B-S2-H4 (13%) than in specimen B-S2-H2 (30%). This indicates that the gain in load capacity due to strengthening in the sagging regions decreases as the amount of reinforcement increases in the hogging region. Finally, it should be noted that the load capacity of specimen B-S2-H4 was the same as that of specimen B-S2-H2. This demonstrates that for RC continuous slab strips heavily reinforced in the sagging region, increasing the amount of NSM-CFRP reinforcement in the hogging region has insignificant effect on the load capacity.

4.2.2.2 Failure Mode

Specimen B-NS failed in a flexural mode of failure. The tensile steel yielded first in the hogging region then in the sagging region. Following yielding of tensile steel, crushing of concrete occurred at the bottom face of the specimen over the middle support then at the top face in the mid-span section. Photos of specimen B-NS at failure are shown in Figure 4.21.

Specimen B-S0-H2 failed in a flexural mode of failure. The tensile steel yielded first in the sagging region then in the hogging region. Following yielding of tensile steel, crushing of concrete occurred at the top face of the specimen in the mid-span section and at the bottom face over the middle support. Due to the weakness of the section over the middle support caused by the cutout, a shear crack developed in the hogging region at the onset of failure after concrete crushing. Photos of specimen B-S0-H2 at failure are shown in Figure 4.22.

Specimen B-S0-H4 failed in a flexural mode of failure. The tensile steel yielded first in the sagging region then in the hogging region. Following yielding of tensile steel, crushing of concrete occurred at the top face of the specimen in the mid-span section and at the bottom face over the middle support. A photo of specimen B-S0-H4 at failure is shown in Figure 4.23.

Failure of mid-span section   Failure of section over central support

(sagging region)   (hogging region)

Figure 4.21: Photos of specimen B-NS at failure

Failure of mid-span section   Failure of section over central support

(sagging region)   (hogging region)

Figure 4.22: Photos of specimen B-S0-H2 at failure

Figure 4.23: Photo of specimen B-S0-H4 at failure

Specimen B-S2-H2 failed in a flexural mode of failure. The tensile steel yielded in the hogging region at a load value of 112 kN. The last yielding occurred in the east sagging region at a load value of 124.7 kN. Following yielding of tensile steel, crushing of concrete occurred at the bottom face of the specimen over the middle support and at the top face in the mid-spans. A minor shear crack developed in the hogging region at the onset of concrete crushing due the weakness caused by the cutout. A photo of specimen B-S2-H2 at failure is shown in Figure 4.24.

The specimen B-S2-H4 failed in a flexural mode of failure. The tensile steel in the sagging and hogging regions yielded almost at the same time. Following yielding of tensile steel, crushing of concrete occurred at the top face of the specimen in the mid-spans and at the bottom face over the middle support. At the onset of failure, crushing of concrete took place in the concrete section over the middle support accompanied by formation of a shear crack in the hogging region. The shear crack developed because of the reduced concrete section caused by the cutout. A photo of specimen B-S2-H4 at failure is shown in Figure 4.25.

Figure 4.24: Photo of specimen B-S2-H2 at failure
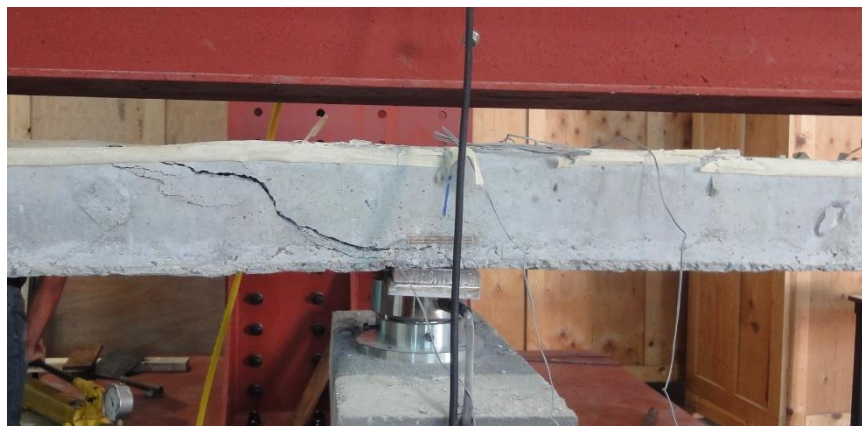
Figure 4.25: Photo of specimen B-S2-H4 at failure

4.2.2.3 Load-Deflection Response

The load-deflection responses for specimens of group [B] are given in Figures 4.26 to 4.30. For specimen B-NS, both spans experienced a very similar deflection response. A linear response was maintained up to an average mid-span deflection of approximately 1 mm. Then, the specimen exhibited a quasi-linear deflection response until first yielding took place in the hogging region at an average

deflection of approximately 8.5 mm. The second (last) yielding occurred in the hogging region at an average mid-span deflection of approximately 11.2 mm. Following last yielding, the deflection continued to increase but at a higher rate until a peak load of 89.80 kN was achieved at corresponding east mid-span deflection of 20.6 mm as shown in Figure 4.26.

Specimen B-S0-H2 featured a linear deflection response in both spans until initiation of cracks at a deflection value of approximately 1 mm where the first deviation from linearity took place. Following cracking, the specimen experienced a quasi-linear deflection response until yielding of tensile steel took place in the sagging region at approximately 10 mm. then, the deflection increased at a higher rate until yielding of tensile steel in the hogging region (last yielding) took place at a deflection of approximately 17 mm. Following last yielding, the specimen exhibited a plastic deflection response until a peak load of 105.5 kN at corresponding east and west span deflections of 24.4 mm and 24.2 mm, respectively as shown in Figure 4.27.

Specimen B-S0-H4 exhibited a linear deflection response up to an average deflection of approximately 1.2 mm where first change in slope took place due to cracking. In the second stage, the deflection continued to increase but at a higher rate until first yielding took place in the sagging region at an average deflection of 9.5 mm. Following first yielding, the deflection increased rapidly until the specimen reached its last yielding in the hogging region at east and west deflections of 10 mm and 16 mm, respectively. In the last stage, the mid-span deflection of the west span experienced a plastic response until a peak load of 122.5 kN was achieved at a west mid-span deflection of 33.2 mm as shown in Figure 4.28.
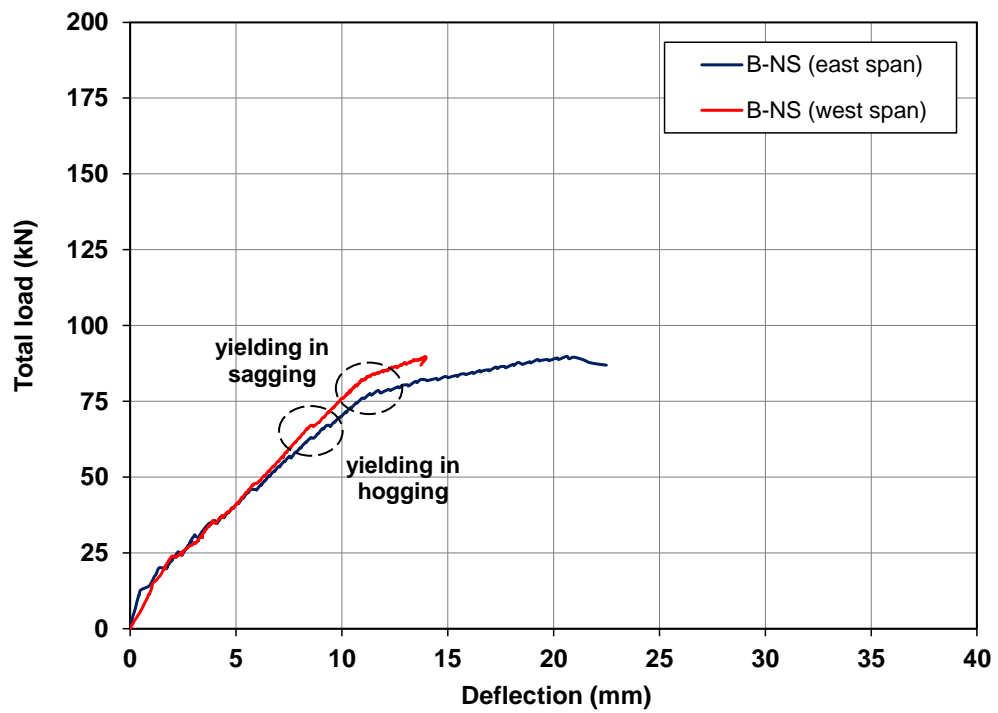
Figure 4.26: Load-deflection response of specimen B-NS
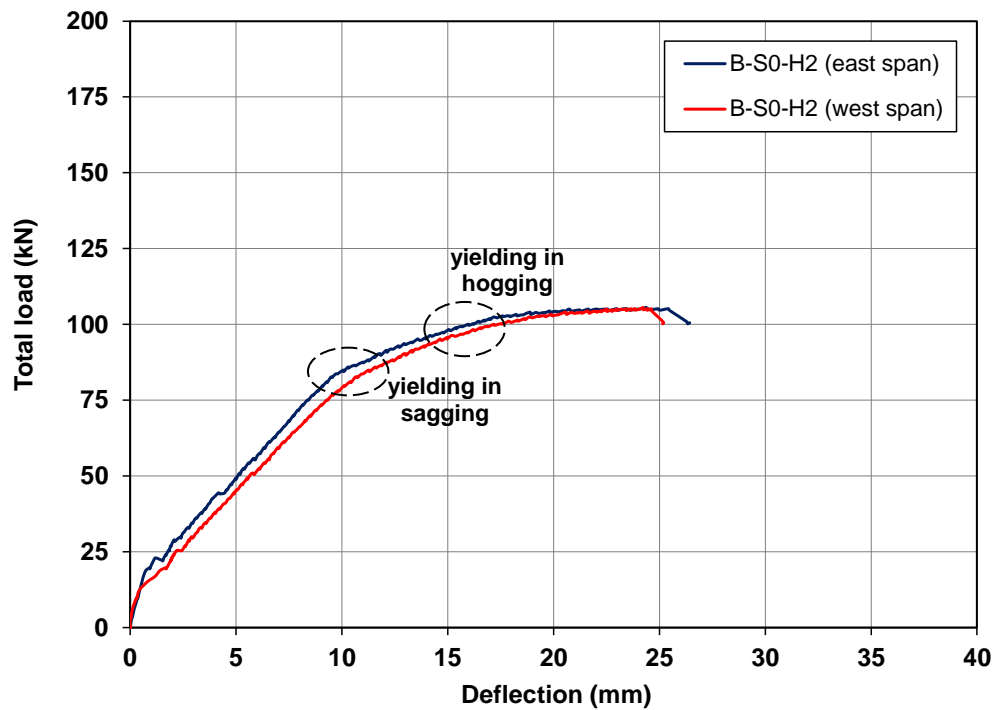
Figure 4.27: Load-deflection response of specimen B-S0-H2
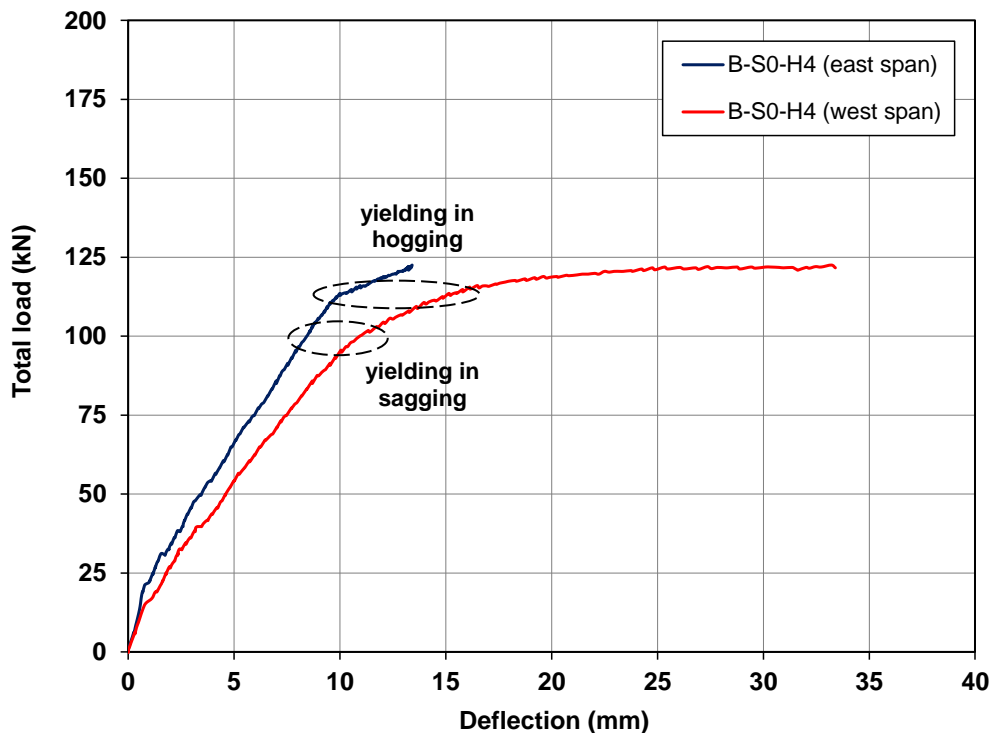
Figure 4.28: Load-deflection response of specimen B-S0-H4

For specimen B-S2-H2, the linear deflection response was maintained up to an average mid-span deflection of approximately 3.5 mm. Then, the deflection increased at a higher rate until first yielding of steel took place in the hogging region at east and west mid-span deflections of 10 mm and 12 mm, respectively. Following first yielding, the deflection further increased at a higher rate until second (last) yielding occurred in the sagging region at east and west deflections of 13 mm and 15.2 mm, respectively. In the last stage, the deflection continued to increase at a higher rate until the specimen reached its peak load of 136.9 kN at east and west mid-span deflections of 22.30 mm and 24.4 mm, respectively as shown in Figure 4.29.

Specimen B-S2-H4 featured a linear deflection response in both spans until initiation of cracks at a deflection value of approximately 1.25 mm where the first deviation from linearity took place. Following cracking, the deflection increased linearly until yielding of tensile steel took place in the sagging and hogging region at an average deflection of 10.3 mm. Following yielding of steel, the deflection continued to increase but at a higher rate until the specimen reached a peak load of 138 kN at an average mid-span deflection of approximately 14.5 mm as shown in Figure 4.30.
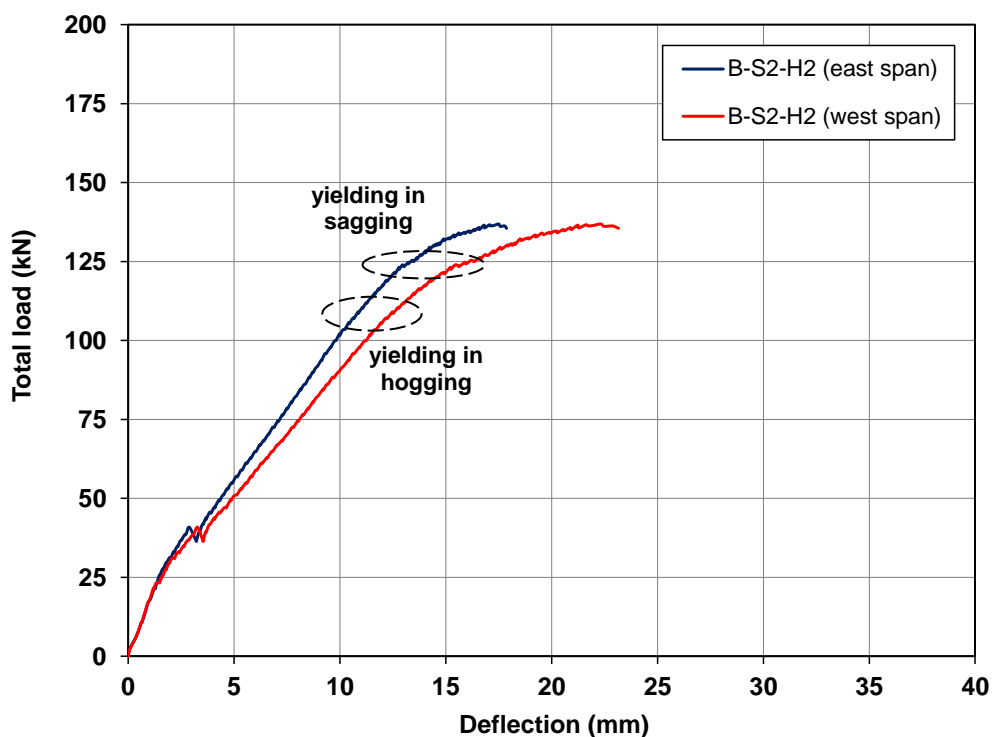
Figure 4.29: Load-deflection response of specimen B-S2-H2
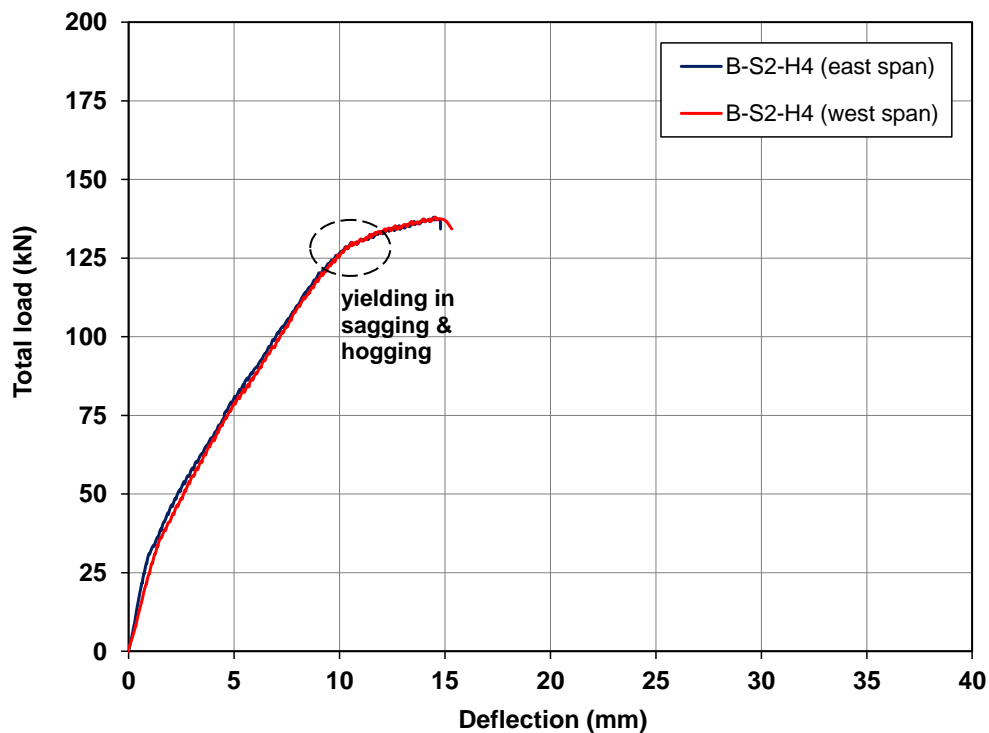
Figure 4.30: Load-deflection response of specimen B-S2-H4

The load-deflection responses of all specimens of group [B] with a cutout in the hogging region along with that of the control specimen are plotted in Figure 4.31. The deflection response of the span that featured the greater mid-span deflections was considered in Figure 4.31. It is clear that the flexural stiffness and load capacity of specimen B-NS were significantly lower than those of the control specimen. For instance at 50 kN, the deflection of the control specimen was 3.6 mm whereas for specimen B-NS it was 6.5 mm. The deflection at peak load for specimen B-NS was slightly lower than that of the control specimen. Although the stiffness of specimens B-S0-H2 and B-S2-H2 having two NSM-CFRP strips in the hogging region was higher than that of the unstrengthened specimen B-NS, it was slightly lower than that of the control specimen. Specimen B-S0-H4 with four NSM-CFRP strips in the hogging region fully restored the stiffness of the control specimen. The stiffness of

specimen B-S2-H4 with four NSM-CFRP strips in the hogging region and two NSM-CFRP strips in the sagging region was even better than that of the control.
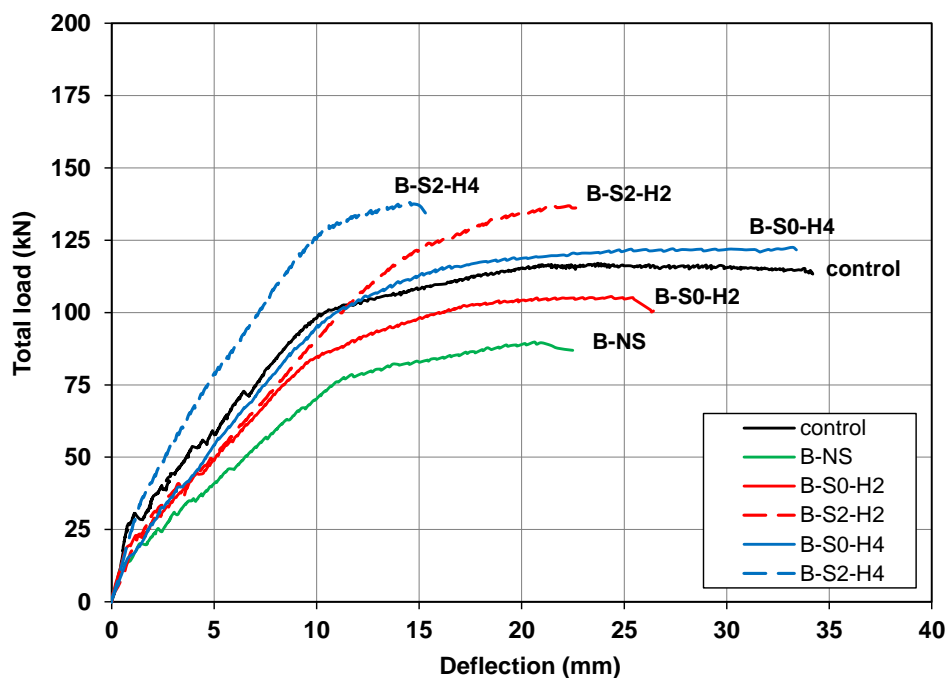
Figure 4.31: Load-deflection response for specimens of group [B]

4.2.2.4 Ductility Index

The ductility indices for specimens of group [B] are compared to that of the control specimen in Table 4.7. The deflection values at first yielding and at peak load are taken from Figure 4.31.

Table 4.7: Ductility indices for specimens of group [B]

Specimen	Δ_{y1} (mm)	Δ_p (mm)	μ
control	10.5	23.8	2.27
B-NS	11.8	20.6	1.75
B-S0-H2	9.2	24.4	2.65
B-S0-H4	11.4	33.2	2.90
B-S2-H2	11.2	22.3	2.0
B-S2-H4	10.4	14.5	1.4

The ductility index of specimen B-NS with a cutout in the hogging region, 1.75, was 23% lower than that of the control specimen. This indicates that installation of a cutout in the hogging region significantly comprised the slab ductility and resulted in insignificant reduction in ductility index. The ductility index of specimens B-S0-H2 and B-S0-H4 strengthened only in the hogging region was higher than that of specimen B-NS and even better than that of the control. This occurred because in these two specimens yielding of steel occurred first in the sagging region that was unstrengthened, and then the specimens had to undergo a significant deformation until yielding of steel followed by crushing of concrete took place in the hogging region. Installation of NSM-CFRP reinforcement in both sagging and hogging regions reduced the slab ductility index. The ductility index of specimen B-S2-H4 was 50% lower than that of specimen B-NS. The ductility of specimen B-S2-H4 was compromised significantly because it was heavily strengthened with two NSM-CFRP strips in the sagging region and four NSM-CFRP strips in the hogging region.

4.2.2.5 Tensile Steel Strain Response

The tensile steel strain response of specimens of group [B] along that of the control specimens are shown in Figure 4.32. The specimens exhibited a tri-linear tensile steel strain response. No steel strains were recorded prior to initiation of flexural cracks. Following cracking, the steel strain increased at an almost constant rate until yielding. In most of specimens, a plastic steel strain response was then recorded after yielding. In some other specimens heavily reinforced with NSM-CFRP strips, the steel strain increased at a higher rate after yielding until the peak load was reached.

The steel strain in the hogging region for the unstrengthened specimen B-NS, with a cutout in the hogging region, increased at a rate higher than that of the control specimen. As a result, the tensile steel of specimen B-NS in both hogging and sagging regions yielded at load values lower than those of the control. Specimen B-NS exhibited yielding of tensile steel in the hogging region at a load value of approximately 63 kN. The post-yield steel strain response of specimen B-NS in the hogging region was not recorded due to failure of the strain gauge. The tensile steel in the sagging yielded at a load value of approximately 71 kN, after yielding of steel in the hogging region.

The hogging yield load of specimen B-S0-H2, with two NSM-CFRP strips in the hogging region, was higher than that of specimen B-NS and slightly lower than that of the control. The steel in the sagging region yielded first at approximately 75 kN followed by yielding of steel in the hogging region at approximately 81 kN. The post-yield tensile steel strain response of specimen B-S0-H2 in the sagging region was not recorded due to failure of the strain gauge.

Specimen B-S0-H4, with four NSM-CFRP strips in the hogging region, experienced yielding of tensile steel in the sagging region first then in the hogging region. This occurred because of the significant amount of NSM-CFRP reinforcement provided in the hogging region that delayed yielding of tensile steel in that region. The yield load of specimen B-S0-H4 in both sagging and hogging regions was higher than that of the control specimen.

The tensile steel of specimen B-S2-H2, with two NSM-CFRP strips in both sagging and hogging regions, yielded earlier in the hogging region than the steel in the sagging region. This occurred because the specimen was strengthened with the same amount of NSM-CFRP reinforcement in both sagging and hogging regions but

it had a cutout in the hogging region. The rate of increase of tensile steel strain in specimen B-S2-H2 was significantly lower than that of specimen B-NS. This in turn increased the yield load of specimen B-S2-H2 in both sagging and hogging regions to a level even higher than that of the control specimen.

The tensile steel of specimen B-S2-H4 in both sagging and hogging regions yielded concurrently. Specimen B-S2-H4 experienced tensile steel strains in the hogging region slightly lower than those of specimen B-S2-H2. This occurred because specimen A-S2-H4 was strengthened with four NSM-CFRP strips in the hogging region whereas specimen A-S2-H2 had only two NSM-CFRP reinforcements in the hogging region. As a result, the yield load of specimen A-S2-H4 in the hogging region was slightly higher than that of specimen A-S2-H2. The tensile steel response of specimen B-S2-H4 in the sagging region coincided with that of specimen B-S2-H2 because both specimens had the same concrete geometry, same amount of internal steel and NSM-CFRP reinforcement in the sagging region.
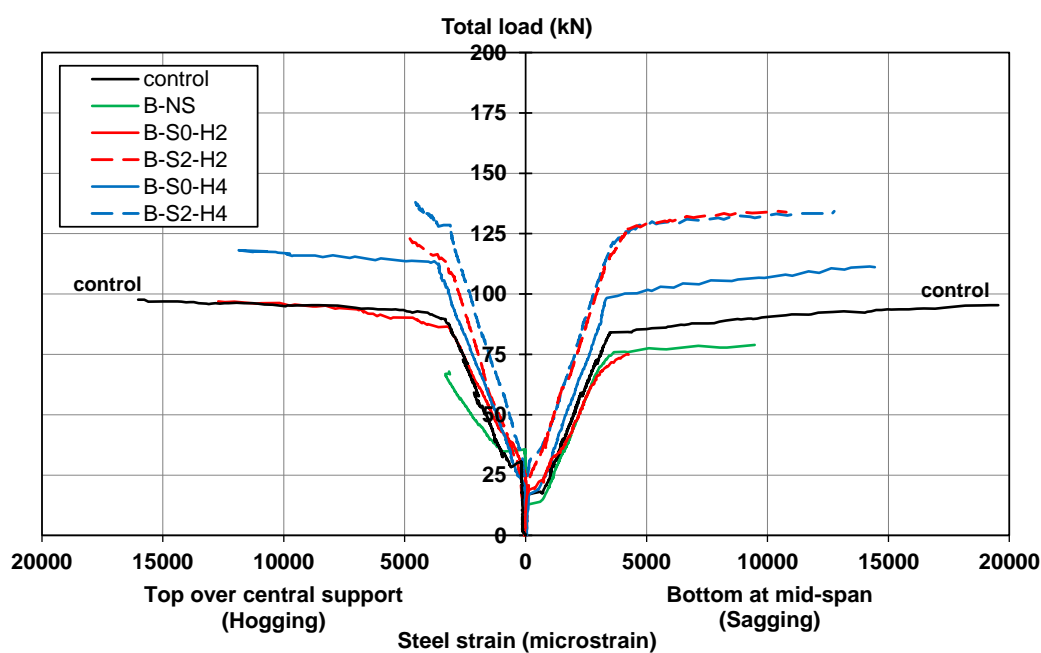
Figure 4.32: Tensile steel strain response for specimens of group [B]

4.2.2.6 CFRP Strain Response

The CFRP strain responses of specimens of group [B] are plotted in Figure 4.33. The CFRP strain response featured three phases during loading. Initially, no or minimal FRP strains were recorded. Following flexural cracking, the CFRP strain increased at an almost constant rate as the load progressed until yielding of steel took place. Following yielding, the CFRP strain continued to increase but at a higher rate until failure. It is evident that specimens B-S0-H4 with four NSM-CFRP strips in the hogging regions exhibited lower CFRP strains than those exhibited by specimen B-S0-H2 with two NSM-CFRP strips. Similarly, specimen B-S2-H4 exhibited lower CFRP strains in the hogging region than those exhibited by specimen B-S2-H2. This indicates that the CFRP strain in a certain regions decreases with an increase in the amount of NSM-CFRP reinforcement in the corresponding region. The CFRP strain response of specimens B-S2-H4 and B-S2-H2 in the sagging region was almost identical as shown in Figure 4.33 because both specimens were strengthened with two NSM-CFRP strips in the sagging region.

Specimens B-S0-H2, B-S0-H4, B-S2-H2, and B-S2-H4 reached their peak loads at hogging CFRP strain values of 8647, 6843, 4939, and 5232 microstrain, respectively. The ratios of the CFRP strain at peak load to the rupture CFRP strain for specimens of group [B] are given in Table 4.8. In this table $\varepsilon_{f,max}$ refers to the CFRP strain at peak load whereas ε_{fr} refers to the rupture CFRP strain. The ratios of CFRP strain at peak load to the rupture CFRP strain for specimens B-S0-H2, B-S0-H4, B-S2-H2, and B-S2-H4 were 46%, 36%, 26%, and 28%, respectively. The CFRP strain at peak load in the sagging region for specimens B-S2-H2 and B-S2-H4 were 6252 and 6411 microstrain, which corresponded to CFRP strain ratios of 33% and 34%.
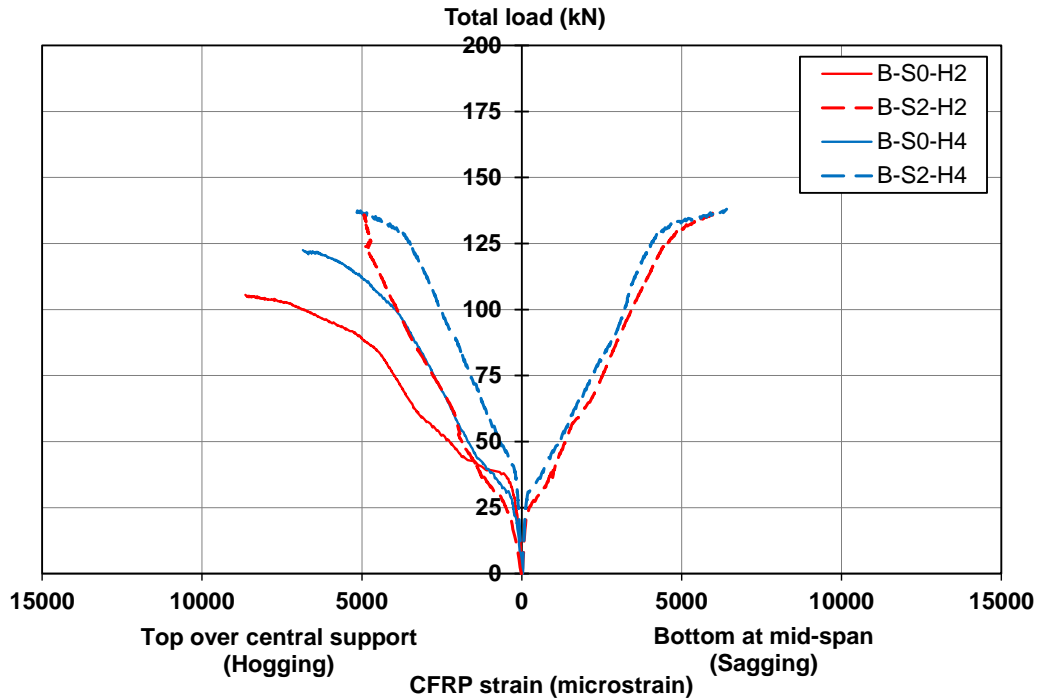
Figure 4.33: CFRP strain response for specimens of group [B]

Table 4.8: Ratio of CFRP strain at peak load to rupture CFRP strain (group [B])

Specimen	$(\varepsilon_{f,max})$ CFRP strain at peak load (microstrain)		$(\varepsilon_{f,max} / \varepsilon_{fr})$ (%)	
	Sagging	Hogging	Sagging	Hogging
B-S0-H2	-	8647.0	-	46
B-S0-H4	-	6843.0	-	36
B-S2-H2	6252.0	4939.0	33	26
B-S2-H4	6411.0	5232.0	34	27

4.2.2.7 Concrete Strain Response

The concrete strain responses for specimens of group [B] along with that of the control specimen are depicted in Figure 4.34. The concrete strain response was not recorded or incomplete in some specimens due to malfunction of the strain

gauge. Generally, the rate of increase of concrete strain increased after cracking then increased further after yielding of tensile steel.

From Figure 4.34, it can be seen that the unstrengthened specimen B-NS exhibited higher concrete strains than those exhibited by the control specimen. The tensile steel in the hogging and sagging regions of specimen B-NS yielded at corresponding concrete strains of approximately 900 and 1250 microstrains, respectively. Specimen B-NS reached its peak load at concrete strain values of approximately 1800 and 2200 microstrains in the hogging and sagging regions, respectively.

The strengthened specimens exhibited a lower rate of increase of concrete strain than that of the unstrengthened specimen B-NS. Increasing the amount of NSM-CFRP reinforcement in a certain region decreased the rate of increase of the CFRP strain in that region.

The concrete strain of specimen B-S0-H2 at the onset of yielding was on average 1000 microstrain. Specimen B-S0-H2 reached its peak load at concrete strain values of approximately 3100 and 2700 microstrains in the hogging and sagging regions, respectively.

Specimen B-S0-H4 exhibited lower concrete strain than that of specimen B-S0-H2, particularly in the sagging region, because of the increased amount of NSM-CFRP strips. Maximum concrete strain values of 2500 and 3750 microstrains were recorded in the hogging and sagging regions of specimen B-S0-H4, respectively prior to failure.

Specimen B-S2-H2 experienced lower rate of increase of concrete strain than that of specimen B-S0-H2, particularly in the sagging region. This occurred because

specimen B-S2-H2 had two NSM-CFRP strips in the sagging region but specimen B-S0-H2 did not include any NSM-CFRP strips in the sagging region. The strain gauge in the hogging region was debonded at approximately 2000 microstrain prior reaching the peak load because of local concrete crushing. Specimen B-S2-H2 reached its peak load at a concrete strain value of approximately 2000 microstrain in the sagging region.

Specimen B-S2-H4 experienced a concrete strain response in the sagging region similar to that of specimen B-S2-H4 because both had two NSM-CFRP strips in the sagging region. The concrete strains of specimen B-S2-H4 in the sagging region increased at a lower rate than that of specimen B-S0-H2. This occurred because specimen B-S2-H2 had two NSM-CFRP strips in the sagging region but specimen B-S0-H2 did not include NSM-CFRP reinforcement in the sagging region. The concrete strain response of specimen B-S2-H4 in the hogging region was not recorded due to malfunction of the strain gauge. A maximum concrete strain of 1715 microstrain was recorded in the sagging region of specimen B-S2-H4 just prior to failure.

It should be noted that due to the presence of the load and support plates, the concrete strain gauges were not placed on the top surface of the specimen at the mid-spans or at the bottom surface over the middle support. The concrete strain gauges were placed on the concrete lateral faces slightly away from the extreme compression fibers. This explains why some concrete strain values at peak load were lower than the concrete crushing strain value of 3000 microstrain specified by the ACI 318-08.
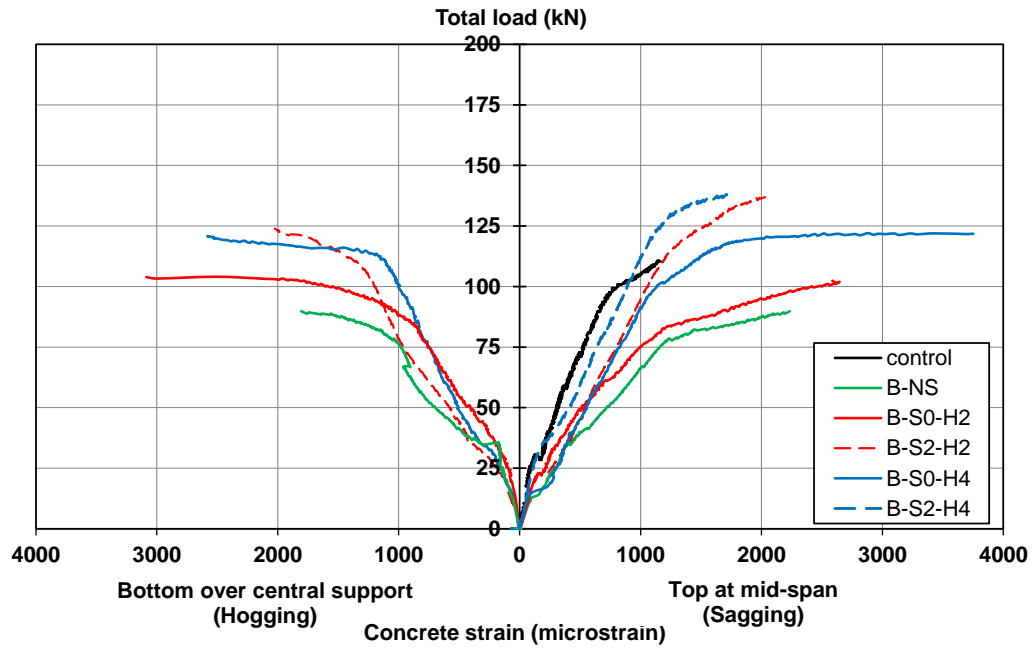
Figure 4.34: Concrete strain response for specimens of group [B]

4.2.2.8 Support Reactions

The load versus support reactions from the experiments are plotted in Figure 4.35. The support reactions of specimen B-S2-H4 were not recorded due to malfunction of the load cell placed between the specimen and middle support during testing. The middle and end support reactions of the control specimen were nearly elastic. On the contrary, the middle support reactions of specimen B-NS were lower than the elastic reactions whereas the end support reactions were higher than the elastic ones. The presence of a cutout in the hogging region reduced the flexural rigidity of the specimen in the hogging region, reduced the middle support reaction, and hence increased the load transferred to the end supports.

The middle and end support reactions of specimen B-S0-H2 almost coincided with the elastic reactions. This occurred because of flexural strengthening in the hogging region with two NSM-CFRP strips, which counteracted the weakness in

flexural rigidity caused by the cutout and controlled propagation and growth of cracks in the hogging region. Increasing the amount of NSM-CFRP reinforcement in the hogging region further increased the middle support reactions and decreased the end support reactions. This explains why specimen B-S0-H4 exhibited middle support reactions slightly higher than the elastic reactions and end support reactions slightly lower than the elastic reactions.

Specimen B-S2-H2 experienced middle support reactions lower than the elastic reactions and end support reactions higher than the elastic ones. Although this specimen had two NSM-CFRP strips in both sagging and hogging regions, it contained a cutout in the hogging region. The cutout reduced the concrete section and amount of internal steel in the hogging region. This in turn reduced the flexural rigidity of the hogging region relative to that of the sagging region, and hence reduced the load transferred to the middle support and increased the load transferred to the end support.
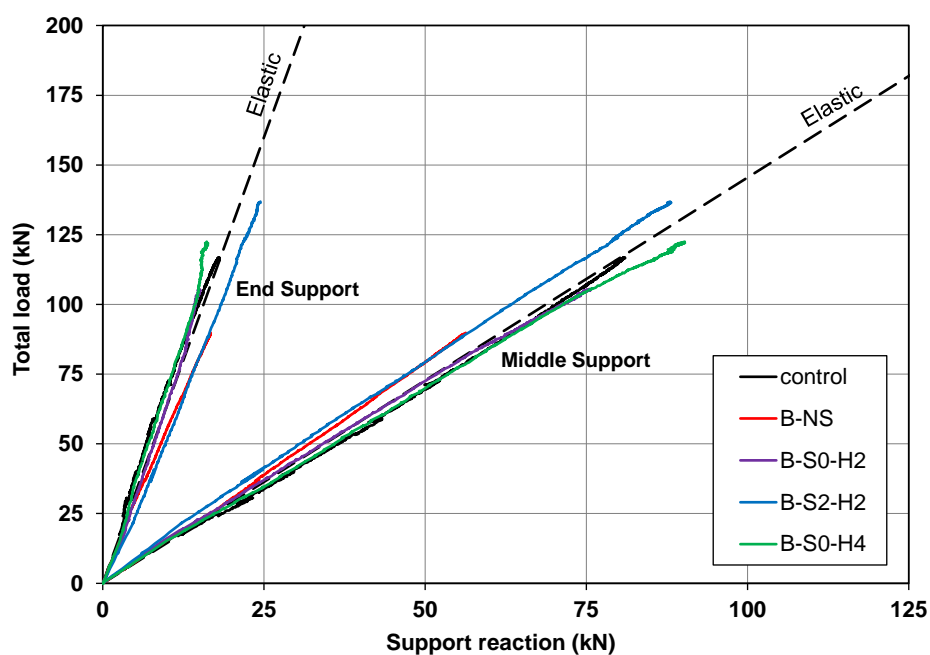
Figure 4.35: Load versus support reactions for specimens of group [B]

4.2.2.9 Moment – Deflection Response

The moment-deflection responses of specimens of group [B] along with that of the control specimen are shown in Figure 4.36. The moment-deflection response of B-S2-H4 was not plotted because the support reactions were not recorded during testing of this specimen. In this figure, the deflection was taken as the average of the west and east mid-span deflections, and the moments were calculated based on the measured supports reactions. The maximum moments from experiments in the sagging and hogging regions are given in Table 4.9 along with the moment enhancement ratio cause by strengthening.
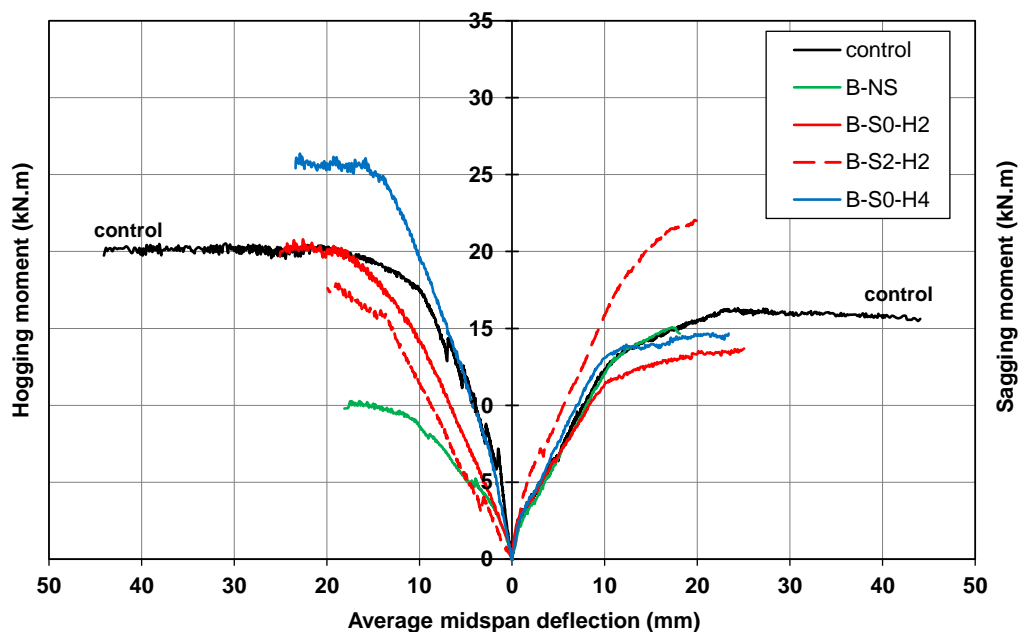
Figure 4.36: Moment-deflection response for specimens of group [B]

Table 4.9: Moment capacity and enhacemenet ratio for specimens of group [B]

Specimen	Moment capacity from experiment		MER^*
	$M_{s,exp}$ (kN.m)	$M_{h,exp}$ (kN.m)	
control	16.3	20.1	-
B-NS	15.1	10.3	1.0
B-S0-H2	13.5	20.5	2.0
B-S0-H4	14.5	26.1	2.5
B-S2-H2	22.0	17.6	1.7

[*]Moment enhancement ratio with respect to hogging moment of specimen B-NS

From Figure 4.36, it is clear that installation of a cutout in the hogging region significantly reduced the hogging yield and ultimate moments of specimen B-NS relative to those of the control specimen. The hogging yield and ultimate moments of specimen B-NS were approximately 50% lower than those of the control specimen. The sagging moment response of specimen B-NS was insignificantly different from that of the control.

Specimen B-S0-H2 with two NSM-CFRP strips in the hogging region featured a hogging moment response similar to that of the control. This demonstrates the effectiveness of the NSM-CFRP system in restoring the moment capacity of the deficient section. The hogging moment capacity further increased as the amount of NSM-CFRP reinforcement increased in the hogging region. The hogging moment capacity of specimen B-S0-H4 with four NSM-CFRP strips in the hogging region was approximately 2.5 times that of specimen B-NS and 1.3 times that of the control (i.e. flexural strengthening with four NSM-CFRP strips not only restored but exceeded the hogging moment capacity of the control specimen).

The sagging moment response of specimens B-S0-H2 and B-S0-H4 were insignificantly different from that of the control specimen. This occurred because

both specimens had neither a cutout nor NSM-CFRP reinforcement in the sagging region. On the contrary, the sagging moment capacity of specimen B-S2-H2 was significantly higher than that of the control because it had two NSM-CFRP strips in the sagging region. The hogging moment capacity of specimen B-S2-H2 was approximately 70% higher than that of specimen B-NS and 12% lower than that of the control. The sagging moment capacity of specimen B-S2-H2 was 46% and 35% higher than those of specimen B-NS and the control specimen, respectively.

4.2.2.10 Load – Moment Relationship

The load-moment relationships for specimens of group [B] along with that of the control are shown in Figure 4.37. The load-moment response of specimen B-S2-H4 was not plotted because the support reactions of this specimen were not recorded during testing. The sagging and hogging moments are proportional to the end and middle support reactions, respectively. The moments in specimens B-NS and B-S2-H2 deviated from the elastic response because of a variation in flexural rigidity of the sagging and hogging regions caused by the presence of the cutout in the hogging region. The presence of the cutout in the hogging region reduced the load transferred to the middle support, and hence reduced the hogging moment and increased the sagging moment relative to the elastic ones.

Flexural strengthening of specimen B-S0-H2 with two NSM-CFRP strips in the hogging region counteracted the deficiency caused by the cutout, and hence the sagging and hogging moments of specimen B-S0-H2 coincided with the elastic moments up to a load value of approximately 75 kN where yielding of tensile steel in the sagging region took place. Following yielding of steel in the sagging region, the sagging moment tended to be lower than the elastic whereas the hogging moment tended to be higher.

Flexural strengthening with four NSM-CFRP strips in the hogging region, where the cutout was installed, further improved the flexural rigidity of the specimen in the hogging region to a level even better than that of the intact sagging regions that contained no cutouts. This in turn increased the hogging moment and reduced the sagging moment of specimen B-S0-H4 relative to the elastic moments. The deviation from the elastic behavior further increased after yielding of tensile steel in the sagging region at approximately 97 kN. Following yielding of steel in the sagging region, the specimen exhibited sagging moments lower than the elastic moments and hogging moments higher than the elastic moments.
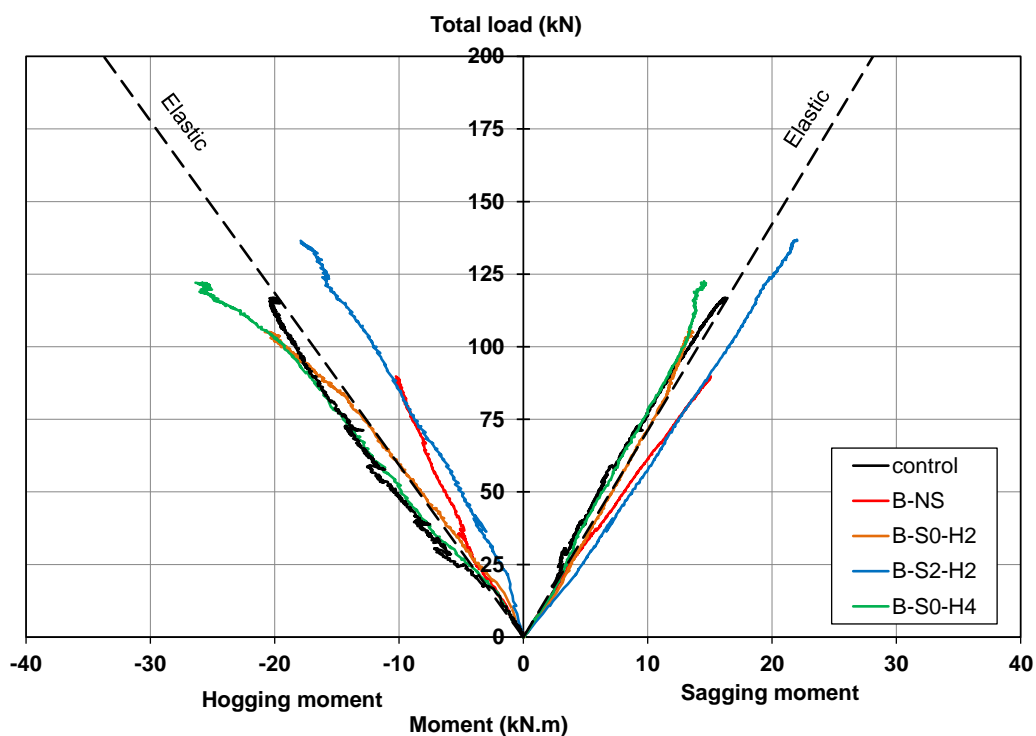
Figure 4.37: Load moment relationship curves for group [B]

4.2.2.11 Moment Redistribution

The moment redistribution ratios for specimens of group [B] along that of the control specimen are given in Table 4.10. The moment redistribution ratio, β, was

calculated using Equation 4.2. A positive value of moment redistribution ratio indicates that the concerned region has gained moments greater than the elastic moment whereas a negative value indicates that the concerned region has gained moments less than the elastic moments.

Table 4.10: Moment redistribution ratios for speicmens of group [B]

Slab Name	Moment form experiment		Elastic Moment		β (%)	
	$M_{s,exp}$ (kN.m)	$M_{h,exp}$ (kN.m)	$M_{s,e}$ (kN.m)	$M_{h,e}$ (kN.m)	Sagging	Hogging
control	16.3	20.1	16.5	19.7	-1.2	+2.0
B-NS	15.1	10.3	12.6	15.2	+19.8	-32.2
B-S0-H2	13.5	20.5	14.8	17.8	-8.8	+15.2
B-S0-H4	14.5	26.1	17.2	20.7	-15.7	+26.1
B-S2-H2	22.0	17.6	19.3	23.1	+14.0	-23.8

From Table 4.10, it can be seen that the unstrengthened specimen B-NS with a cutout in the hogging region exhibited significant moment redistribution ratios of +19.8% and -32.2% in the sagging and hogging regions, respectively. This occurred because of the presence of a cutout in the hogging region which reduced the flexural rigidity of the hogging region relative to that of the sagging region. The control specimen exhibited almost no moment redistribution because both sagging and hogging regions had same concrete geometry and amount of steel reinforcement. Specimen B-S0-H2 exhibited moment redistribution ratios of -8.8% and +15.2% in the sagging and hogging regions, respectively. Specimen A-S0-H4 exhibited higher moment redistribution ratios than those of specimen B-S0-H4 because increasing the amount of NSM-CFRP reinforcement in the hogging region increased the variation in flexural rigidity between the sagging and hogging regions. The moment redistribution ratios for specimen B-S0-H4 were -15.7% and +26.1% in the sagging and hogging regions, respectively. Specimen B-S2-H2 featured moment

redistribution ratios of +14% and -23.8% in the sagging and hogging regions, respectively.

4.3 Efficiency of the Strengthening Schemes

Table 4.11 compares the efficiency of the strengthening schemes adopted in the present study. Equations 4.3 to 4.5 have been used to calculate the efficiency factor of each strengthening scheme. The efficiency factor (EF) for a strengthening scheme has been calculated by multiplying the ratio of the strength gain to the effective tensile strength of all CFRP strips used in strengthening (S_g/T_{fe}) times the ratio of the load capacity of the control specimen without cutouts to the load capacity of the specimen after strengthening (C_c/C_s). The strength gain is the difference between the load capacity before and after strengthening. To fully restore the load capacity, the ratio C_c/C_s must be less than or equal to unity, otherwise the strengthening scheme is considered inefficient with an efficiency factor of $EF = zero$.

$$EF = \begin{cases} \dfrac{S_g}{T_{fe}} \cdot \dfrac{C_c}{C_s} & \text{for} & \dfrac{C_c}{C_s} \leq 1 \\[2em] zero & \text{for} & \dfrac{C_c}{C_s} > 1 \end{cases} \tag{4.3}$$

$$T_{fe} = A_{fe} f_{fr} \tag{4.4}$$

$$A_{fe} = \frac{A_{f,s} L_{f,s} + A_{f,h} L_{f,h}}{\sum L_i} \tag{4.5}$$

where:

A_{fe} = effective cross section area of all CFRP strips used in strengthening

$A_{f,s}$ = cross section area of all CFRP strips used in the sagging regions

$A_{f,h}$ = cross section area of all CFRP strips used in the hogging region

C_c = load capacity of the control specimen without cutouts

C_s = load capacity of the strengthened specimen with cutouts

$L_{f,s}$ = length of all CFRP strips used in the sagging regions

$L_{f,h}$ = length of all CFRP strips used in the hogging region

L_i = length of span i of the continuous slab

Table 4.11: Efficiency of the strengthening schemes

Group	Specimen	A_{fe} (mm^2)	T_{fe} (kN)	S_g (kN)	S_g/T_{fe} (%)	C_c/C_s	EF (%)
[A]	A-S2-H0	241.6	748.9	45.2	6.0	0.89	5.4
	A-S4-H0	966.3	2995.6	65.3	2.2	0.77	1.7
	A-S2-H2	289	895.7	54.2	6.1	0.84	5.0
	A-S4-H2	1013.7	3142.4	69.2	2.2	0.75	1.7
[B]	B-S0-H2	47.4	146.8	15.7	10.7	1.1	0
	B-S0-H4	189.5	587.4	32.7	5.6	0.95	5.3
	B-S2-H2	289	895.7	47.1	5.3	0.85	4.5
	B-S2-H4	431.1	1336.3	48.2	3.6	0.85	3.1

For specimens of group [A] with a cutout in each sagging region, it can be seen that scheme S2-H0 with two NSM-CFRP strips in each sagging region and no strengthening in the hogging region was the most efficient strengthening scheme followed by scheme S2-H2 with two NSM-CFRP strips in both sagging and hogging regions. Schemes S4-H0 with four NSM-CFRP strips in each sagging region, and S4-H2 with four NSM-CFRP strips in each sagging region and two NSM-CFRP strips in the hogging region, were the least efficient strengthening schemes. Although

scheme S2-H0 had half of the amount of the NSM-CFRP reinforcement used in scheme S4-H0, its efficiency factor was approximately 3-fold higher. This occurred because failure of strengthened specimens was controlled by concrete crushing rather than rupture of CFRP, and hence the added amount of NSM-CFRP reinforcement was not efficiently utilized. It can then be concluded that for a slab strip with a cutout in each sagging region having w_c/b of 0.375 and l_c/L of 0.25, the optimal strengthening solution was using two NSM-CFRP strips in each sagging region with a CFRP reinforcement ratio of $\rho_f = 0.35\%$.

For specimens of group [B] with a cutout in the hogging region, the use of two NSM-CFRP strips in the hogging region only was not efficient because the load capacity after strengthening was less than the load capacity of the control specimen without cutouts (i.e. scheme S0-H2 was not able to restore the original load capacity). A minimum of four NSM-CFRP strips had to be used in the hogging region (scheme S0-H4) to fully restore the original load capacity. Scheme S0-H4 with four NSM-CFRP strips in the hogging region was the most efficient scheme followed by scheme S2-H2 with two NSM-CFRP strips in each sagging region and two NSM-CFRP strips in the hogging region. Although scheme S2-H4 had double the amount of the hogging NSM-CFRP reinforcement used in scheme S2-H2, its efficiency factor was approximately 30% lower. This occurred because strengthened specimens failed by concrete crushing without rupture of CFRP. This mode of failure concealed the effect of increasing the amount of the NSM-CFRP reinforcement. It can then be concluded that for a slab strip with a cutout in the hogging region having w_c/b of 0.375 and l_c/L of 0.25, the optimal strengthening solution was using four NSM-CFRP strips in the hogging region with a CFRP reinforcement ratio of $\rho_f = 0.7\%$.

CHAPTER 5: ANALYTICAL MODLEING

5.1 Introduction

This chapter presents an analytical model that can predict the load capacity of two-span continuous RC slab strips with cutouts strengthened with NSM-CFRP reinforcement. The analytical model adopts realistic material laws, and accounts for the effect of NSM-CFRP strengthening on the load capacity. Properties of the concrete, steel and NSM-CFRP reinforcement described in Chapter 3 were used as input data in the analysis. The accuracy of the analytical approach was examined by comparing its predictions with test results.

5.2 Material Constitutive Laws

5.2.1 Concrete

The assumed stress–strain relationship of concrete in compression is illustrated in Figure 5.1 (Hognestad et al. 1955). The ascending branch of the stress–strain relationship of the concrete in compression is described by a second-degree parabola. The softening concrete law in compression is assumed linearly descending until concrete crushing at a strain value of $\varepsilon_{cu} = 0.0038$ and a corresponding post-peak stress value of $f_c = 0.85f_c^{'}$ (Hognestad et al. 1955). The assumed stress-strain relationship is given by Equations 5.1 to 5.3.

$$f_c = \begin{cases} f_c^{'}\left[\dfrac{2\varepsilon_c}{\varepsilon_{co}} - (\dfrac{\varepsilon_c}{\varepsilon_{co}})^2\right] & \varepsilon_c \le \varepsilon_{co} \\[4mm] 0.85f_c^{'} + \dfrac{0.15f_c^{'}(\varepsilon_{cu} - \varepsilon_c)}{(\varepsilon_{cu} - \varepsilon_{co})} & \varepsilon_{co} \le \varepsilon_c \le \varepsilon_{cu} \end{cases} \qquad (5.1)$$

$$\varepsilon_{co} = \frac{2f_c'}{E_c}$$

(5.2)

$$E_c = 4700\sqrt{f_c'}$$

(5.3)

Where:

f_c' = concrete compressive strength.

ε_{c_o} = concrete strain corresponding to the concrete compressive strength.

ε_c = concrete strain for a given loading condition.

f_c = concrete stress for a given concrete strain.

E_c = Young's modulus of concrete.
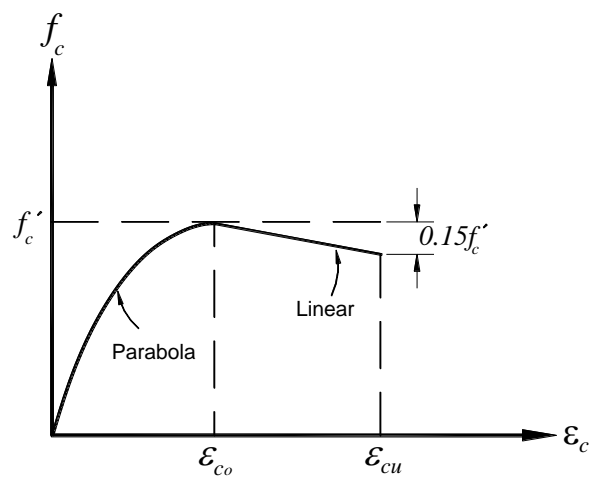
Figure 5.1: Assumed stress-strain relationship of concrete (Hognestad et al. 1955)

5.2.2 Steel Reinforcement

The stress-strain relationship of the steel reinforcement is idealized to be linear elastic-plastic with a post-yield strain hardening of 1% (MacGregor and Bartlett 1997; Park and Paulay 1975) as shown in Figure 5.2. The stress-strain relationship of steel is given by Equation 5.4.

$$f_s = \begin{cases} \varepsilon_s E_s & Pre\text{ - }yield\ \ stage \\[2ex] f_y + E_{sp}\left(\varepsilon_s - \varepsilon_{sy}\right) & Post\text{ - }yield\ \ stage \end{cases}$$

(5.4)

where:

ε_s = steel strain for a given load condition.

f_s = steel stress corresponding to ε_s.

f_y = steel yielding stress.

ε_{sy} = steel strain corresponding to the yield stress f_y.

E_s = modulus of the steel reinforcement before yielding (pre-yield stage).

E_{sp} = modulus of the steel reinforcement after yielding (post-yield stage).

f_{su} = steel ultimate strength.

ε_{su} = steel strain corresponding to the steel ultimate strength f_{su}.
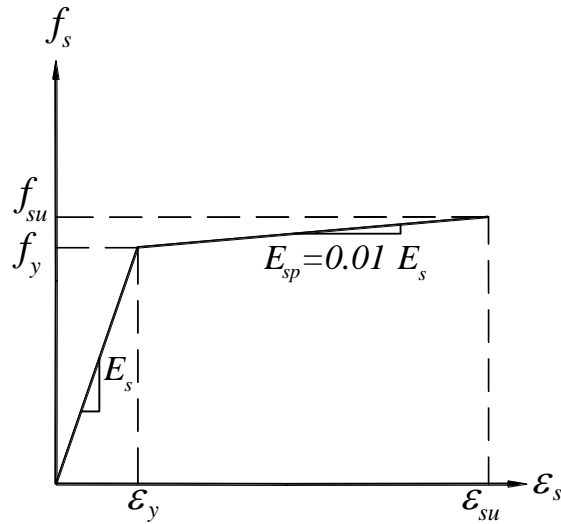
Figure 5.2: Idealized stress-strain relationship of steel

5.2.3 Carbon Fiber Reinforced Polymer

The stress-strain relationship of the CFRP composite strips is idealized to be linear-elastic up to failure as shown in Figure 5.3. The stress-strain relationship of steel is given by Equation 5.5.

$$f_f = \varepsilon_f E_f \leq f_{fr} \qquad (5.5)$$

where:

f_f = stress in NSM-CFRP reinforcement.

ε_f = CFRP strain for a given load condition.

E_f = Young's modulus of the CFRP.

f_{fr} = tensile strength of the CFRP.
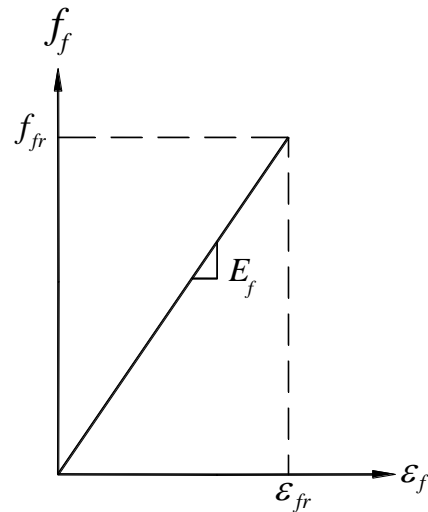
Figure 5.3: Idealized stress-strain relationship of CFRP

5.2.4 Compatibility Requirements

Strain and stress distributions along section depth are shown in Figure 5.4. The strains in the compression steel, tensile steel, and NSM-CFRP reinforcement are given by Equations 5.6, 5.7, and 5.8, respectively.

$$\varepsilon_s^{'} = \frac{\varepsilon_c(c-d^{'})}{c}$$

(5.6)

$$\varepsilon_s = \frac{\varepsilon_c(d-c)}{c}$$

(5.7)

$$\varepsilon_f = \frac{\varepsilon_c(h-c)}{c}$$

(5.8)

where:

$\varepsilon_s^{'}$ = strain in compression steel reinforcement.

ε_s = strain in tensile steel reinforcement.

ε_f = strain in longitudinal NSM-CFRP reinforcement.

c = depth of neutral axis measured from the compression face of the slab.

d' = depth of compression steel measured from the compression face of the slab.

d = depth of tensile steel measured from the compression face of the slab.

h = thickness of slab.
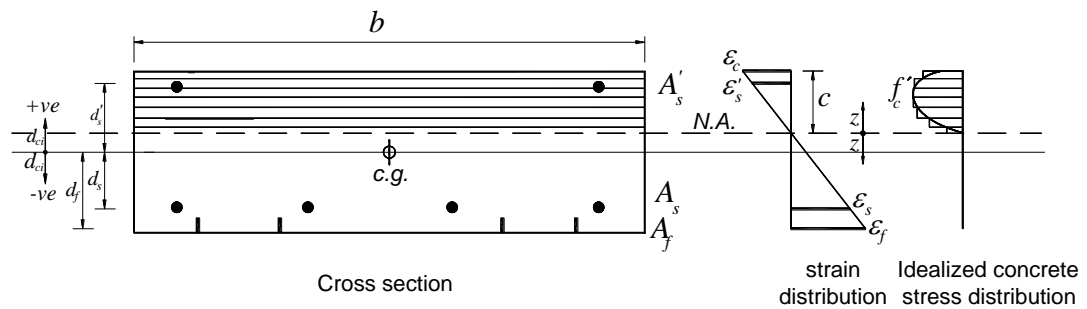
Figure 5.4: Strain and stress distributions along section depth

5.2.5 Equilibrium Requirements

Equilibrium conditions are imposed in terms of axial force and bending moment (Equations 5.9 and 5.10). In order to calculate the compression force in concrete, the cross-section is discretized into finite layers. The compression force in concrete is calculated by numerical integration of forces in each layer. The steel reinforcing bars and FRP strip are represented by discrete elements.

$$\sum_{1}^{n} f_{ci} A_i + \sum A_{si} f_{si} + \sum A_f f_f = 0 \tag{5.9}$$

$$\sum_{1}^{n} f_{ci} A_i d_{ci} + \sum A_{si} f_{si} d_{si} + \sum A_f f_f d_f = M_n \tag{5.10}$$

where:

A_i = area of concrete layer i.

A_{si} = cross sectional area of steel bar i.

A_f = cross sectional area of a NSM-CFRP strip.

d_f = distance between plastic centroid of concrete section and center of the CFRP strip.

d_{ci} = distance between plastic centroid of concrete section and centroid of concrete layer i.

d_{si} = distance between plastic centroid of concrete section and center of steel bar i.

f_f = stress in NSM-CFRP reinforcement.

f_{ci} = concrete stress at the center of the layer i.

f_{si} = stress in the steel bar i.

M_n = nominal moment strength.

In Equations 5.9 and 5.10, compressive stresses are taken as positive and tensile stresses are taken as negative. The distance d_{ci} is taken as positive if the corresponding concrete layer is located above the plastic centroid of the concrete section, otherwise the distance will be taken as negative as shown in Figure 5.4. Similarly, the distance d_s' is taken as positive whereas the distances d_s and d_f are taken as negative.

5.2.6 Model Procedure

For a given strain distribution along the section depth at peak load, the sectional forces are integrated numerically and the nominal moment capacity of both sagging and hogging regions was calculated using an iterative process. It should be noted that all specimens failed by concrete crushing without rupture of the NSM-CFRP

reinforcement, and hence the concrete strain at peak load was assumed as $\varepsilon_{cu} =$ 0.0038 (see section 5.2.1). The model procedure used to predict the nominal moment strength can be summarized as follows:

- Assume depth of the neutral axis c.

- Calculate the strain in each layer of concrete, steel bars, and NSM-CFRP reinforcement using compatibility requirements.

- Calculate the stress in each layer of concrete, steel bars, and NSM-CFRP strips using the materials' constitutive laws.

- Calculate the forces in concrete, steel and NSM-CFRP reinforcement.

- Iterate the assumed neutral axis depth until equilibrium of forces is satisfied.

- Calculate the moment capacity that satisfies equilibrium requirements.

Once the sagging and hogging moment capacities are calculated the load carrying capacity for a two equal-span continuous slab, with a concentrated load of $P/2$ at each mid-span, can be predicted using Equation 5.11 (Park and Paulay 1975).

$$P_n = \frac{4}{L}(2M_{ns} + M_{nh})$$

(5.11)

where:

P_n = nominal load capacity predicted by the model.

L = length of one of the two equal spans.

M_{ns} = nominal moment strength of the sagging section.

M_{nh} = nominal moment strength of the hogging section.

5.2.7 Analytical Results

The predicted nominal moment strengths of the sagging and hogging sections are presented in Table 5.1. The concrete dimensions, amount of internal steel reinforcement, and NSM-CFRP reinforcement used as input data in the analysis are presented in the same table. Properties of concrete, steel and NSM-CFRP reinforcement used in the analysis are described in Chapter 3. A comparison between the experimental and predicted load carrying capacities is given in Table 5.2. The model tended to provide a conservative prediction for the load capacity of test specimens. The predicted load capacity of the control specimen was approximately 22% lower than the experimental load capacity. For specimens of group [A], with a cutout in the sagging region, the ratio of the predicted to measured load capacity was in the range of 0.74 to 0.87. The model provided more accurate predictions for the load capacities of specimens of group [B] with a cutout in the hogging region where the ratio of the predicted to measure load capacity was in the range of 0.85 to 1.02. The contribution of the sagging moment to the load capacity is two times that of the hogging moment (see Equation 5.11). As a result, the predicted load capacity is less sensitive to the predicted hogging moment capacity than the sagging moment capacity. This explains why the model had better predictions for specimens of group [B] with a cutout in the hogging region.

The ratio of the predicted to measured load capacity was on average 0.85 with a standard deviation of 0.09, and a coefficient of variation of 10%. The difference between the predicted load capacity and that measured experimentally is within the acceptable margin of error for such a complex problem. It can then be stated that the analytical approach adopted in this study can give reasonable predictions for the load

capacity of two-span continuous RC slab strips with a cutout and strengthened with NSM-CFRP reinforcement.

Table 5.1: Predicted moment capacity

Specimen	Sagging section				M_{ns}	Hogging section				M_{nh}
	b	A_s	$A_s{}'$	A_f	(kN.m)	b	A_s	$A_s{}'$	A_f	(kN.m)
control	400	314.2	157.1	0	13.7	400	314.2	157.1	0	13.7
A-NS	250	157.1	157.1	0	7.5	400	314.2	157.1	0	13.7
A-S2-H0	250	157.1	157.1	75	15.24	400	314.2	157.1	0	13.7
A-S4-H0	250	157.1	157.1	150	19.25	400	314.2	157.1	0	13.7
A-S2-H2	250	157.1	157.1	75	15.24	400	314.2	157.1	75	22.1
A-S4-H2	250	157.1	157.1	150	19.25	400	314.2	157.1	75	22.1
B-NS	400	314.2	157.1	0	13.7	250	157.1	157.1	0	7.5
B-S0-H2	400	314.2	157.1	0	13.7	250	157.1	157.1	75	15.24
B-S0-H4	400	314.2	157.1	0	13.7	250	157.1	157.1	150	19.25
B-S2-H2	400	314.2	157.1	75	22.1	250	157.1	157.1	75	15.24
B-S2-H4	400	314.2	157.1	75	22.1	250	157.1	157.1	150	19.25

Table 5.2: Comparison between analytical and experimental load capacities

Group	Specimen	Predicted load capacity P_n (kN)	Experimental load capacity P_u (kN)	*Difference (%)	Ratio (P_n/P_u)
Control	control	91.3	116.9	-21.9	0.78
[A]	A-NS	63.8	85.8	-25.6	0.74
	A-S2-H0	98.2	131.0	-25.0	0.75
	A-S4-H0	116.0	151.1	-23.2	0.77
	A-S2-H2	116.8	140.0	-16.6	0.83
	A-S4-H2	134.7	155.0	-13.1	0.87
[B]	B-NS	77.6	89.8	-13.6	0.86
	B-S0-H2	94.8	105.5	-10.1	0.90
	B-S0-H4	103.7	122.5	-15.3	0.85
	B-S2-H2	132.1	136.9	-3.5	0.96
	B-S2-H4	141.0	138.0	+2.2	1.02
Average					0.85
Standard deviation					0.09
Coefficient of variation (%)					10%

*Difference (%) = 100 x $(P_n – P_u)/(P_u)$

CHAPTER 6: CONCLUSIONS AND RECOMMENDATIONS

6.1 Introduction

The flexural response of two-span continuous RC slab strips with cutouts strengthened with NSM-CFRP reinforcement has been investigated in this thesis. The research comprised experimental testing and analytical modeling. The experimental study comprised testing of eleven slabs. One unstrengthened slab without a cutout acted as a benchmark. Five slabs had a cutout in each sagging region and five slabs had a cutout in the hogging region. The specimens with cutouts were strengthened in the sagging, hogging, or both regions using NSM-CFRP reinforcement. An analytical model that can predict the load capacity of unstrengthened and strengthened two-span RC slab strips with a cutout either in the mid-span sections or over the middle support has been introduced. The validity of the model has been demonstrated by comparing its predictions with the experimental results of the present study.

Main conclusions of the work along with recommendations for future studies on the subject are presented in this chapter. The outcomes of the present study are limited to two-span RC slab strips with a width of $b = 400$ mm, depth of $h = 125$ mm, and span length of $L = 1800$ mm subjected to monotonic loading. The cutout went completely through the full thickness of the slab, and was installed either in the mid-span sections or over the middle support. The cutout had a width of $w_c = 0.375b$ and a length of $l_c = 0.25L$. A variation in the location and/or size of the cutouts would change the structural response of the slabs before and after strengthening.

6.2 Conclusions

Based on results of this research work, the following conclusions can be drawn:

- Installation of a cutout in the sagging region reduced the load capacity by approximately 27% and ductility index by approximately 12%. When the cutout was installed in the hogging region, a 23% reduction in both load capacity and ductility index was recorded.

- The NSM-CFRP strengthening system was very effective in improving the load capacity but tended to reduce the slab ductility. For the specimens with a cutout in the sagging region, the strengthening system fully restored the load capacity of the control slab regardless of the amount and distribution of the NSM-CFRP reinforcement. For the specimens with a cutout in the hogging region, two NSM-CFRP strips restored only 90% of the load capacity of the control specimen. The load capacity of all other strengthened specimens with a cutout in the hogging region was higher than that of the control specimen. The increase in load capacity due to strengthening was more pronounced when the NSM-CFRP reinforcement was installed in the sagging region.

- Strengthening of continuous RC slab strips having a cutout in the sagging region using two and four NSM-CFRP strips increased the load capacity by 53% and 76%, respectively relative to that of the unstrengthened specimen with a cutout. Installation of NSM-CFRP reinforcement in the hogging region, in addition to the NSM-CFRP reinforcement in the sagging region, resulted in an insignificant additional increase in the load capacity. The additional increase in load capacity due to installation of NSM-CFRP reinforcement in the hogging region was 3% for the specimen with two

NSM-CFRP strips in the sagging region and 7% for the specimen with four NSM-CFRP strips in the sagging region. This indicated that the additional increase in load capacity due to installation of NSM-CFRP reinforcement in the hogging region decreased with an increase in the amount of NSM-CFRP reinforcement in the sagging region.

- Strengthening of continuous RC slab strips having a cutout in the hogging region using two and four NSM-CFRP strips increased the load capacity by 18% and 36%, respectively relative to that of the unstrengthened specimen with a cutout. Installation of NSM-CFRP reinforcement in the sagging region, in addition to the NSM-CFRP reinforcement in the hogging region, resulted in 30% additional increase in the load capacity for the specimen with two NSM-CFRP strips in the hogging region and 13% increase in the load capacity for the specimen with four NSM-CFRP strips in the hogging region. This indicated that the additional increase in load capacity due to installation of NSM-CFRP reinforcement in the sagging region decreased with an increase in the amount of NSM-CFRP reinforcement in the hogging region.

- The ductility index of the strengthened specimens with a cutout, except those heavily strengthened in both sagging and hogging regions, was the same as or higher than that of the corresponding unstrengthened specimen with a cutout. The specimen heavily strengthened in both sagging and hogging regions was an average 28% lower than that of the corresponding specimen with a cutout.

- Unlike simply-supported structures, the enhancement in moment capacity of the critical sections in continuous RC slab strips due to strengthening was not the same as the enhancement in the load capacity. Two and four NSM-CFRP strips enhanced the moment capacity by approximately 2 and 2.5 folds

respectively. The enhancement in the load capacity due to strengthening was in the range of 53% to 81% for the specimens with a cutout in the sagging region and 18% to 54% for the specimens with a cutout in the hogging region.

- The moment redistribution was dependent on variation in flexural rigidity between the sagging and hogging regions. The control unstrengthened specimen exhibited almost no moment redistribution because it contained the same amount of internal steel reinforcement in both sagging and hogging regions. The unstrengthened specimens with a cutout exhibited moment redistribution ratios in the range of 20% to 50% due to the significant variation in cross section and amount of steel reinforcement between the sagging and hogging regions. The moment redistribution values in strengthened specimens depended on the amount and distribution of the NSM-CFRP reinforcement between the sagging and hogging regions. Proper distribution of NSM-CFRP reinforcement between the sagging and hogging regions resulted in up to 26% moment redistribution in continuous RC slab strips with cutouts.

- The CFRP reinforcement used in strengthening was not fully utilized. The ratio of the CFRP strain at peak load to the ruptured CFRP strain was in the range of 37% to 51% for the specimens with a cutout in each sagging region, and 33% to 46% for the specimens with a cutout in the hogging region.

- The optimal strengthening solution for the slabs with a cutout in each sagging region was using two NSM-CFRP strips in each sagging region with a CFRP reinforcement ratio of $\rho_f = 0.35\%$. For the slabs with a cutout in the hogging

region, the optimal strengthening solution was using four NSM-CFRP strips in the hogging region with a CFRP reinforcement ratio of $\rho_f = 0.7\%$.

- The analytical model proposed in this study tended to provide a conservative prediction for the load capacity of test specimens. The predicted load capacity of the control specimen was approximately 22% lower than the experimental load capacity. For the specimens with a cutout in the sagging region, the ratio of the predicted to measured load capacity was in the range of 0.74 to 0.87. The model provided more accurate predictions for the load capacities of the specimens with a cutout in the hogging region where the ratio of the predicted to measure load capacity was in the range of 0.85 to 1.02. The ratio of the predicted to measured load capacity was on average 0.85 with a standard deviation of 0.09, and a coefficient of variation of 10%.

6.3 Recommendations for Future Studies

The following are recommendations for future studies in the field of strengthening of continuous structures with composites.

- Study the effect of varying the location and size of the cutouts on the flexural response of strengthened and unstrengthened continuous RC slab strips.
- Study the viability of using externally-bonded composites with and without anchors rather than NSM-CFRP reinforcement to upgrade the flexural response of continuous RC beams and slab strips.
- Investigate the durability performance of continuous RC beams and slab strips strengthened with composites under elevated temperatures and high humidity.

- Investigate the response of continuous RC beams and slab strips strengthened with composite under fatigue loading.

- Develop finite element (FE) models for the specimens tested in the present study. The FE models can be used as a numerical platform for performance prediction of continuous RC slab strips containing cutouts and strengthened with composites.

BIBLIOGRAPHY

ACI 318-08. (2008). "Building code requirements for structural concrete." ACI 318-08, Farmington Hills, MI.

ACI 214R-02 (2002). "Evaluation of strength test results of concrete." ACI 214R-02, Farmington Hills, MI.

Aiello, M., and Ombres, L. (2011). "Moment redistribution in continuous fiber-reinforced polymer-strengthened reinforced concrete beams." *ACI Structural Journal,* Vol. 108 No. 2, March-April, pp. 158-166.

Arduini, M., Nanni, A., and Romagnolo, M. (2004). "Performance of one-way reinforced concrete slabs with externally bonded fiber-reinforced polymer strengthening." *ACI Structural Journal,* Vol. 101 No. 2, March-April, pp. 193-20.1.

Ashour, A. F., El-Refaie, S. A., and Grrity, S. W. (2004). "Flexural strengthening of RC continuous beams using CFRP laminates." *Cement & Concrete Composites,* pp. 765-775.

Boon, K. (2009). "Flexural behavior of reinforced concrete slab with opening." *Malaysian Technical Universities Conferences on Engineering and Technology,* June.

Coccia, S., Ianniruberto, U., and Rinaldi, Z. (2008). "Redistribution of bending moment in continuous reinforced concrete beams strengthened with fiber-reinforced polymer." *ACI Structural Journal,* Vol. 105 No. 3, May-June, pp. 318-326.

Dalfre, G., and Barros, J. (2011). "Assessing the effectiveness of a NSM-CFERP flexural strengthening technique for continuous RC slabs by experimental research." *First Middle East Conference on Smart Monitoring, Assessment and Rehabilitation of Civil Structure,* 8-10 February.

El-Refaie, S., Ashour, A., and Garrity, W. (2003). "Sagging and hogging strengthening of continuous reinforced concrete beams using carbon fiber-reinforced polymer sheets." *ACI Structural Journal,* Vol. 100 No. 4, August, pp. 446-453.

Farahdad, F., and Mostonfinejad, D. (2011). "Experimental study of moment redistribution in RC frames strengthened with CFRP sheets." *Composite Structures,* 93(2011), pp. 1168-1177.

Grace, N., Ragheb, W., and Abdel-Sayed, G. (2004). "Strengthening of cantilever and continuous beams using new triaxially braided ductile fabric." *ACI Structural Journal,* Vol. 101 No. 2, March-April, pp. 237-244.

Hongstad, E., Hanson,N., and McHenry, D. (1955). "Concrete stress distribution in ultimate strength design." *ACI Structural Journal,*52 (6), PP. 455-479.

ISIS Canada Educational Module No. 4 (2004). "An introduction to FRP-strengthening of concrete structures." ISIS Canada. Section 2S, Canadian Network of Centers of Excellence on Intelligent Sensing for Innovative Structures., Winnipeg, Manitoba, Canada, p 5 .

Jumaat, M., Rahman, M., and Alam, M. (2010). "Flexural strengthening of RC continuous T beam using CFRP laminate: a review." *International journal of the physical sciences,* Vol. 5(6), June, pp. 619-625.

Kai, X., Guo-hui, W., Ting, Z., and Zhou-dao, L. (2011). "Experiment and analysis of CFRP strengthened fire-damaged reinforced concrete continuous T-beams." *The 5th Conference on Performance-based Fire and Fire Protection Engineering*, pp. 541-549.

Kim, S., and Smith, S. (2009). "Strengthening of RC slabs with large penetrations using anchored FRP composites." *Asia-Pacific Conference on FRP in Structures*, December , pp.111-116.

Liu, I., Oehlers, D., Seracino, R., and Ju, G. (2006). "Moment redistribution parametric study of CFRP, GFRP and steel surface plated RC beams and slabs." *Construction and Building Materials,* June, pp. 59-70.

MacGregor, J. G., and Bartlett, F. M. (1997). "Reinforced concrete: mechanics and design." Prentice Hall Canada Inc., Ontario, Canada, p. 939.

Park, R., and Paulay, T. (1975). "Reinforced concrete structures." John Willey & Sons, NY, USA, p. 800.

Seliem, H., Seracino, R., Summer, E., and Smith, S. (2011). "Case study on the restoration of flexural capacity of continuous one-way RC slabs with cutouts." *Journal of Composites for Construction,* November-December, pp. 992-998.

Silva, P., and Ibell, T. (2008). "Evaluation of moment distribution in continuous fiber-reinforced polymer-strengthened concrete beams." *ACI Structural Journal,* Vol. 105 No. 6, November-December, pp. 729-739.

Smith, S., and Kim, S. (2009). "Strengthening of one-way spanning RC slabs with cutouts using FRP composites." *Construction and Building Materials*, pp. 1578-1590.

Tan, K., and Zhao, H. (2004). "Strengthening of opening in one-way reinforced-concrete slabs using carbon fiber-reinforced polymer systems." *Journal of composites for construction ASCE*, September-October, pp. 393-401.

Vasquez, A., and Karbhari, V. (2003). "Fiber reinforced polymer composite strengthening of concrete slabs with cutouts." *ACI structural journal,* Vol. 100 No. 5, September- October, pp. 665-673.